

**SIGNAL PROCESSING FOR BIT-PATTERNED MEDIA
RECORDING**

WU TONG

NATIONAL UNIVERSITY OF SINGAPORE

2014

**SIGNAL PROCESSING FOR BIT-PATTERNED MEDIA
RECORDING**

WU TONG

(B. Eng., Huazhong University of Science and Technology, China)

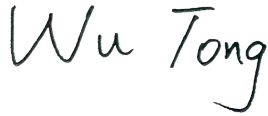
A THESIS SUBMITTED
FOR THE DEGREE OF DOCTOR OF PHILOSOPHY
DEPARTMENT OF ELECTRICAL AND COMPUTER ENGINEERING
NATIONAL UNIVERSITY OF SINGAPORE

2014

DECLARATION

I hereby declare that this thesis is my original work and it has been written by me in its entirety. I have duly acknowledged all the sources of information which have been used in the thesis.

This thesis has also not been submitted for any degree in any university previously.

A handwritten signature in black ink, reading "Wu Tong", written in a cursive style. The signature is positioned above a horizontal line.

Wu Tong

15 August 2014

Acknowledgments

Foremost, I would like to express my sincere gratitude and deepest appreciation to my supervisor Professor Marc Andre Armand for his invaluable guidance and great support throughout my Ph.D course. Had it not been for his solid expertise, continuous advices, enthusiastic encouragements and enormous patience, this thesis would certainly not exist in its current form. His profound thinking, positive and prudential attitude, and academic rigour has been and will always be an inspiring role model for my future career.

I would like to give my special thanks to Dr. Xiaopeng Jiao and Ahmed Mahmood, for their helpful suggestions and stimulating discussions, especially during the early stage of my Ph.D study when I was intimidated by various difficulties encountered in my research.

I want to thank Professor J. R. Cruz for his help and insightful comments on my research. I am also grateful to Saima Ahmed, Nguyen Phan Minh and Dr. Haifeng Yuan for the fruitful discussions and valuable suggestions they have provided.

My sincere thanks also go to my former and current colleagues in the Communications & Networks Laboratory for their warm friendship and kindness. These include Yu Wang, Liang Liu, Gaofeng Wu, Shixin Luo, Xuzheng Lin, Jie Xu, Xun Zhou, Yi Yu, Chenglong Jia, Tianyu Song, Eric and many others.

I am forever indebted to my parents for their endless love and support. I would definitely not be able to finish my education, not even to mention the Ph.D study, if

not for their continuous support and encouragements. I also owe my deepest gratitude to my wife, who encouraged me to pursue a Ph.D degree in the very first place and experienced all of the ups and downs of my research. Her love, understanding and encouragements have been and will always be my motivation to succeed.

Finally, the support of the Singapore National Research Foundation under CRP Award No. NRF-CRP 4-2008-06 in the form of a research scholarship is gratefully acknowledged.

Contents

Summary	ix
List of Tables	xii
List of Figures	xiii
List of Notations	xix
List of Abbreviations	xx
1 Introduction	1
1.1 Bit-Patterned Media Recoding	5
1.1.1 Fabrication Imperfections of BPMR	7
1.1.2 Challenges of Signal Processing for BPMR	8
1.2 Motivations and Contributions	13
1.2.1 Davey-MacKay Construction with RS Codes as Outer Codes .	13
1.2.2 Improved Write Channel Model with Data-Dependent IDS Er- rors	14
1.2.3 Detection-Decoding on Rectangular and Staggered BPMR Chan- nels with WIE Correction and ITI Mitigation	16
1.3 Organization of the Thesis	18

CONTENTS

2	On Reed-Solomon Codes as Outer Codes in the Davey-MacKay Construction for Channels with Insertions and Deletions	20
2.1	IIDS Channel Model	21
2.2	DM Coding Scheme	23
2.2.1	Bit-Level DM Inner Decoding	25
2.2.2	Symbol-Level DM Inner Decoding	29
2.3	LDPC Codes and BP Decoding	30
2.4	RS Codes and Iterative Soft-Decision RS Decoding	31
2.4.1	The Hybrid ABP-ASD Decoder	32
2.5	Advantages of Using RS Codes as Outer Codes in the DM Construction	34
2.5.1	Effective Substitution Error Rate	34
2.5.2	Uncertainty in Inner Decoder's Output	36
2.5.3	Implications	38
2.5.4	Simulation Results	39
2.6	Concluding Remarks	43
3	The Davey-MacKay Coding Scheme for BPMP Write Channels with Data-Dependent Insertion, Deletion and Substitution Errors	44
3.1	Data-Dependent Characteristics of WIEs in BPMP	46
3.2	The DIDS Channel Model	49
3.2.1	Modeling Insertion-Deletion & Deletion-Insertion Pairs	49
3.2.2	Modeling Substitution Errors	51
3.3	Applying the DM Construction to the DIDS Channel Model	52
3.3.1	Modifying the Inner Decoder	54
3.3.2	Reduced-Complexity Inner Decoding	58
3.3.3	Iterative Decoding	59
3.4	Simulation Results	59

CONTENTS

3.4.1	Distribution of the Length of Negative/Positive Cycles	60
3.4.2	FER Performance on the DIDS Channel	60
3.5	Conclusion	70
4	Detection-Decoding on Rectangular BPMR Channels with Written-In Error Correction and ITI Mitigation	72
4.1	Two-Dimensional Pulse response of Isolated Bit Island	73
4.2	Rectangular BPMR Channel Model	77
4.3	Read Channel Equalization and Detection	79
4.4	Channel Detection and Decoding	80
4.4.1	BCJR Detection with Binary-Input-Inner-Decoding	81
4.4.2	Joint Detection-Inner-Decoding	83
4.4.3	BCJR Detection with Soft-Input-Inner-Decoding	87
4.5	Simulation Results and Discussions	90
4.5.1	Performance Comparison of the BCJR-BIID, JDD and BCJR-SIID with SE	91
4.5.2	Performance Comparison of the BCJR-BIID, JDD and BCJR-SIID with M-2D2D (5 tracks)	96
4.5.3	Performance of Increased Code Rate and Higher Areal Density	101
4.6	Conclusion	108
5	Detection-Decoding on Staggered BPMR Channels with Written-In Error Correction and ITI Mitigation	109
5.1	BPMR Channel Model with JE	110
5.2	Channel Detection and Decoding	111
5.3	Simulation Results and Discussions	113
5.3.1	Performance Comparison of M-JE on Rectangular and Staggered BPMR Read Channels	116

CONTENTS

5.3.2	Performance of DM Construction on Single-Track Staggered BPMR Channels	116
5.4	Conclusion	122
6	Summary of Contributions and Suggestions for Future Work	124
6.1	Summary of Contributions	124
6.2	Proposals for Future Research	127
6.2.1	Efficiently Handle Relatively Long Burst Errors	127
6.2.2	Improving the DM Coding Scheme for DIDS Channel	128
6.2.3	Applying Marker Codes to the DIDS Channels	129
6.2.4	Detection-Decoding on BPMR Channels with Media Noise	130
Appendix A	Channel Capacity Bounds for DIDS Channel	132
A.1	Channel Capacity Bounds for DIDS Channel with Stationary and Er- godic Input Process	132
A.2	Symmetric Information Rate Lower and Upper Bounds of the DIDS Channel	137
	Bibliography	141
	List of Publications	154

Summary

Due to the onset of the superparamagnetic effect, conventional continuous magnetic recording technology is expected to reach its data storage areal density limit in the near future. To sustain the continuous growth of areal density, bit-patterned media recording (BPMR) has emerged as a competitive candidate for next-generation magnetic recording. BPMR can dramatically delay the onset of the superparamagnetic effect and bring many advantages compared to continuous magnetic recording; however, it also poses new and challenging technical issues. Two major and unique challenges are the written-in errors (WIE), i.e., insertion, deletion and substitution (IDS) errors, that occur during the write process, and the 2D interference comprising inter-symbol interference (ISI) and inter-track interference (ITI) that deteriorates the readback performance. In this thesis, we investigate and address WIE and 2D interference in BPMR from the perspective of signal processing.

The Davey-MacKay (DM) construction is a promising concatenated coding scheme for channels with independent IDS (IIDS) errors. It employs an inner watermark code to recover synchronization errors and an outer low-density parity-check (LDPC) code to correct residual substitution errors. Inspired by the fact that Reed-Solomon (RS) codes are still considered for BPMR and powerful iterative RS decoding schemes are available, we investigate and compare the performance of the DM construction with LDPC and RS codes as the outer code. We show that when the insertion and deletion probabilities are sufficiently small, using a q^2 -ary $(q^2 - 1, (q^2 - 1)R)$ RS code in place

of a q -ary $(2(q^2 - 1), 2(q^2 - 1)R)$ LDPC code as the outer code along with an iterative soft-decision RS decoder, improves frame-error-rate (FER) performance for moderate to high-rate applications involving relatively short blocklengths.

Experiments and simulations revealed that WIE are data-dependent. Hence, we propose a dependent IDS (DIDS) channel model to mimic the write channel found in BPMR systems. The proposed channel consists of a ternary Markov state channel and a two-state binary symmetric channel (BSC). The ternary Markov state channel produces data-dependent and paired insertion-deletion errors while the two-state BSC produces random substitution errors, as well as burst-like substitution errors in the vicinity of insertions and deletions. In addition, we modify the inner decoder of the DM coding scheme for the proposed channel model. As the (computational) complexity of our inner decoder increases with the length of the burst-like substitution errors, we further propose a reduced-complexity variant of our inner decoder to handle these errors.

As intervals between adjacent islands need to be reduced to achieve high areal densities, ITI arises as a new performance-limiting factor besides the conventional and ever-increasing ISI. Hence, we first consider a rectangular BPMR channel model consisting of the DIDS write channel followed by a partial response read channel with high ITI corresponding to high areal densities. Three detection-inner-decoding schemes are proposed to work with an outer decoder to recover the data encoded by the DM coding scheme on the BPMR channel, namely the BCJR-binary-input-inner-decoder (BCJR-BIID) algorithm, the joint detection-inner-decoder (JDD) algorithm and the BCJR-soft-input-inner-decoder (BCJR-SIID) algorithm. Computer simulations show that: i) at low to moderate (resp., high) signal-to-noise ratios (SNRs), BCJR-SIID (resp., BCJR-BIID) provides good performance-complexity trade-offs; ii) the burst-like substitution errors preceding and following an insertion or deletion have a significant impact on the overall performance. Further, since staggered BPMR reduces ITI at the expense of enhanced ISI which can nevertheless be effectively dealt with longer

SUMMARY

generalized partial-response targets, we consider data recovery on a staggered BPMP channel at ultra high areal density with BCJR-BIID and BCJR-SIID. We show that a soft-input inner decoder for the DM construction provides significantly better robustness against burst-like substitution errors compared to its binary-input counterpart at low insertion/deletion probabilities.

List of Tables

2.1	An example of the mapping LUT employed by the DM spsifier inner encoder when $k = 3, n = 4$	24
2.2	Effective substitution error rates for different q and R_w	36
3.1	Number of valid SCSWs for $L = 0, 1, 2, 3, 4, 5$ with $T_{max} = 1, 2$	58

List of Figures

1.1	(a) longitudinal magnetic recording; (b) perpendicular magnetic recording.	3
1.2	Bit-patterned media recording.	6
1.3	Illustration of written-in errors in the recording process of BPMR systems. The gray squares are the magnetic pattern island and the number in the square represents the bit recorded, the writing head with writing span larger than one island is represented using a dashed rectangle. The sequence of bits to be recorded, i.e., 010101, are shown on the left side of the figure along the time axis. The written-in errors are indicated in the figure using white square and the deleted bit is denoted by a dashed white square.	10
2.1	State diagram of the IIDS channel model with insertion, deletion and substitution probabilities.	22
2.2	Block diagram of the DM coding scheme.	24
2.3	Trellis representation of the IIDS channel with channel state x_i	27
2.4	Structure of iterative DM decoder	30
2.5	Illustration of the hybrid ABP-ASD algorithm.	33
2.6	Average entropy of the likelihoods $P(\mathbf{r} c_i)$ generated by the inner decoder, as a function of $P_i = P_d$	37

LIST OF FIGURES

2.7	Performance comparison of 64-ary (63,45) RS code and 8-ary (126,90) LDPC code.	40
2.8	Performance comparison of 256-ary (255,239) RS code and 16-ary (510,478) LDPC code.	42
3.1	Modeling insertion and deletion errors that are surrounded by burst substitution errors.	48
3.2	The DIDS channel model. The input is $\{X_i\}$ and the output from the ternary Markov channel model is $\{X_{i-Z_i}\}$ which feeds to the two-state BSC to yield the final output $\{Y_i\}$	49
3.3	Numerical overall substitution error rates obtained via simulations and corresponding overall substitution error rates computed by (3.2). . . .	53
3.4	Illustration of the DIDS channel model. The arrow shows how the input bits map into the received sequence \mathbf{Y} according to the channel state sequence \mathbf{Z} . Inserted (resp., deleted) bits are indicated by gray (resp., dashed) square. Crosses in the figure denote the received bits resulting from substitution errors. The burst substitution errors in the vicinity of an insertion and vicinity of a deletion are indicated by I and D , respectively. The initial state of \mathbf{Z} is denoted by (0).	54
3.5	Illustration of the 16 valid SCSWs for $L = 0$	55
3.6	Illustration of the received bits needed by the inner decoder.	56
3.7	Positive cycle rate vs. Positive cycle length.	61
3.8	Negative cycle rate vs. Negative cycle length.	62
3.9	FER performance under iterative and non-iterative decoding over the DIDS channel with inner decoder A for $L = 0$	64
3.10	FER performance under iterative and non-iterative decoding over the DIDS channel with inner decoder C for $L = 0$	65

LIST OF FIGURES

3.11	Number of codewords corrected vs. Number of outer iterations performed with inner decoder A for $P_I = P_D = 0.01$ and $L = 0$	66
3.12	(a) Average entropy of the likelihoods $\Pr(\mathbf{Y} c_i)$ generated by inner decoder B, as a function of $P_I = P_D$, for $1 \leq T_{max} \leq 2L + 2$ and $L = 0, 1$; (b) FER performance under non-iterative decoding with inner B for the different values of T_{max} and L considered in part (a).	68
3.13	Symmetric information rate for the DIDS channel with independent and uniformly distributed input for $L = 0, 1, 2$	69
3.14	FER performance under iterative decoding with inner decoder B for $L = 0, 1, 2, 3, 4, 5$, $T_{max} = 1$ and $(\alpha, \beta) = (10, 10)$	70
4.1	Geometry of MR/GMR read head sensing an individual square island of length a and thickness σ	75
4.2	(a) DIDS write channel model; (b) Rectangular read channel model with MTD and 2D equalization.	78
4.3	The BCJR-BIID detection-decoding scheme.	82
4.4	The JDD detection-decoding scheme.	84
4.5	The BCJR-SIID detection-decoding scheme.	87
4.6	Iterative decoding framework for the BIID, JDD and SIID.. . . .	89
4.7	(a) BER under non-iterative decoding with the proposed BCJR-BIID, JDD and BCJR-SIID on the single-track equalized BPMR channel with $L = 1$ for different SNR values; (b) The distribution of LLRs generated by the BCJR detector for different SNRs considered in part (a).	93
4.8	BER under non-iterative decoding with the proposed BCJR-BIID, JDD and BCJR-SIID on the BPMR channel with $L=5$ for different SNR values.	94

LIST OF FIGURES

4.9	BER under iterative decoding with the proposed BCJR-BIID, JDD and BCJR-SIID on the BPMR channel with $L=5$ for different SNR values.	95
4.10	(a) BER and BLER under non-iterative decoding with the proposed BCJR-BIID, JDD and BCJR-SIID on the BPMR channel with $L = 1$ for different SNR values; (b) The PDF of LLRs generated by the BCJR detector for different SNRs considered in part (a).	97
4.11	BER and BLER under iterative decoding with the proposed BCJR-BIID, JDD and BCJR-SIID on the BPMR channel with $L = 1$ for different SNR values.	98
4.12	Average entropy of the likelihoods generated by the BCJR-BIID, JDD and BCJR-SIID of Fig.4.10(a).	100
4.13	BER performance of BCJR-SIID under iterative decoding on the BPMR channels with $L = 0, \dots, 5$ for different SNRs.	102
4.14	Normalized 2D pulse response of a length-5 nm square island.	104
4.15	Normalized pulse response for numerical and Gaussian fitted analytical pulses in the (a) along-track and (b) cross-track directions of a length-5 nm square island.	105
4.16	BER performance of the BCJR-SIID under iterative decoding on the BPMR channel with different areal density and $L = 0, \dots, 5$, when $\text{SNR} = 12$ dB.	106
4.17	PDF of LLRs generated by the BCJR detector with the read channel of different areal densities considered in Fig.4.16.	107
5.1	(a) DIDS write channel model; (b) Read channel model with joint-track equalization.	110
5.2	(a) Rectangular BPMR; (b) single-track staggered BPMR; (c) double-track staggered BPMR.	112

LIST OF FIGURES

5.3	Normalized 2D pulse response of an isolated square island, which has length of 5 nm and thickness of 10 nm. The GMR read head is of width 10 nm and thickness 4 nm. The fly height is 10 nm and shield to sensor spacing is 6 nm.	114
5.4	Normalized pulse response for numerical and Gaussian fitted analytical pulses in the (a) along-track and (b) cross-track directions of Fig.5.3.	115
5.5	BER performance of M-JE on single-track staggered, double-track staggered and rectangular BPMR read channels at an areal density of 6 Tb/in ²	117
5.6	BER of rate-0.71 DM code with BCJR-BIID and BCJR-SIID under iterative decoding on the single-track staggered BPMR channel for $L = 0, \dots, 5$	118
5.7	BER of BCJR-BIID and BCJR-SIID under iterative decoding on the single-track staggered BPMR channel with two rate-0.71 DM codes: a) DM-1 and b) DM-2.	120
5.8	Average entropy of the likelihoods generated by BCJR-BIID and BCJR-SIID under non-iterative decoding against inner code rate for $L = 3, 4, 5$ and $P_I = P_D = 0.002, 0.003, 0.004$	121
5.9	BER of rate-0.8 DM code with BCJR-BIID and BCJR-SIID under iterative decoding on the single-track staggered BPMR channel for $L = 0, \dots, 5$	122
A.1	Symmetric information rate lower and upper bounds for DIDS channel with $L = 0$	138
A.2	Symmetric information rate lower and upper bounds for DIDS channel with $L = 1$	139

LIST OF FIGURES

A.3 Symmetric information rate lower and upper bounds for DIDS channel with $L = 2$	140
--	-----

List of Notations

a	lowercase letters are used to denote scalars
\mathbf{a}	boldface lowercase letters are used to denote column vectors
\mathbf{A}	boldface uppercase letters are used to denote matrices
$(\cdot)^T$	the transpose of a vector or a matrix
$E[\cdot]$	the statistical expectation operator
$H(\cdot)$	the entropy computation
$I(\cdot)$	the mutual information computation
$w_H(\cdot)$	the Hamming weight computation

List of Abbreviations

2D	Two Dimensional
3D	Three Dimensional
2D2D	2D Equalization with 2D Optimized GPR Target
ABP	Adaptive Belief-Propagation
ABS	Air Bearing Surface
ASD	Algebraic Soft-Decision
AWGN	Additive White Gaussian Noise
BCJR	Bahl-Cocke-Jelinek-Raviv
BER	Bit Error Rate
BIID	Binary-Input-Inner-Decoder
BLER	Block Error Rate
BP	Belief-Propagation
BPMR	Bit-Patterned Media Recording
BPSK	Binary Phase-Shift Keying
BSC	Binary Symmetric Channel
DIDS	Data-Dependent Insertion, Deletion and Substitution
DM	Davey-MacKay
EAMR	Energy-Assisted Magnetic Recording
E-Beam	Electron Beam

Abbreviations

ECC	Error Correction Code
EXIT	Extrinsic Information Transfer
FER	Frame Error Rate
FFT	Fast Fourier Transform
GB	Gigabyte
GF	Galois Field
GMR	Giant Magneto-Resistive
GPR	Generalized Partial-Response
HAMR	Heat-Assisted Magnetic Recording
HDD	Hard Disk Drive
HMM	Hidden Markov Model
i.i.d	independent and identically distributed
i.u.d	independent and uniformly distributed
ID	Insertion and Deletion
IDS	Insertion, Deletion and Substitution
IIDS	Independent Insertion, Deletion and Substitution
IPR	Integer Partial-Response
ISI	Intersymbol Interference
ITI	Inter-Track Interference
JDD	Joint Detection-Inner-Decoder
JE	Joint-Track Equalization
KV	Koetter and Vardy
LDPC	Low-Density Parity-Check
LLR	Log-Likelihood Ratio
LMR	longitudinal Magnetic Recording
LUT	Look-Up Table

Abbreviations

M-2D2D	MTD with 2D2D Equalization
MAMR	Microwave-Assisted Magnetic Recording
MDS	Maximum Distance Separable
M-JE	MTD with Joint-Track Equalization
ML	Maximum Likelihood
MR	Magneto-Resistive
MTD	Multi-Track Detection
PDF	Probability Density Function
PDNP	Pattern-Dependent Noise Predication
PEG	Progressive Edge-Growth
PMR	Perpendicular Magnetic Recording
PR	Partial-Response
PRML	Partial-Response Maximum Likelihood
RS	Reed-Solomon
SaE	Stationary and Ergodic
SCSW	Sliding Channel State Window
SE	Single-Track Equalization
SFD	Switch Filed Distribution
SIID	Soft-Input-Inner-Decoder
SIR	Symmetric Information Rate
SMR	Shingled Magnetic recording
SNR	Signal-to-Noise Ratio
SUL	Soft Underlayer
Tb	Terabit
TB	Terabyte
TDMR	Two-Dimensional Magnetic Recording

Abbreviations

TMR	Track Mis-Registration
WIE	Written-In Errors

Chapter 1

Introduction

After entering the information age, the demand for high-capacity digital storage systems has exponentially increased. To this end, various information storage techniques have been developed and/or improved to meet the increasing demand. Magnetic hard disk drive (HDD) has been the primary storage device since it was invented by IBM in 1956. In the past decades, HDD has enjoyed a tremendous growth in storage capacity as well as a continuous reduction in cost, which give HDD a great advantage over other contenders that appeared even later than HDD, for instances, solid state drive, optical recording, etc. With the rapid growth of social media network, cloud computing and storage, high-definition audio and video streaming, etc, the HDD industry has to keep increasing storage capacity and reducing the price per gigabyte (GB) to satisfy the ever-increasing storage demand as well as maintain its predominance in the data storage market [1]. The most effective way is to increase the data storage areal density, which is measured by the number of bits recorded per square inch. The areal density growth rate has served as the technology growth rate indicator for the HDD industry.

Recall that the areal density of the first commercial HDD manufactured by IBM was merely 2 Kb/inch². For almost fifty years of extensive research and investment, the conventional longitudinal magnetic recording (LMR) technique enjoyed an annual

1. Introduction

30% ~ 100% increase in areal density till it reached its limit at around 150 Gb/inch². The areal density in LMR is mainly increased by scaling down the grain size while maintaining a certain number of grains per bit to achieve sufficient signal-to-noise ratio (SNR). However, the superparamagnetic effect imposes a fundamental constraint on the minimum grain size, below which either the ambient temperature will be sufficient to cause the magnetization of the grain to reverse spontaneously in a short time or the write head itself will not be able to generate a strong enough write field to reverse the magnetization of each grain [2, 3]. This phenomenon is also known as *media trilemma* for it actually describes trade-offs between three physical limitations of the media: the SNR, the thermal stability and the writability.

To keep increasing areal density, perpendicular magnetic recording (PMR) was developed and first commercially implemented by Toshiba in 2005. The two magnetic recording mechanisms are illustrated in Fig. 1.1, from which we observe that the main difference between LMR and PMR is the orientation of the anisotropy of media grains. As shown in Fig. 1.1(b), the magnetic soft underlayer (SUL) underneath the recording layer conducts magnetic flux very readily thus efficiently strengthens the write field penetrating recording layer and field gradient. A stronger write field permits the use of a medium with higher coercivity, which can maintain thermal stability with minimum grain size smaller than that of LMR. Therefore, PMR promised to deliver at least three times the areal density of conventional LMR and bring many additional technical advantages, such as stronger readback signal, thicker recording layer, etc [4–6].

However, the areal density in PMR is still mainly increased by scaling down the grain size, which means the areal density growth will still be ultimately limited by the superparamagnetic effect. It has been reported in [7, 8] that the areal density limit for PMR is around 1 Tb/inch². In 2014, Seagate started to ship its 6 Terabyte (TB) enterprise HDDs with areal density of 643 Gigabit/inch², which is already more than half of the areal density limit predicted for PMR. Recently, shingled magnetic record-

1. Introduction

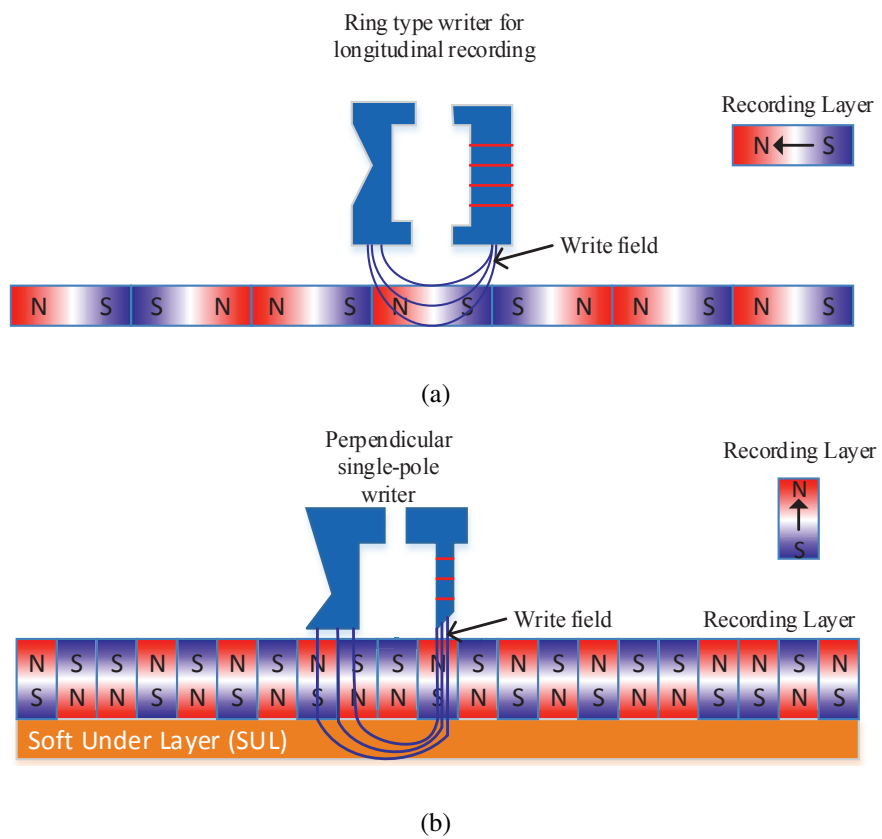


Figure 1.1: (a) longitudinal magnetic recording; (b) perpendicular magnetic recording.

1. Introduction

ing (SMR) and two-dimensional magnetic recording (TDMR) have been proposed and developed to boost the areal density towards or even beyond 2 Tb/inch² with the conventional PMR system [9–11].

SMR utilizes a wide write head to ensure the writability of a medium with high coercivity. In SMR, each written track will be partially overwritten by its adjacent track that is written sequentially, which resembles the way roof shingles are applied. The overlap effectively reduces track pitch and thus increases the areal density. The guard bands that separate adjacent tracks in PMR and LMR are eliminated in SMR, which requires the read head to be narrower than the track pitch to reduce influence from adjacent tracks during the readback process. On the other hand, TDMR strikes the trilemma from the SNR and signal processing perspective. It employs an array reader or a single reader to read multiple adjacent tracks, and then applies powerful 2D signal processing and 2D coding techniques to process the 2D readback waveform to compensate for the reduction in SNR and take advantage of the inter-track interference (ITI) resulting from placing adjacent tracks close to each other, which is typically avoided in the conventional magnetic recording. Obviously, the combination of SMR and TDMR can further increase the areal density, since it allows the use of a medium with good coercivity while alleviating the need for a read head narrower than the track pitch.

To further delay the onset of the superparamagnetic effect and achieve even higher areal density, intensive research has been conducted on two major candidates for next-generation magnetic recording techniques: bit-patterned media recording (BPMR) and energy-assisted magnetic recording (EAMR) [12–14]. Both technologies have the potential to achieve areal densities up to 10 Tb/inch², but require significant changes in the media and head designs.

EAMR ensures the thermal stability of each grain at ultra-high areal density by using media with high coercivity, and utilizing an additional energy source to momentar-

1.1 Bit-Patterned Media Recoding

ily reduce the coercivity of the media during the writing process. Based on the energy source employed, EAMR can be divided into two categories: heat-assisted magnetic recording (HAMR) using laser as the energy source [15] and microwave-assisted magnetic recording (MAMR) that applies a high frequency magnetic field during the write process [16].

Compared to the other three candidates, BPMR is a more advanced technology for it fundamentally changes the recording physics of conventional continuous recording. In BPMR, bits are recorded on a lithographic pre-patterned media where each single domain magnetic island is surrounded by non-magnetic material and stores one bit only. The radically redesigned BPMR introduces novel engineering challenges that cannot be well handled by existing techniques developed for conventional magnetic recording. In this thesis, some of these challenges are investigated and addressed from the signal processing and coding perspective.

In the remainder of this chapter, a brief review of BPMR along with its advantages over the conventional continuous magnetic recording will be given. Further, main challenges in BPMR implementation will be discussed with an emphasis placed on the ones that are relevant to signal processing. Thereafter, the motivations and contributions of this thesis are given. At the end of this chapter, the organization of this dissertation is presented.

1.1 Bit-Patterned Media Recoding

In Fig. 1.2, the recording mechanism of BPMR is illustrated. Compared to the conventional continuous magnetic recording schemes shown in Fig. 1.1, the major difference is that the information bits are stored on discretely distributed magnetic islands which are fabricated by masking the strongly exchange coupled medium surface with non-magnetic material using nano-lithography [17–19]. By using medium material with

1.1 Bit-Patterned Media Recording

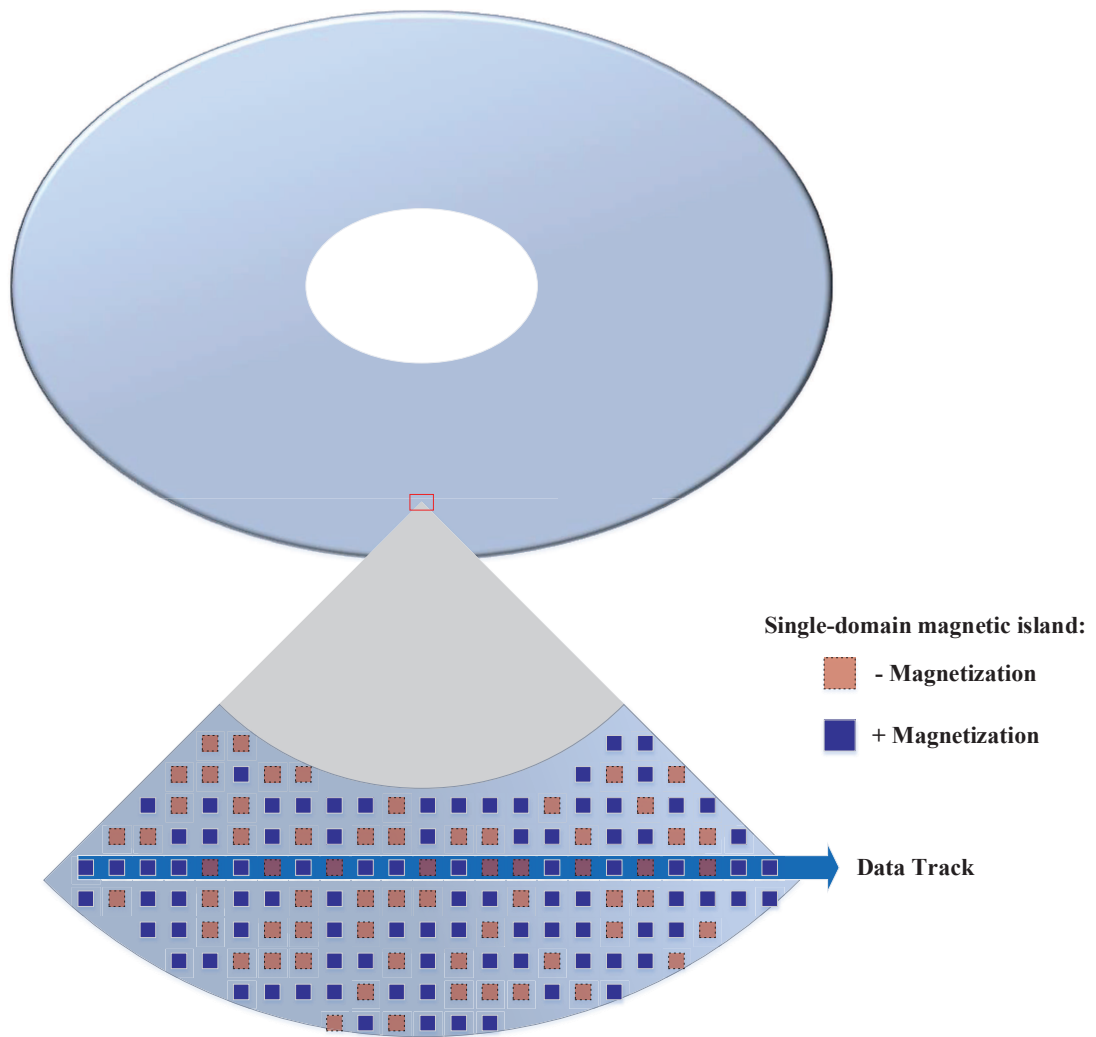


Figure 1.2: Bit-patterned media recording.

strong exchange coupling, the thermal stability is now proportional to the island volume instead of grain size. Therefore, the use of small grains is no longer a concern for BPMR and the onset of the superparamagnetic limit is significantly delayed. Further, the restrictions on the recording head and media material are also relaxed compared to EAMR.

In BPMR, the nonmagnetic barrier between magnetic islands effectively reduces or even eliminates transition noise [20], which is a dominant data-dependent me-

1.1 Bit-Patterned Media Recoding

dia noise in conventional continuous magnetic recording [2]. Similarly, track edge noise [21] that degrades the performance of conventional magnetic recording systems especially at high areal densities is also eliminated. Thanks to the elimination of non-linear transition noise, the SNR in BPMR is no longer determined by the number of grains per bit. Hence, it is possible that each magnetic island contains only one grain in the extreme case. In addition, the non-linear bit shift and side writing found in conventional magnetic recording are also eliminated as bit positions in BPMR are predetermined [22]. Further, the tracking problem, which becomes more and more difficult in magnetic recording systems with increasing areal density and decreasing track pitch, is simplified while the error signal for the tracking system improves due to the patterned media [20].

1.1.1 Fabrication Imperfections of BPMR

Despite the attractive advantages promised by BPMR, the implementation of BPMR raises an enormous amount of technical challenges. Although the write and read head design, servo and signal processing systems in BPMR can more or less inherit the corresponding relatively mature techniques utilized in current continuous magnetic recording systems, fabricating patterned media requires a radical paradigm shift in the current HDD industry. On the bright side, the mature nano-lithographic tools and technology developed by the semiconductor industry can be utilized to fabricate the patterned media [13]. Cutting-edge semiconductor techniques can achieve an areal density around 2.5 Tb/inch², however; they cannot keep up with the areal density evolution envisioned for BPMR [13, 23].

To date, feasible mass production method envisioned for BPMR utilizes electron beam (e-beam) lithography, self-assembly, and nano-imprint lithography for the creation and replication of patterns [24]. Current challenges and promising solutions for

1.1 Bit-Patterned Media Recoding

BPMR fabrication have been discussed in details in [23].

In general, the fabrication of BPMR requires high resolution, high placement accuracy and high throughput at relatively low cost. However, it is impossible to effectively fabricate perfect and uniform patterned media with ultra-high areal densities over a large area. Consequently, the imperfection leads to geometrical variation in patterned islands which is generally assumed to be Gaussian in nature and can be classified mainly into two categories: bit size variation and bit position variation [25]. In addition, the fabrication imperfection also introduces bit shape variation and thickness variations [13]. Those variations essentially contribute to the media noise of BPMR that degrades the replay waveform and reduces the SNR. Furthermore, these variations also induce a broad switch field distribution (SFD), which has a significant impact on recording performance. Another major disadvantage originating from the physical nature of BPMR is the roughness of the surface after patterning, which complicates the head disc interface design and may necessitate a dynamic air bearing system to maintain stability of the fly height of the write/read head over each island [26, 27].

1.1.2 Challenges of Signal Processing for BPMR

Because of the discrete data storage structure of BPMR, near-perfect synchronization between the clock that times the writing of bits and the island period is required to ensure that the effective write window is positioned over the correct island. Although the correct island position may be located during the read process, it is impractical to write and read simultaneously. Therefore, write synchronization is one of the most critical and major challenges in BPMR, which is however not a concern for continuous magnetic recording where bit positions are determined by the write field [12, 22, 28, 29].

Due to unpredictable mechanical disturbances, variation in spindle motor speed, geometrical variation, etc., it is only feasible to maintain write synchronization in a

1.1 Bit-Patterned Media Recoding

statistical sense in a practical BPMR system and the unavoidable mis-synchronization may result in random insertions and deletions of bits. In addition, even with perfect write synchronization, random substitution write errors occur when magnetic islands cannot be correctly written due to variations in media SFD and/or demagnetization field from adjacent islands. Since those errors occur during the write process, they are generally referred to as written-in errors (WIEs).

Fig. 1.3 illustrates the write process with WIEs in practical BPMR systems, where influence of the magnetic write field along the down-track direction typically spans multiple islands [30]. As shown in Fig. 1.3, when a bit is written on the media, the write field of the currently recorded bit affects a number of subsequent islands which will eventually be overwritten by the following bits. As shown in Fig. 1.3, an insertion occurs when an island is skipped without being written while a deletion occurs when an island is overwritten by the following bit. In addition, the inserted bit is typically the same as the last recorded bit, which implies that the write channel has memory and WIEs are data-dependent. The data-dependencies of the BPMR write process will be discussed in detail in Chapter 3.

The causes for WIEs as well the corresponding error rates have been investigated and analyzed in [12], where all variations are assumed to be Gaussian. In addition, a lot of research effort has been expended in statistically characterizing the error rates for WIEs, e.g., [31–34]. WIEs have been widely recognized as one dominant factor that limits the overall system performance of BPMR [12]. As pointed out in [29], the implementation of accurate timing estimate techniques as well as the reduction in mechanical and motor jitter can effectively reduce WIEs.

WIEs also pose challenges to the error correction coding techniques developed for and employed in current HDDs, which is mainly due to the timing errors, i.e., insertions and deletions. Timing errors if not well compensated will lead to a burst of substitution errors, which may be too long to be successfully handled even by the most

1.1 Bit-Patterned Media Recoding

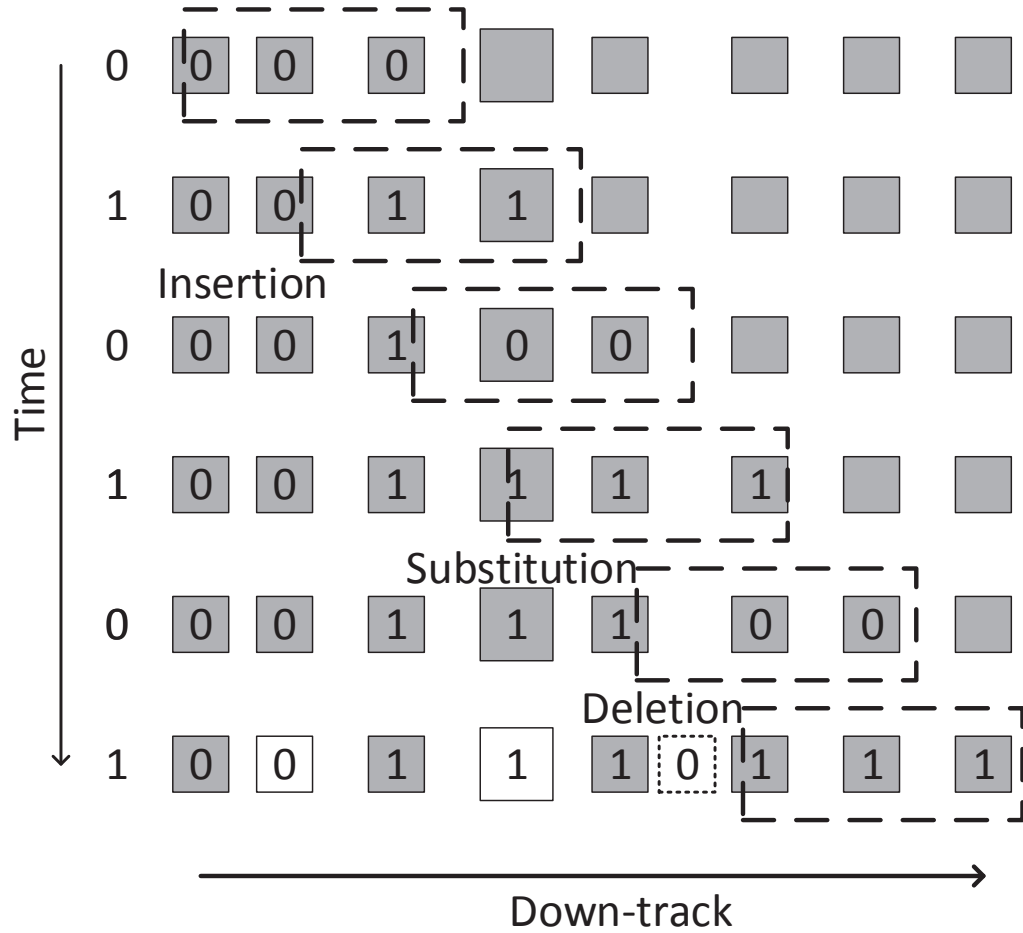


Figure 1.3: Illustration of written-in errors in the recording process of BPMR systems. The gray squares are the magnetic pattern island and the number in the square represents the bit recorded, the writing head with writing span larger than one island is represented using a dashed rectangle. The sequence of bits to be recorded, i.e., 010101, are shown on the left side of the figure along the time axis. The written-in errors are indicated in the figure using white square and the deleted bit is denoted by a dashed white square.

1.1 Bit-Patterned Media Recoding

powerful error correction codes (ECCs) that are currently available, e.g., low-density parity-check (LDPC) codes and Turbo codes.

Due in part to the development of BPMR, channels with insertion, deletion and substitution (IDS) errors have recently received increased attention and a variety of coding schemes have been developed or improved to combat IDS errors. In [35], the achievable information rates for channels with insertions, deletions, substitutions, additive white Gaussian noise (AWGN) and inter-symbol interference (ISI) are investigated. In [36], upper and lower bounds of channels with independent and identically distributed insertion, deletion and substitution errors are presented. To handle WIEs, a picket-shift coding scheme involving a double-error correction Reed-Solomon (RS) code to encode the row data and a much stronger RS code to encode the column data has been proposed in [37], which shows significant performance improvement when applied in BPMR with WIEs. Marker codes, where a known sequence of bits is inserted periodically to offer synchronization correction capability, have also been widely investigated for BPMR [38, 39].

In the readback process, one major challenge would be the mitigation of the 2D interference among adjacent bits, i.e., ISI and ITI [40], which will significantly degrade overall system performance if not well compensated. In conventional magnetic recording, adjacent tracks are placed far from each other to avoid interference from adjacent tracks. However, magnetic islands in BPMR are placed close to each other in both the along-track and across-track directions to achieve ultra-high areal densities. Consequently, ITI arises as a new performance limiting factor in BPMR in addition to the ever-increasing ISI.

Conventional magnetic recording systems have relied heavily on partial-response maximum likelihood (PRML) channel detection to deal with ISI [41–43]. This channel detection scheme consists of two parts: partial-response (PR) equalization and maximum-likelihood (ML) detection, which are jointly designed. This detection scheme

1.1 Bit-Patterned Media Recoding

has also been extended to mitigate the 2D interference by equalizing the channel to 2D PR targets and employing a reduced-complexity ML detector [44, 45]. It was shown in [46] that the optimized generalized partial-response (GPR) target of [47] significantly outperforms integer partial-response (IPR) targets when employed in BPMR. Subsequently, [48] proposed to use two-dimensional (2D) GPR targets to mitigate ITI in BPMR. Furthermore, the multi-track detection (MTD) scheme of [49] that utilizes a 2D GPR target has also been proposed to mitigate ITI in BPMR. This scheme uses a 2D or 1D equalizer to equalize the read channel readback sequence to a 2D GPR target. Notably, it can approach the performance bound obtained when data on sidetracks are known. In BPMR, bit islands can be distributed on a rectangular array (rectangular BPMR) or hexagonal array (staggered BPMR) depending on the lithographic technique employed in the fabrication process [50]. Simulations in [50] show that staggered BPMR improves performance compared to rectangular BPMR at the same areal density. Further, switching from rectangular to staggered BPMR can effectively reduce ITI as the bits in the neighboring tracks do not align with the bits in the center track [51].

Another big signal processing challenge for BPMR is the presence of the aforementioned media noise due to imperfect fabrication. It has been reported in [46] that the read channel is very sensitive to the presence of media noise. Further, the presence of media noise exacerbates the difficulty of write synchronization and 2D interference mitigation. The modeling of media noise in BPMR readback process has been considered in [52, 53]. In [52], the study on the influence of media noise on the readback process reveals that the readback performance is more sensitive to size fluctuation than location fluctuation, while both fluctuations should be smaller than 8% to achieve a bit error rate (BER) around 10^{-4} at an areal density of 1.5 Tb/inch². In [53], an analytical approach has been proposed to jointly design a 2D equalizer and a 1D GPR target to combat media noise. In [54], a 1D equalizer and a 1D GPR target were jointly designed

1.2 Motivations and Contributions

to mitigate the 2D interference, media noise and AWGN in staggered BPMR channel with an areal density of 4 Tb/inch². Further, as media noise is data-dependent, the pattern-dependent noise prediction (PDNP) scheme, which considers data patterns in the computation of branch metrics in the ML detection, has been proposed to improve the performance of PRML detection in media noise dominant channels [55].

1.2 Motivations and Contributions

In summary, many technical challenges are still to be overcome before the mass production of BPMR HDDs. Two major challenges of BPMR from the perspective of signal processing are the presence of WIEs in the write process and the 2D interference influencing the readback performance. Therefore, we investigate both challenges in this thesis and propose coding and detection schemes to effectively address them.

1.2.1 Davey-MacKay Construction with RS Codes as Outer Codes

As mentioned in Section 1.1.2, the presence of WIEs dominates the overall performance and cannot be corrected by conventional coding schemes due to synchronization drifts (the difference between the position of a bit being actually recorded and the position it is intended to be recorded) introduced by insertion and deletion errors. Notably, a comprehensive survey of ECCs for channels corrupted by IDS errors has been presented in [56]. It has been identified in [56] that the most promising ECCs for IDS channels are those having a concatenated structure, where an inner code is used to regain synchronization and an outer code corrects additive noise and imperfect resynchronization by the inner code. The Davey-MacKay (DM) coding scheme developed in [57] for independent IDS (IIDS) channels that introduce independent insertion, deletion and substitution errors, is of this type.

1.2 Motivations and Contributions

In the original DM coding scheme, non-binary LDPC codes are used as outer codes. However, LDPC codes do not always guarantee the best performance. For an example, it has been shown in [58] that low-rate turbo codes provide better frame-error-rate (FER) performance on poor channels. In view of this observation and further inspired by the fact that RS codes are still been considered for future magnetic recording and powerful iterative soft-decision RS decoding schemes are available, we propose the use of RS codes as outer codes in the DM construction and investigate the performance improvements RS codes as outer codes can bring. Our *contributions* resulting from the investigation of using RS codes as outer codes in the DM construction are as follows.

We first show that for a fixed inner code rate, increasing the order of Galois field q of the outer non-binary code has the potential to improve the overall performance of the DM coding scheme. The largest q of practical interest for non-binary LDPC codes is 16 [59] while 128-ary and 256-ary RS codes are widely used in practice. Hence, we compare the performance of the DM coding scheme with q^2 -ary $(q^2 - 1, (q^2 - 1)R)$ RS code and q -ary $(2(q^2 - 1), 2(q^2 - 1)R)$ LDPC code as the outer code and show that the DM coding scheme with the former RS code as the outer code improves the FER performance for moderate to high-rate applications involving relatively short blocklengths.

1.2.2 Improved Write Channel Model with Data-Dependent IDS Errors

To investigate and address WIEs, many write channel models have been proposed to model the BPMR write process, such as the binary symmetric channel (BSC) when insertion and deletion errors are assumed to be very rare [60, 61], the channel model of [39] which consists of a subchannel introducing i.i.d insertion and deletion errors

1.2 Motivations and Contributions

followed by an AWGN subchannel, and the channel model of [37] which introduces insertion/deletion errors controlled by a uniformly distributed random variable denoting the frequency offset between the ideal write frequency and the actual frequency. In those channel models, insertion and deletion WIEs were either assumed to be sufficiently rare to be ignored or occur independently. A probabilistic write channel model driven by a binary channel state process has been proposed to capture some of the data-dependence characteristics of the WIEs in [30]. This channel model employs either a Bernoulli or first order binary Markov process to produce errors resembling substitution errors or paired insertion-deletion errors with the inserted bit being the same as the last written bit. The phenomenon that insertions and deletions occur in pairs with almost equal probabilities has been reported in [62]. However, the aforementioned channel models have their limits in capturing some of the characteristics of WIEs. Therefore, we develop a new channel model to better mimic the actual BPMR write process in this thesis and our corresponding *contributions* are summarized as follows.

First, a data-dependent IDS (DIDS) write channel model is proposed to mimic the BPMR write process, which is a concatenation of a ternary Markov state channel and a two-state BSC. The former augments the binary Markov state channel model of [30] by introducing a new channel state such that deletion-insertion pairs can occur in addition to insertion-deletion pairs. The latter models random substitution errors owing to write failures and dead islands that have an effective switching field exceeding the maximum applied write field. It also produces burst-like substitution errors in the immediate neighborhood of an insertion or deletion error, which are mainly due to relatively large phase offsets between the write field and the islands preceding and following each insertion/deletion error [37].

Secondly, the DM coding scheme proposed for IIDS channel is applied to the DIDS channel with a modified inner decoding algorithm that takes all data-dependencies into account. As the computational complexity of the inner decoder increases expo-

1.2 Motivations and Contributions

nentially in the length of burst substitution errors in the immediate neighborhood of an insertion or deletion error, a reduced-complexity variant of the modified inner decoding algorithm is also proposed and investigated.

1.2.3 Detection-Decoding on Rectangular and Staggered BPMR Channels with WIE Correction and ITI Mitigation

In general, a complete BPMR channel can be modeled as a concatenation of two independent sub-channels – a noisy write channel followed by a PR read channel with ITI.

The BPMR read channel is characterized by the 2D replay pulse response of an isolated bit island, which depends on the medium design and read head configuration. In [52], the 2D pulse response is obtained numerically using 3D reciprocity while assuming a magneto-resistive (MR) read head. It has been further noted in [63] that the 2D replay response can be well fitted by a 2D Gaussian pulse in both the along-track and across-track directions. The 2D Gaussian pulse is thus used to represent the channel response in [49], where single-track equalization (SE), joint-track equalization (JE), multi-track detection (MTD) and 2D equalization are investigated for read channel detection.

Since there will still be errors in the detector output, including substitution errors from imperfect read channel detection and WIEs, coding schemes and corresponding detection-decoding strategies are needed to be developed to ensure that the data written to the BPMR system can be reliably recovered. Therefore, various detection-decoding schemes will be proposed and investigated in this thesis for data-recovery on the BPMR channel model consisting of a DIDS write channel model and a rectangular or staggered BPMR read channel model with 2D interference. Our main *contributions* in detection and decoding on rectangular and staggered BPMR channels with WIE

1.2 Motivations and Contributions

correction and ITI mitigation are summarized as follows.

First of all, we start with a rectangular BPMR write-read channel model and propose three detection-inner-decoding schemes to work with an outer decoder to recover the data encoded by the DM coding scheme on the channel, namely the BCJR-binary-input-inner-decoder (BCJR-BIID) algorithm, the joint detection-inner-decoder (JDD) algorithm and the BCJR-soft-input-inner-decoder (BCJR-SIID) algorithm. The performance of these three detection-decoding schemes employing different read channel detection schemes are investigated and compared. We observe that BCJR-BIID and BCJR-SIID achieve good performance-complexity trade-offs, while JDD yields the optimal performance at the expense of relatively high computation complexity. Further, we consider the performance degradation due to an increase in the areal density and code rate, and investigate the performance degradation due to burst-like substitution errors around each insertion/deletion error.

Furthermore, as the DIDS write channel does not depend on the specific distribution of islands on the media, we investigate the data recovery problem for staggered BPMR where the write process is still modeled by the DIDS channel. The read channels corresponding to two possible staggered BPMR systems, i.e., single-track staggered BPMR and double-track staggered BPMR as investigated in [51], are adopted. The read channel performance of rectangular BPMR, single-track staggered BPMR and double-track staggered BPMR are compared at an areal density of 6 Tb/inch². Our study reveals that single-track staggered BPMR read channel with extended MTD [51] exhibits the best performance among all the detection schemes and island distributions that we consider at such a high areal density. Therefore, the BCJR-BIID and BCJR-SIID are employed to work with the extended MTD to recover the data encoded by the DM coding scheme on the single-track staggered BPMR channel. The performance of BCJR-BIID and BCJR-SIID are compared and analyzed, which reveals that BCJR-SIID provides significantly better robustness against burst errors compared to

BCJR-BIID at sufficiently low insertion/deletion probabilities (e.g., $\leq 3 \times 10^{-3}$).

1.3 Organization of the Thesis

The remainder of the thesis is organized as follows.

In Chapter 2, we will first give a short review of the IIDS channel. Then, the encoding and decoding algorithms for the DM coding scheme, LDPC codes and RS codes will be reviewed. Further, we will investigate and compare the performance of the DM coding scheme with LDPC and RS codes as the outer code on the IIDS channel.

In Chapter 3, analysis and explanation concerning the data-dependent characteristics of WIEs as well as corresponding evidence reported in experiments and simulations will be discussed first. Based on the discussion, the DIDS write channel model is then proposed. Further, a modified DM inner decoder that takes into account all those data-dependencies is developed to make the DM coding scheme applicable to the DIDS channel. To complete the investigation, the channel capacity bounds of the DIDS channel are also investigated.

In Chapter 4, we consider data-recovery on rectangular BPMR channels consisting of a DIDS write channel followed by a rectangular BPMR read channel with 2D interference. The read channel is modified according to the specific distribution of islands. Three detection-decoding schemes involving different level of interaction between the channel detector and decoder are proposed and their performance compared and analyzed.

In Chapter 5, we investigate data-recovery on staggered BPMR channels consisting of a DIDS write channel followed by a staggered BPMR read channel with areal density increased to 6 Tb/inch². The performance of MTD on staggered and rectangular BPMR read channels are first compared and analyzed. Then, detection-decoding

1.3 Organization of the Thesis

schemes developed in Chapter 4 are employed on the staggered BPMR channel to correct data-dependent WIEs and mitigate 2D interference.

Finally, Chapter 6 concludes this thesis and discusses future work.

Chapter 2

On Reed-Solomon Codes as Outer Codes in the Davey-MacKay Construction for Channels with Insertions and Deletions

Insertion and deletion WIEs in the BPMR channel have recently motivated many research works on the development and investigation of ECCs for channels with timing errors. Synchronization is a critical requirement for any communication and recording systems, however, the majority of ECCs merely focus on the correction of substitution errors while assuming perfect synchronization maintained by other techniques. Insertion and deletion errors can make the boundaries of codewords hard to identify and induce bursts of substitution errors that can be too long to be successfully handled even by capacity-approaching ECCs, such as LDPC codes, turbo codes.

Since it has been widely conjectured that overall system performance could be improved with ECCs that are capable of correcting synchronization errors [56], a number

2.1 IIDS Channel Model

of ECCs have been developed for channels corrupted by synchronization errors over the past decades. However, most of them have quite limited synchronization error correction capability or were designed for a specific IDS channel having certain restrictions or unrealistic assumptions. According to [56], concatenated coding schemes where an inner code recovers synchronization and an outer code corrects residual substitution errors are the most promising ECCs for IDS channels. One prominent coding scheme falling under this category is the DM coding scheme.

Originally, nonbinary LDPC codes are employed as outer codes in the DM construction. Although LDPC codes are recognized as capacity-approaching codes, the use of turbo codes as outer codes result in better FER performance on poor channels [58]. Inspired by the fact that RS codes are still considered for future BPMR systems [37, 64] and powerful iterative soft-decision RS decoding schemes are available in the literature, we investigate the performance improvements RS codes as outer codes could bring in this chapter.

In this chapter, we will first review the IIDS channel which has been widely used for the development and evaluation of ECCs with synchronization error correction capability. Further, a brief review of the DM coding scheme and its bit-level and symbol-level DM inner decoding algorithms will be given. LDPC codes and RS codes with their iterative soft-decision decoding schemes will also be reviewed. Then, we will analyze and show the advantages of using RS codes as outer codes in the DM coding scheme.

2.1 IIDS Channel Model

The IIDS channel is a probabilistic binary channel model which was initially proposed in [65]. This channel has been widely considered as the channel model on which various of synchronization ECCs have been developed and investigated, e.g.,

2.1 IIDS Channel Model

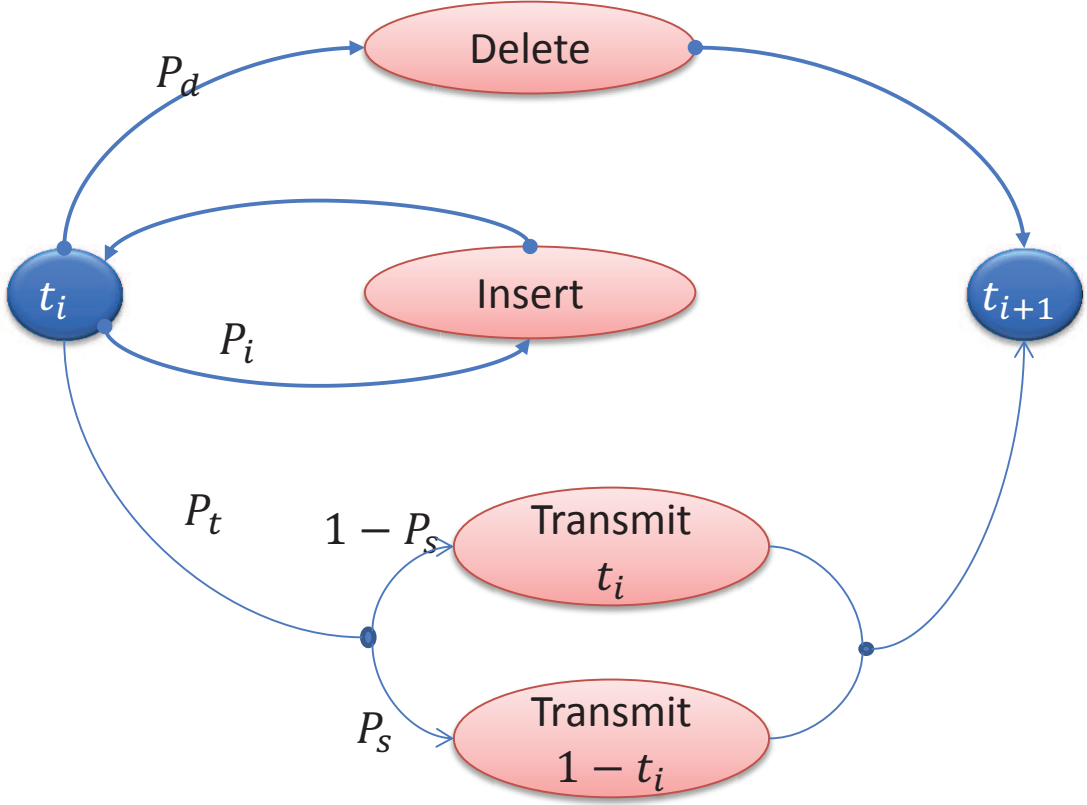


Figure 2.1: State diagram of the IIDS channel model with insertion, deletion and substitution probabilities.

[38, 57, 66, 67]. This channel model and its variant where the substitution errors are generated by an AWGN channel have also been used to model the BPMR write process producing WIEs in [39] and [68], respectively. Although it has been stated in Chapter 1 that BPMR write channel actually introduces dependent IDS errors, we use the IIDS channel as a first approximation to the BPMR write channel. A more realistic BPMR write channel model that captures data-dependent characteristics of WIEs will be developed and investigated later in Chapter 3.

The state diagram of the IIDS channel is illustrated in Fig. 2.1, where P_i , P_d and P_s control the rates of insertions, deletions and substitutions, respectively. Imagine that at time i , a bit t_i is ready to enter the channel, one of the following three events

2.2 DM Coding Scheme

can occur:

- a random bit is inserted with probability P_i while t_i remaining untransmitted;
- t_i is deleted with probability P_d ;
- t_i is transmitted with probability $P_t = 1 - P_i - P_d$, but it may be suffering a substitution error with probability P_s during the transmission.

Consequently, the probability of successfully transmitting bit t_i at time i is $(1 - P_i - P_d)(1 - P_s)$.

2.2 DM Coding Scheme

The DM coding scheme was initially proposed by Davey and MacKay for the IIDS channel in [57]. A block diagram of this coding scheme is presented in Fig. 2.2, where the information is first encoded by a non-binary (N, K) LDPC code constructed over $\text{GF}(q = 2^k)$ and subsequently encoded by the inner watermark code. Therefore, the DM coding scheme is sometimes referred to as watermark codes, e.g., in [69]. However, it should not be confused with the watermarking technique used for encryption.

As shown in Fig. 2.2, each LDPC outer codeword $\mathbf{d} = \{d_i\}_{i=0}^{N-1}$ is converted into a sparse binary string $\mathbf{s} = \{s_i\}_{i=0}^{N-1}$ by mapping each outer code symbol d_i into a binary sparse string $s_i = \{s_{i,j}\}_{j=0}^{n-1}$ of length n , $n > k$, using a look-up table (LUT) of size q . The 2^k sparse strings are those with lowest Hamming weight chosen from in total 2^n binary strings of length n . The density of \mathbf{s} is defined as $f = P(s_{i,j} = 1)$, which is less than 0.5 since sparse strings with lowest Hamming weight are chosen. An example of the LUT is given in Table 2.2 for $k = 3, n = 4$.

Further, the binary sparse string \mathbf{s} is added modulo-2 to a binary watermark string \mathbf{w} of length Nn to generate the ultimate transmitted codeword \mathbf{t} . Thus the overall

2.2 DM Coding Scheme

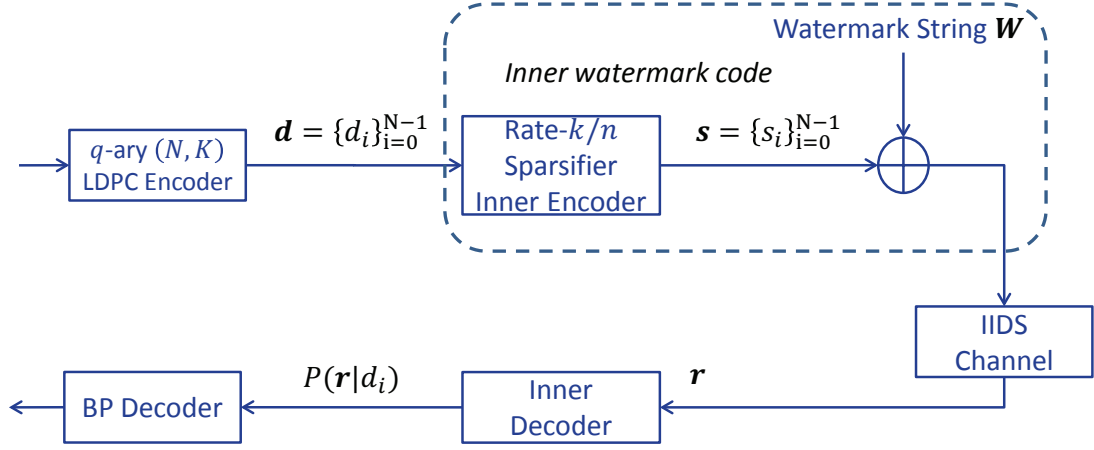


Figure 2.2: Block diagram of the DM coding scheme.

d_i	000	001	010	011	100	101	110	111
s_i	0000	0001	0010	0100	1000	0101	1010	1001

Table 2.1: An example of the mapping LUT employed by the DM sparsifier inner encoder when $k = 3, n = 4$.

2.2 DM Coding Scheme

code rate is $\frac{Kk}{Nn}$. The watermark strings is known to both encoder and decoder and thus provides synchronization capability of the code. It has been reported in [57] that useful choices of \mathbf{w} include random and run-length-limited sequences and it has been further confirmed in [70] the carefully designed watermark strings can significantly improve performance. In this thesis, we nevertheless always use randomly generated watermarking strings, which can be directly replaced by other carefully designed and optimized watermark strings without further modifications being made to the encoding and decoding algorithms.

The basic idea of the DM coding scheme is to use the predefined and fixed watermark string \mathbf{w} as a pilot sequence and ensure on average only $f < 0.5$ of bits in t are different from the corresponding bits in \mathbf{w} by mapping each outer codeword to a sparse string of density f . Then, the inner decoder can identify and locate the synchronization errors by detecting the discontinuity of the watermark pattern in \mathbf{r} [57].

Corresponding to the encoding process, the decoding also consists of two stages. First, the inner decoder corrects synchronization errors and generates log-likelihood ratios (LLRs) for LDPC code symbols. Then, those LLRs are fed to the outer LDPC belief-propagation (BP) decoder to correct the residual substitution errors.

2.2.1 Bit-Level DM Inner Decoding

To facilitate the inner decoding, the received vector is modeled to be produced by a hidden Markov model (HMM) while ignoring the correlations among \mathbf{s} and \mathbf{d} . The hidden states are formed by the synchronization *drift* sequence $\{x_i\}_0^{Nn}$, where x_i represents the number of insertions minus the number of deletions that have occurred before t_i is transmitted.

Based on the HMM model, a trellis representing the IIDS channel can be easily constructed. In Fig. 2.3, an illustration of the trellis with typical state transitions are

2.2 DM Coding Scheme

presented. The total number of states considered in the trellis is limited to $2x_{max} + 1$, where $\pm x_{max}$ is the maximum synchronization drift assumed by the decoder. In addition, the maximum number of consecutive insertions at each time is assumed to be I for computational convenience.

From Fig. 2.3, the *a priori* probability $P(x_{i+1} = b|x_i = a)$ can be computed as

$$P(x_{i+1} = b|x_i = a) = \begin{cases} P_d, & \text{when } b = a - 1 \\ \alpha_I P_i P_d + P_t, & \text{when } b = a \\ \alpha_I ((P_i)^{b-a+1} P_d + (P_i)^{b-a} P_t), & \text{when } a < b < a + I \\ \alpha_I (P_i)^I P_t, & \text{when } b = a + I \\ 0, & \text{otherwise} \end{cases} \quad (2.1)$$

where α_I is a normalizing constant to account for the constraint imposed by I and it is computed by

$$\alpha_I = \frac{\sum_{u=1}^{\infty} P_i^u}{\sum_{u=1}^I P_i^u} = \frac{1}{1 - P_i^I}. \quad (2.2)$$

Then the state transition probability of receiving subsequence $\bar{\mathbf{r}} = \{\mathbf{r}\}_{i+a}^{i+b}$ is computed by

$$P(\bar{\mathbf{r}}, x_{i+1} = b|x_i = a) = P(\bar{\mathbf{r}}|x_i = a, x_{i+1} = b) \cdot P(x_{i+1} = b|x_i = a) \quad (2.3)$$

By defining the effective substitution error probability of receiving a bit which is not equal to the corresponding watermark bit as

$$P_f = P_s(1 - f) + f(1 - P_f), \quad (2.4)$$

the conditional probability $P(\bar{\mathbf{r}}|x_i = a, x_{i+1} = b)$ with respect to the predefined watermark string can be computed by

$$\begin{aligned} & P(\bar{\mathbf{r}}|x_i = a, x_{i+1} = b) \\ = & \frac{1}{P(x_{i+1} = b|x_i = a)} \cdot \begin{cases} \alpha P_d / 2^{b-a+1} + \beta P_t (1 - P_f) / 2^{b-a}, & \text{when } \mathbf{r}_{i+b} = w_i \\ \alpha P_d / 2^{b-a+1} + \beta P_t P_f / 2^{b-a}, & \text{when } \mathbf{r}_{i+b} \neq w_i \end{cases} \end{aligned}$$

2.2 DM Coding Scheme

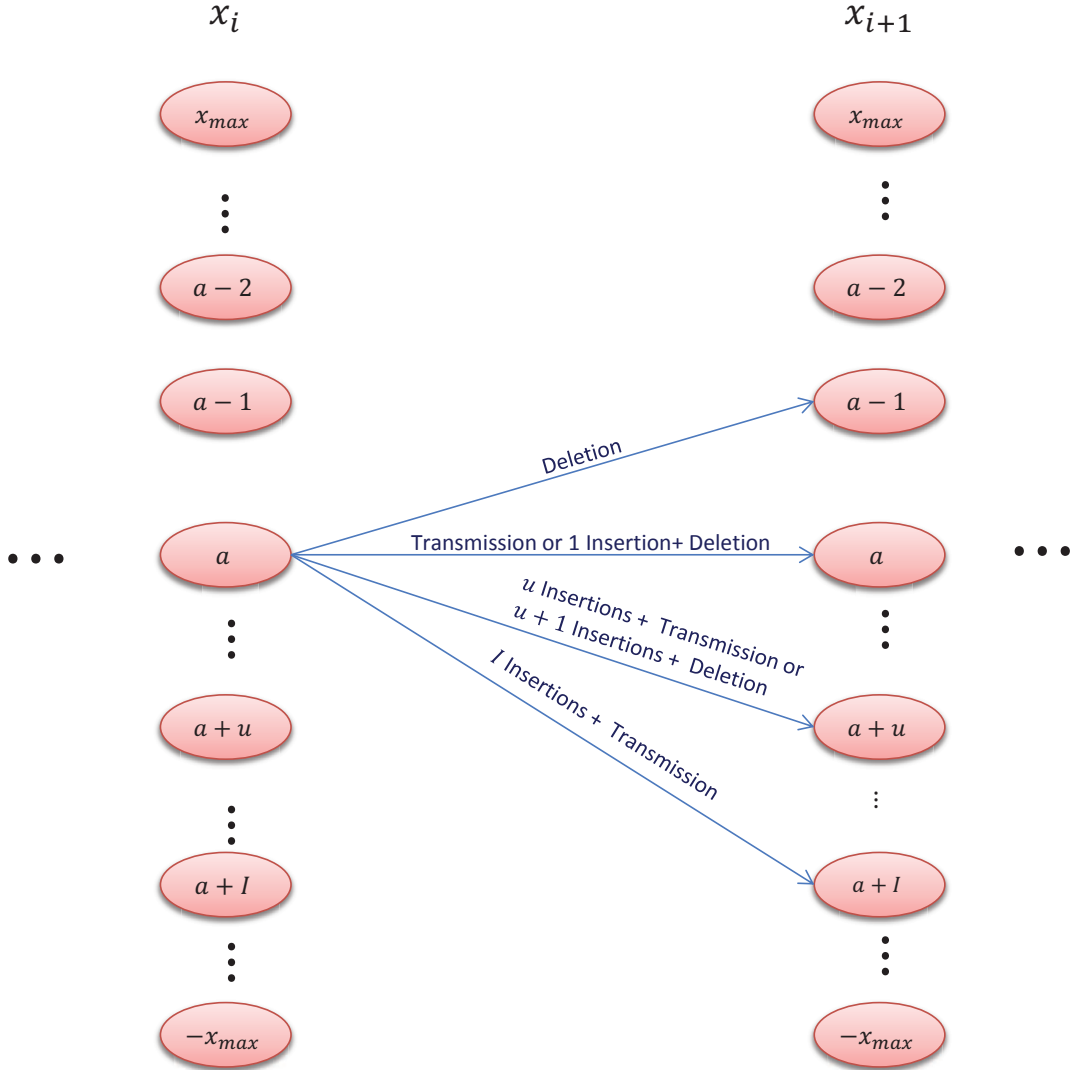


Figure 2.3: Trellis representation of the IIDS channel with channel state x_i .

2.2 DM Coding Scheme

where $\alpha = P_i^{b-a+1}$ and $\beta = P_i^{b-a}$ represent the probability of making $b - a + 1$ and $b - a$ insertions in the channel, respectively. The term $\frac{1}{P(x_{i+1}=b|x_i=a)}$ normalizes the summation $\sum_{\bar{\mathbf{r}}} P(\bar{\mathbf{r}}|x_i = a, x_{i+1} = b)$ to be 1. Finally, (2.3) can be written as

$$P(\bar{\mathbf{r}}, x_{i+1} = b|x_i = a) = \begin{cases} \alpha P_d/2^{b-a+1} + \beta P_t(1 - P_f)/2^{b-a}, & \text{when } \mathbf{r}_{i+b} = w_i \\ \alpha P_d/2^{b-a+1} + \beta P_t P_f/2^{b-a}, & \text{when } \mathbf{r}_{i+b} \neq w_i \end{cases} \quad (2.5)$$

Denoting $(r_a, r_{a+1}, \dots, r_{b-1})$ of \mathbf{r} by $\mathbf{r}|_a^b$, the likelihood $P(\mathbf{r}|d_i)$ can be computed via a forward-backward algorithm on the trellis of $\{x_i\}$ as follows:

$$P(\mathbf{r}|d_i) = \sum_{x_{in}, x_{in+n}} F_{in}(x_{in}) P(\mathbf{r}_{in+x_{in}}^{in+n+x_{in+n}}, x_{in+n}|x_{in}, d_i) B_{in+n}(x_{in+n}) \quad (2.6)$$

where

$$F_j(x_j) = \sum_{x_{j-1}=x_j+1}^{x_j-I} F_{j-1}(x_{j-1}) P(\mathbf{r}_{j-1+x_{j-1}}^{j+x_j}, x_j|x_{j-1}) \quad (2.7)$$

$$B_j(x_j) = \sum_{x_{j+1}=x_j-1}^{x_j+I} B_{j+1}(x_{j+1}) P(\mathbf{r}_{j+x_j}^{j+1+x_{j+1}}, x_{j+1}|x_j) \quad (2.8)$$

are the forward and backward metrics, respectively, and

$$P(\mathbf{r}_{in+x_{in}}^{in+n-1+x_{in+n-1}}, x_{in+n-1}|x_{in}, d_i)$$

can be computed via a forward pass between x_{in} and x_{in+n-1} using (2.3) by fixing s_i according to d_i and replacing w_i and P_f with corresponding t_i and P_s , respectively. Assuming the received sequence has length L_r , the initial values for $F_i(x_i)$ and $B_i(x_i)$ are set to be

$$F_0(x_0) = \begin{cases} 1, & \text{when } x_0 = 0 \\ 0, & \text{otherwise} \end{cases} \quad (2.9)$$

$$B_{Nn}(x_{Nn}) = \begin{cases} 1, & \text{when } x_{Nn} = L_r - Nn \\ 0, & \text{otherwise} \end{cases} \quad (2.10)$$

2.2 DM Coding Scheme

2.2.2 Symbol-Level DM Inner Decoding

Recall, the bit-level inner decoding algorithm developed in [57] ignores the correlations among sparse strings. Therefore, a symbol-level inner decoding algorithm that takes advantage of the underlying correlations has been developed in [71], which significantly improves the overall performance without inducing obvious complexity increase.

The symbol-level DM inner decoder still computes the $P(\mathbf{r}|d_i)$ via (2.6), while the computation for the forward and backward metrics takes into account the correlation introduced by the LUT as follows:

$$F_{in}(x_{in}) = \sum_{x_{(i-1)n}, d_{i-1}} F_{(i-1)n}(x_{(i-1)n})P(d_{i-1})P(\mathbf{r}|_{(i-1)n+x_{(i-1)n}}^{in+x_{in}}, x_{in}|x_{(i-1)n}, d_{i-1}) \quad (2.11)$$

$$B_{in}(x_{in}) = \sum_{x_{(i+1)n}, d_{i+1}} B_{(i+1)n}(x_{(i+1)n})P(d_{i+1})P(\mathbf{r}|_{in+x_{in}}^{(i+1)n+x_{(i+1)n}}, x_{(i+1)n}|x_{in}, d_i) \quad (2.12)$$

where $P(\mathbf{r}|_{(i-1)n+x_{(i-1)n}}^{in+x_{in}}, x_{in}|x_{(i-1)n}, d_{i-1})$ and $P(\mathbf{r}|_{in+x_{in}}^{(i+1)n+x_{(i+1)n}}, x_{(i+1)n}|x_{in}, d_i)$ are computed similarly as $P(\mathbf{r}|_{in+x_{in}}^{in+n+x_{in+n}}, x_{in+n}|x_{in}, d_i)$ in (2.6).

Further, it has been proved in [72] that

$$P(\mathbf{r}|_{in+x_{in}}^{in+n+x_{in+n}}, x_{in+n} = b|x_{in} = a, d_i) = P(\mathbf{r}|_{in+x_{in}}^{in+n+x_{in+n}}, x_{in+n} = b - a|x_{in} = 0, d_i).$$

Therefore, a LUT based implementation of the symbol-level inner decoding algorithm has been proposed in [72], which computes and stores the probability

$$P(\mathbf{r}|_{in+x_{in}}^{in+n+x_{in+n}}, x_{in+n} = b - a|x_{in} = 0, d_i)$$

for every possible combination of $\mathbf{r}|_{in+x_{in}}^{in+n+x_{in+n}}$, d_i and $b - a$ in a LUT. A sufficiently large δ is set to limit the size of the LUT to achieve a good performance-complexity trade-off.

2.3 LDPC Codes and BP Decoding

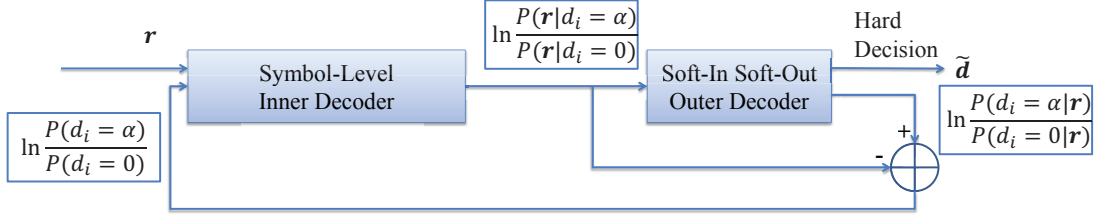


Figure 2.4: Structure of iterative DM decoder

In addition, the *a priori* probabilities $P(d_{i-1})$ and $P(d_{i+1})$ in (2.11-2.12) enable the inner decoder to iteratively admit the extrinsic information from the outer decoder. Therefore, an iterative decoding structure has been proposed in [72], which is illustrated in Fig. 2.4. It has been shown in [72] that the iterative decoding structure with the LUT based symbol-level inner decoding can significantly improve the overall performance while only induces a small increase in the decoding complexity compared to the non-iterative counterparts when insertion/deletion probabilities are small.

2.3 LDPC Codes and BP Decoding

LDPC codes were initially proposed by Gallager in 1962 [73] and were mostly forgotten until their capacity-approaching capability was rediscovered by David MacKay in 1996 [74].

An LDPC code C is simply a linear block code specified by an $M \times N$, $M < N$, parity-check matrix $\mathbf{H} = [h_{i,j}]$ that contains mostly zeros and relatively few non-zero entries. Similar to the conventional linear block codes, the code C is the null space of \mathbf{H} , i.e., $\mathbf{x} = [x_0, x_1, x_2, \dots, x_{N-1}]^T$ is a valid codeword if and only if $\mathbf{H}\mathbf{x} = \mathbf{0}$. Note that the rows in \mathbf{H} are not necessarily to be linearly independent, as a consequence, the dimension of code C is $K = N - L$ where $L \leq M$ is the rank of \mathbf{H} . In [73], Gallager proposed constructing a class of regular pseudorandom LDPC codes by randomly se-

2.4 RS Codes and Iterative Soft-Decision RS Decoding

lecting the positions of the nonzero entries in the parity check matrix. However, this random code design does not guarantee good error performance while most of the good LDPC codes are generated through exhaustive computer search. Further, the density evolution [75, 76] and extrinsic information transfer (EXIT) chart [77, 78] are proposed to aid the construction of good LDPC codes.

With Gallager's iterative BP decoding algorithm that was proposed to efficiently decode LDPC codes on the Tanner graph [79], binary LDPC codes have exhibited excellent performance on a large number of different channels [80]. Although many other LDPC decoding algorithms are available, the BP decoding algorithm is widely recognized as the standard decoder for LDPC codes and usually used as a benchmark against which the decoding performance of other decoding schemes are compared.

Further, binary LDPC codes were generalized to finite field $GF(q = 2^k)$, $k \geq 1$, in [81]. Non-binary LDPC codes with non-binary BP decoder have demonstrated even better performance than binary LDPC codes at the expense of relatively high decoding complexity which is dominated by $O(q^2)$. Fortunately, the decoding complexity for non-binary LDPC codes can be greatly reduced to $O(q \log_2 q)$ [82] by implementing the BP decoder using the fast Fourier transform (FFT) based approach of [75]. Due to its superior error correction performance, both binary and non-binary LDPC codes have been investigated and considered for BPMR channels [61, 83].

2.4 RS Codes and Iterative Soft-Decision RS Decoding

RS codes are powerful cyclic non-binary linear block codes developed by Irving S. Reed and Gustave Solomon in 1960 [84], which have been widely used for error control in both digital communication and data storage systems. Unlike the aforementioned LDPC codes, RS codes are algebraic codes and thus can be conveniently designed to satisfy specific requirements. A detailed review of the construction of RS

2.4 RS Codes and Iterative Soft-Decision RS Decoding

codes can be found in [85].

Although RS codes are slowly replaced by modern ECCs such as Turbo codes and LDPC codes in some systems and standards, maximum distance separable (MDS) RS codes may still be of practical interest for magnetic recording applications since high rate LDPC and turbo codes may encounter error floors at high SNR due to their relatively small minimum distance [86]. In magnetic recording, high code rate, high SNR and extremely low error rate are preferred. Therefore, RS codes may still be considered since they are maximum distance separable codes and so offer the best trade-offs between code rate and minimum distance.

Most of the RS decoding algorithms utilized in practical systems are algebraic hard-decision decoding algorithms with relatively low complexity, e.g., Peterson decoding algorithm [87], Berlekamp-Massey decoding algorithm [85]. However, they cannot make use of the soft channel reliability information, which may cause considerable performance loss in applications where soft-information is available. Further, inspired by the superior performance of Turbo and LDPC codes owing to the use of iterative soft-decision decoding, a lot of research effort has been put into the development of iterative soft RS decoding algorithms.

In the rest of this section, we will review the iterative algebraic soft-decision list decoding algorithm developed in [88] that combines two powerful RS decoding algorithms, i.e., the algebraic soft-decision decoding (ASD) algorithm developed by Koetter and Vardy (KV) [89] and iterative adaptive BP (ABP) RS decoding algorithm [90]. The concatenation of ABP followed by ASD is referred to as hybrid ABP-ASD in [88].

2.4.1 The Hybrid ABP-ASD Decoder

As previously stated, the hybrid ABP-ASD decoding algorithm is a powerful iterative soft-decision RS decoder consisting of the ABP algorithm and ASD algorithm. The

2.4 RS Codes and Iterative Soft-Decision RS Decoding

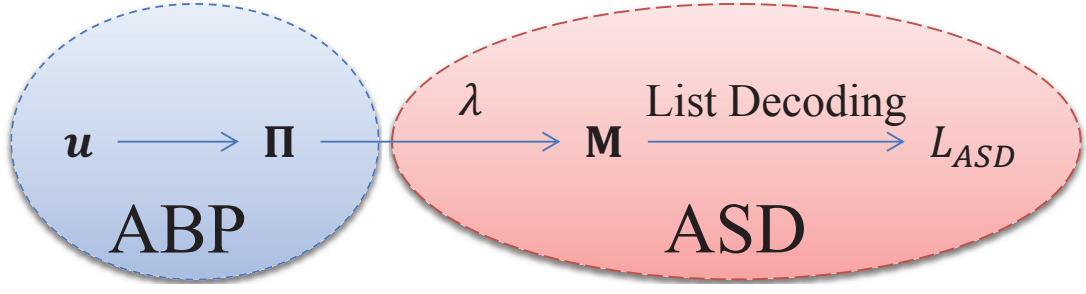


Figure 2.5: Illustration of the hybrid ABP-ASD algorithm.

ABP decoding algorithm is an iterative soft-decision RS decoding algorithm developed based on BP. In this algorithm, BP with a vertical step damping factor θ runs on the dense parity-check matrix of a RS code after reducing all its independent columns, corresponding to the least reliable received bits, to an identity submatrix using Gaussian elimination. The ASD decoding algorithm is developed by adding a multiplicity assignment scheme for the Guruswami-Sudan (GS) list decoding algorithm of [91].

The structure of the hybrid ABP-ASD algorithm is summarized in Fig. 2.5. As we can see from the figure, assuming the code used is a q -ary (N, K) RS code, u represents the log-likelihood ratios (LLRs) of the channel observation which is then processed by the ABP algorithm to generate an enhanced *a posteriori* probability matrix Π . In the ASD decoder, Π is further processed as follows. First, each element of Π will be multiplied by a positive constant λ and the result round down to the nearest integer to generate the multiplicity matrix M . The ASD algorithm then constructs a bivariate polynomial which has qN singularities of order given by M . Finally, by factoring the bivariate polynomial, we will obtain a list \mathcal{L}_{ASD} of codeword estimates.

In the iterative hybrid ABP-ASD decoding, there are two kinds of iterations: outer iterations and inner iterations. The process shown in Fig. 2.5 forms one inner iteration and at the end of the iteration if \mathcal{L}_{ASD} is not empty, the codewords in \mathcal{L}_{ASD} are added to a global list \mathcal{L}_G . Each outer iteration starts with a distinct systematization of the

2.5 Advantages of Using RS Codes as Outer Codes in the DM Construction

RS code's parity-check matrix at the first inner iteration. Assuming that there are N_2 parallel outer iteration, each of which performs N_1 inner iterations, hence the average size of \mathcal{L}_G is at most $N_1 N_2$, since the average size of \mathcal{L}_{ASD} is 1 [92].

In this section, we only provide a brief review of the hybrid ABP-ASD algorithm that is employed as the soft-decision decoder for RS codes in Section 2.5.4. For more details, see [88–90].

2.5 Advantages of Using RS Codes as Outer Codes in the DM Construction

In this section, we investigate the performance improvements RS codes as outer codes could bring when moderate-to-high code rates are considered. First, we analyze the impact of the choice of the size of outer code alphabet $GF(q)$ and the length n of each inner binary sparse string \mathbf{s}_i on the average uncertainty of the soft output from the DM inner decoder. Then we discuss the influence on the overall error performance that results from changing the outer code in the DM construction from a q -ary $(2(q^2 - 1), 2(q^2 - 1)R)$ code to a q^2 -ary $(q^2 - 1, (q^2 - 1)R)$ code. For the performance comparison, the original bit-level inner decoding algorithm reviewed in Section 2.2.1 is considered. The terminology used in this section for the IIDS channel and the DM coding scheme follow the definitions in Sections 2.1 and 2.2.

2.5.1 Effective Substitution Error Rate

Recall that in the DM inner decoding, the effective substitution error rate P_f in (2.4) is an important parameter which denotes the probability that a bit transmitted is not equal to the corresponding watermark bit. Since the resynchronization ability of the inner decoder mainly relies on identifying the discontinuity of watermark pattern in the

2.5 Advantages of Using RS Codes as Outer Codes in the DM Construction

received sequence \mathbf{r} , it is desirable to minimize P_f . Note that for practical value of random substitution error rate P_s and moderate to high-rate applications, P_s is expected to be a few orders of magnitude smaller than f , hence we can approximate Equation. 2.4 to be $P_f \approx f$. Therefore, minimizing f effectively minimizes the effective substitution error rate of the channel.

The following lemma indicates that if all codewords are equally likely, then the statistical mean density of s_i is equal to the arithmetic mean, i.e.,

$$f = \frac{1}{q} \sum_{j=0}^{q-1} \frac{w_H(\mathbf{s}_{i_j})}{n} \quad (2.13)$$

where $w_H(\cdot)$ computes the Hamming weight and $\mathbf{s}_{i_0}, \dots, \mathbf{s}_{i_{q-1}}$ are the distinct elements of the sparsifier's codebook.

Lemma 2.1. *If all codewords of an (N, K) code over $GF(q)$ are equally likely, then each code symbol is uniformly distributed on $GF(q)$.*

Proof. Let $(c_0, c_1, \dots, c_{N-1}) = \mathbf{m}\mathbf{G}$ where $\mathbf{m} = (m_0, m_1, \dots, m_{K-1})$ is a message vector and \mathbf{G} is the generator matrix of the code. Further, let $\mathbf{G} = [\mathbf{g}_0 \ \mathbf{g}_1 \ \dots \ \mathbf{g}_{N-1}]$ where $\mathbf{g}_i = [g_{i,0} \ g_{i,1} \ \dots \ g_{i,K-1}]^T$ is the i th column of \mathbf{G} . Then

$$c_i = \mathbf{m}\mathbf{g}_i = \sum_{j=0}^{K-1} m_j g_{i,j}.$$

Obviously, \mathbf{g}_i cannot be an all-zero vector for all i . Thus, we may assume without loss of generality that $g_{i,s} \neq 0$ and so

$$c_i = m_s g_{i,s} + \sum_{j=0, j \neq s}^{K-1} m_j g_{i,j}.$$

Given $\{m_i\}_{i=0, i \neq s}^{K-1}$, there is a one-to-one correspondence between c_i and m_s . Since each codeword is equally likely, it follows that c_i is uniformly distributed on $GF(q)$ and $\{m_i\}_{i=0, i \neq s}^{K-1}$ is uniformly distributed on $GF(q)^{K-1}$. Based on that, the lemma is immediate. \square

2.5 Advantages of Using RS Codes as Outer Codes in the DM Construction

Therefore, for a particular sparsifier mapping scheme, the effective substitution error rate can be computed using (2.13). Based on this approach, we compute the effective substitution error rates for the watermark code rate $R_w = k/n$ equal to $3/4(4/5)$ by increasing q from 8 to 64 (16 to 256). The results are illustrated in Table 2.2 and from this table, we draw the conclusion that for a fixed watermark code rate, increasing q reduces the effective substitution error rate.

Table 2.2: Effective substitution error rates for different q and R_w .

$R_w = 3/4$		$R_w = 4/5$	
$q = 8$	$q = 64$	$q = 16$	$q = 256$
0.3125	0.2832	0.3125	0.3047

2.5.2 Uncertainty in Inner Decoder's Output

Since increasing q minimizes the effective substitution error rate, it is expected that increasing q will improve the quality of the likelihoods generated by the inner decoder. Note that the outer LDPC decoder is initialized by the likelihoods generated by the inner decoder, improving the quality of the likelihoods will improve the performance of the outer decoder. In Fig. 2.6, we plot the average entropy of the likelihoods generated by the inner decoder as a function of $P_i = P_d$ for those different R_w and q shown in Table 2.2. These plots were made using a histogram estimate of the distribution of the likelihoods $P(\mathbf{r}|c_i)$.

As shown in Fig. 2.6, the average entropy of the likelihoods decreases as q increases for a given watermark code rate and insertion/deletion error rate, which means the quality of the likelihoods increases with q while R_w and $P_i = P_d$ are fixed. Fig. 2.6 also indicates that using a larger q allows a higher watermark code rate while more or less preserving the quality of the likelihoods.

2.5 Advantages of Using RS Codes as Outer Codes in the DM Construction

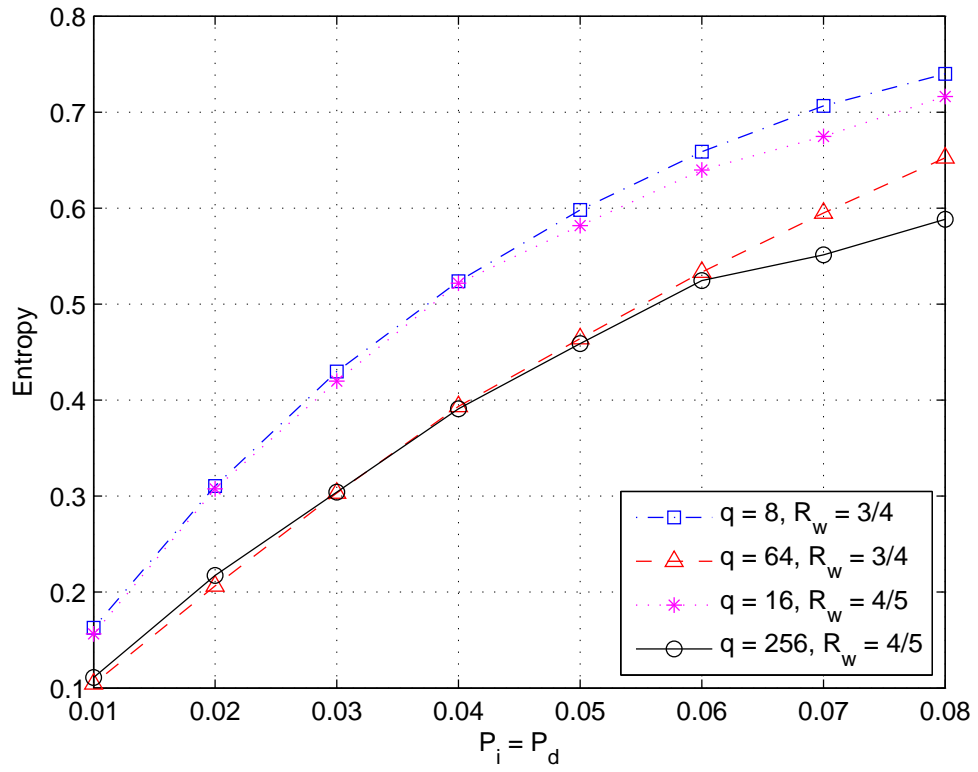


Figure 2.6: Average entropy of the likelihoods $P(\mathbf{r}|c_i)$ generated by the inner decoder, as a function of $P_i = P_d$.

2.5 Advantages of Using RS Codes as Outer Codes in the DM Construction

2.5.3 Implications

From the previous two subsections, we know that for a fixed watermark code rate, increasing q reduces the effective substitution error rate and improves the quality of likelihoods generated by the watermark decoder. Therefore, we compare two outer codes with the same rate and the same length: a q -ary $(2(q^2 - 1), 2(q^2 - 1)R)$ LDPC code and a q^2 -ary $(q^2 - 1, (q^2 - 1)R)$ RS code. For each DM construction with a distinct outer code, the inner code rate is fixed to be r , so the length of the sparse strings is $2(\log_2 q)/r$ with RS outer code and $(\log_2 q)/r$ with LDPC outer code. For the DM coding scheme with RS code as outer code, the hybrid ABP-ASD decoder is employed as the outer decoder.

Due to the complexity concern for decoding non-binary LDPC codes using BP decoder, we hence do not consider $\text{GF}(q^2)$ for outer LDPC codes for $\text{GF}(16)$ is the biggest alphabet of practical interest for LDPC codes [59]. However, the code alphabet size of practical interest for RS codes are much larger, such as $\text{GF}(128)$ and $\text{GF}(256)$. RS codes are widely used in many applications. Further, since the length of an RS code is bounded by its alphabet size plus 1 (except for a very limited class of extended RS code where the length is equal to its alphabet size plus 2) [93], the overall block length considered in this chapter is relatively short.

Based on our previous analysis, using an outer code constructed over larger Galois field improves the performance of the inner decoder. We hence conjecture that q^2 -ary RS code should have a chance to outperform the equivalent q -ary LDPC code when used as the outer code in the DM construction. Given the excellent error correction capability of the LDPC codes, we expect that the DM coding scheme with RS code as outer code to have better error performance than that with LDPC code as outer code, when the insertion/deletion error rates are sufficiently low. The reason to have sufficiently low insertion/deletion error rates is to ensure the frequency of uncertainty

2.5 Advantages of Using RS Codes as Outer Codes in the DM Construction

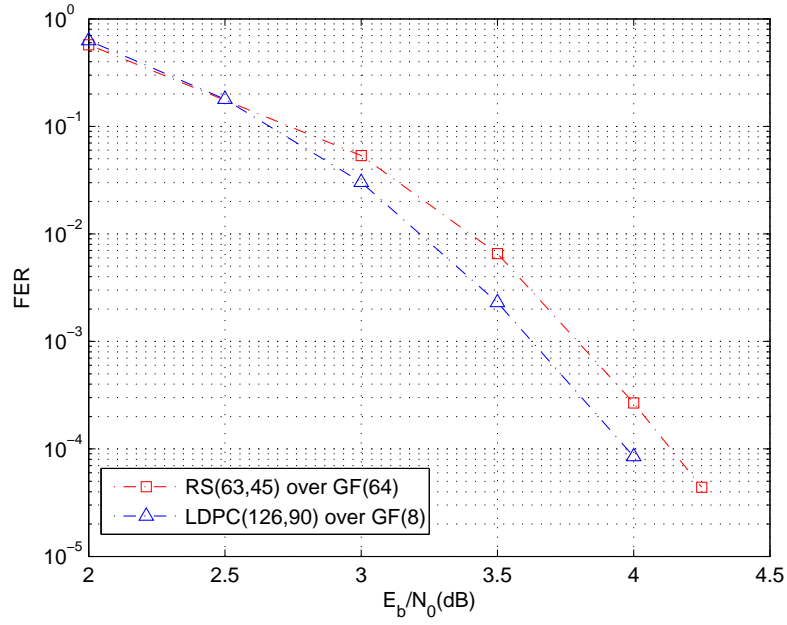
in the vicinity of insertions/deletions does not outweigh the reduction in effective substitution error rate. Further, smaller reduction in the effective substitution error rates indicates lower $P_i = P_d$ are needed to enable the coding scheme with outer RS code to perform better. Our simulation presented in the next section verifies both assertions for moderate to high overall code rates Rr .

2.5.4 Simulation Results

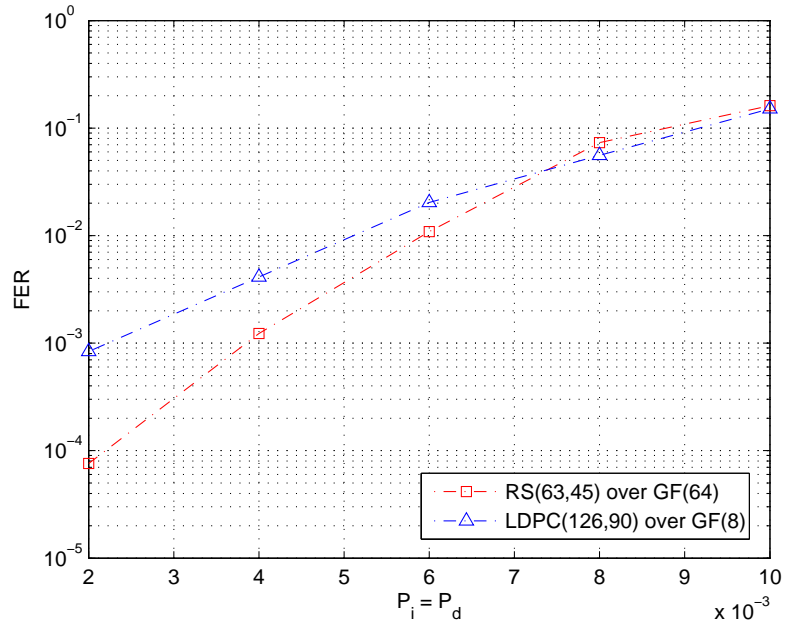
According to Section 2.5.3, short and relatively high rate LDPC codes are needed, we thus use the progressive edge-growth (PEG) algorithm [94] to construct LDPC codes for it is known to produce good, short LDPC codes. The maximum number of BP iterations performed by the outer LDPC code is set to 100. As for the RS hybrid ABP-ASD algorithm, we set $N_1 = 20$, $N_2 = 25$ and $\lambda = 10^3$, also the ASD is performed according to [89, Theorem 3] to further speed up the RS code simulations. The hybrid ABP-ASD algorithm terminates if the transmitted codeword is on the list, or if the maximum number of iterations $N_1 N_2$ is reached. For the IIDS channel, we set $P_i = P_d$, $P_s = 0$ as in [57].

1) 64-ary (63, 45) RS code vs. 8-ary (126, 90) LDPC code: The LDPC code here is an irregular code with column weight 3 and row weights 10 and 11. With a watermark code rate of $3/4$, an overall code rate of 0.54 and overall block length (in bits) of 504 are obtained. Further, the effective substitution error rate is 0.2832 for the coding scheme with the RS outer code and 0.3125 for the coding scheme with the LDPC outer code. Thus, the reduction Δ_1 in the effective substitution error rate obtained by increasing q from 8 to 64 is 0.0293. Fig. 2.7(a) shows the LDPC code having a coding gain of about 0.2 dB over the RS code at a FER of 10^{-4} on an AWGN channel with BPSK signalling. On the other hand, Fig. 2.7(b) shows the DM coding scheme with the RS outer code outperforming the coding scheme with the LDPC outer code on the

2.5 Advantages of Using RS Codes as Outer Codes in the DM Construction



(a) FER over AWGN channel with BPSK signaling.



(b) FER over IDS channel.

Figure 2.7: Performance comparison of 64-ary (63,45) RS code and 8-ary (126,90) LDPC code.

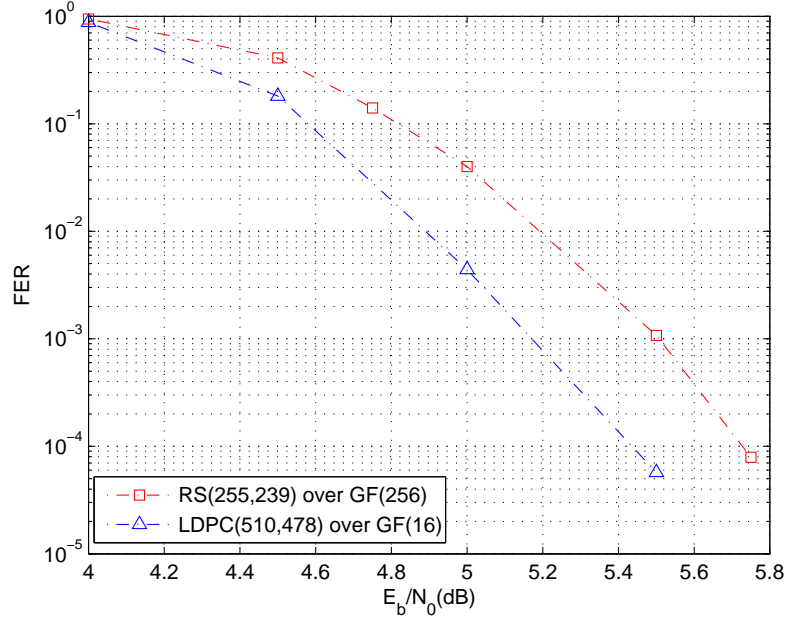
2.5 Advantages of Using RS Codes as Outer Codes in the DM Construction

IIDS channel when $P_i = P_d < 7.3 \times 10^{-3}$.

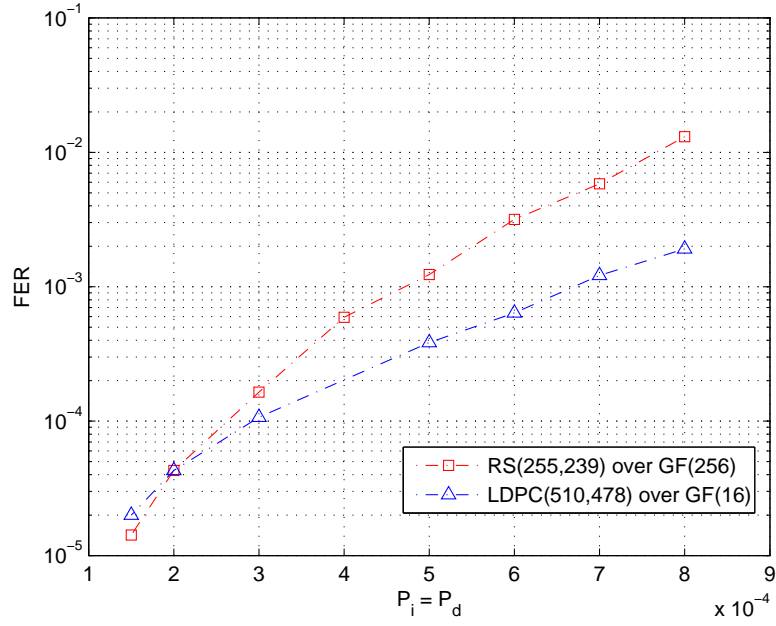
2) 256-ary (255, 239) RS code vs. 16-ary (510, 478) LDPC code: The LDPC code here is an irregular code with column weight 3 and row weights 47 and 48. With a watermark code rate of $4/5$, an overall code rate of 0.75 and overall block length (in bits) of 2550 are obtained. Further, the effective substitution error rate is 0.3047 for the coding scheme with the RS outer code and 0.3125 for the coding scheme with the LDPC outer code. Thus, the reduction Δ_2 in the effective substitution error rate obtained by increasing q from 16 to 256 is 0.0078, which is smaller than that in the previous case. Fig. 2.8(a) shows the LDPC code having a coding gain of about 0.3 dB over the RS code at a FER of 10^{-4} on an AWGN channel with binary phase-shift keying (BPSK) signaling. On the other hand, Fig. 2.8(b) shows the DM coding scheme with the RS outer code outperforming the coding scheme with the LDPC outer code on the IIDS channel when $P_i = P_d < 2 \times 10^{-4}$ which is less than 7.3×10^{-3} , as expected since $\Delta_2 < \Delta_1$.

We note that although the hybrid ABP-ASD decoder is a list decoder, it is still fair to say that below a certain insertion/deletion error rate, the coding schemes with an RS outer code outperform the corresponding coding schemes with an LDPC outer code. This is because the average global list size decreases monotonically with the insertion/deletion error rate and is therefore close to 1 below a certain error rate. For example, when applied to the above coding scheme with the 64-ary (63, 45) RS outer code, the average size of \mathcal{L}_G is 7.18, 1.66 and 1.01 when $P_i = P_d$ is 6×10^{-3} , 4×10^{-3} and 2×10^{-3} , respectively. Further, when applied to the coding scheme involving the 256-ary (255, 239) RS outer code, the average size of \mathcal{L}_G is 1.35 when $P_i = P_d = 4 \times 10^{-4}$ and so is already close to 1 even at insertion/deletion error rates above the point where the two FER curves in Fig. 2.8(b) cross over.

2.5 Advantages of Using RS Codes as Outer Codes in the DM Construction



(a) FER over AWGN channel with BPSK signaling.



(b) FER over IDS channel.

Figure 2.8: Performance comparison of 256-ary (255,239) RS code and 16-ary (510,478) LDPC code.

2.6 Concluding Remarks

In this chapter, we propose to use RS codes in place of LDPC codes as outer codes in the DM coding scheme along with the iterative hybrid ABP-ASD RS decoder for moderate to high-rate applications involving relatively short block length.

We show that for a fixed watermark code rate, the effective substitution error rate decreases as the code alphabet size of the outer code increases. In addition, we eliminate the influence of the outer code and measure the quality of the likelihoods generated by the inner decoder by computing the average entropy of these likelihoods. We observe that for a given watermark code rate, the uncertainty also decreases as the code alphabet size of the outer code increases. Furthermore, in view of the fact that the code alphabet size of practical interest for RS codes are larger than that of LDPC codes, we thus consider two realizations of the DM coding scheme having the same length and same code rate: one employs q -ary $(2(q^2 - 1), 2(q^2 - 1)R)$ LDPC code and the other one uses a q^2 -ary $(q^2 - 1, (q^2 - 1)R)$ RS code. We further show that when insertion and deletion probabilities are sufficiently small, the latter offers better FER performance for moderate to high-rate applications involving relatively short blocklengths.

Chapter 3

The Davey-MacKay Coding Scheme for BPMR Write Channels with Data-Dependent Insertion, Deletion and Substitution Errors

Recall that the presence of WIEs in the BPMR write process is a unique and major challenge which dramatically limits the overall performance of BPMR systems [12]. Intensive research effort has focused on statistically characterizing and modeling WIEs - see [12, 31, 34]. Since the actual write process in BPMR is extremely complicated and there are many factors that may affect the writing performance, a simplified write channel model that captures sufficient characteristics of the WIEs would be of practical interest for the development and evaluation of ECCs designed to handle WIEs.

In some early research works, the insertion and deletion errors caused by mis-synchronization between the write head and the intended islands were ignored to facilitate the performance analysis of a BPMR system under some detection/coding scheme,

3. The Davey-MacKay Coding Scheme for BPMR Write Channels with Data-Dependent Insertion, Deletion and Substitution Errors

e.g., the write process in BPMR was simplified to be a BSC in [60, 61]. The IIDS channel model introduced in the Section 2.1 has also been used to model the WIEs in BPMR, e.g., in [68, 95], an extension of the IIDS channel where the substitution errors are generated by an independent BSC, was considered.

Further, simulations and experiments of the BPMR recording process reveal that WIEs are actually data-dependent and the write channel therefore has memory. In [30], a probabilistic write channel model driven by binary state processes was proposed to model some data dependency between WIEs. By taking the channel state process to be a Bernoulli or first-order binary Markov process, this channel produces errors resembling substitution errors or paired insertion-deletion errors with the inserted bit being identical to the last written bit - a phenomenon that occurs when the timing errors are sufficiently large and the write head field spans several consecutive islands in the along-track direction. However, this write channel model still has its limits in capturing some of the characteristics of WIEs while modeling the BPMR write process.

In this chapter, we will first review the data-dependent characteristics of WIEs that have been reported in the existing literature. Then based on the review, we propose a new write channel model which introduces dependent insertion, deletion and substitution (DIDS) errors as would occur in an actual BPMR system. Further, we modify the DM inner decoder to suit the DIDS channel model and propose a scheme to efficiently reduce the complexity required by the inner decoder. The performance of the DM coding scheme under iterative and non-iterative decoding on the DIDS channel are presented. Our simulation results are indicative of how well the DM coding scheme will perform in an actual BPMR system, when the SNR of the read channel is sufficiently high to enable the channel detector to compensate for all impairments of the read channel.

3.1 Data-Dependent Characteristics of WIEs in BPMR

In BPMR, the combined effect of random island position jitter and variations in the switching field of the islands, is a localized random phase drift between the desired write window and the actual switching position of each island. This localized random phase drift introduces random substitution errors in the writing process [29]. Random substitution errors are also caused by dead islands, i.e., bits with effective switching field exceeding the maximum applied write field [34]. Moreover, the combined effect of mechanical vibration and variations in spindle spin, is a long term slow phase drift which, if not compensated for, will accumulate to a point leading to an insertion or deletion [29].

Remarkably, insertions and deletions occur in pairs, a phenomenon resulting from the frequency mismatch between the islands and the write head, or a group of islands being separated further apart than usual or having larger switching fields [30]. In other words, paired insertions and deletions are a result of the combined effect of the aforementioned localized random phase drift and long term slow phase drift. We note that [29, TABLE I] presents experimental data pertaining to synchronization error pairs whereby synchronization is first lost due to a deletion and subsequently regained following an insertion, and vice-versa.

The tendency of the actual write clock to both accumulate and self-correct has been observed by Keele in [62], which also leads to paired insertions and deletions. It has been further verified by the simulations in [62] that the paired insertions and deletions can average over more than four per sector run with equal probability when the standard deviation of the write clock is equal to 0.1% and the sector lengths is 32 Kbits, which implies an insertion/deletion error rate at the order of 10^{-3} . In addition, the accumulated phase drifts at the end of each sector are below $1/4$ of an island period, we hence can expect that the instantaneous phase drift (which is a combination of a

3.1 Data-Dependent Characteristics of WIEs in BPMR

short-term localized phase drift and accumulated phase drift [29]) will rarely exceed 1.5 times an island period, which implies that with high probability, the write channel inserts/deletes one bit for each insertion/deletion event.

Moreover, it is noted in [30] that since the magnetic write field influences multiple adjacent islands along the down-track direction at any time, the occurrence of an insertion corresponds to a particular island being skipped rather than overwritten by the intended write field. Consequently, the inserted bit is typically the same as the previous recorded bit. (The inserted bit may be different from the previous recorded bit if e.g., the switching field of the island to which the inserted bit is written is larger than the write head field.)

Finally, it is noted in [37] that the magnetic write field may be too weak to write a number of islands before and after an insertion or deletion. This results in bursts of substitution errors before and after a synchronization error. The bursts of substitution errors complicate the code designs, and was thus not considered in [37]. According to [37], insertion and deletion errors are induced by the mismatch Δ_f between the actual write clock frequency f and the ideal write clock frequency f_0 , as shown in Fig. 3.1. In addition, it was reported in [29] that $\Delta_f = |f_0 - f|$ is a long-term steady phase drift, hence it can be considered constant within a number of bits around each synchronization error. Further, according to [33, Fig. 4], the error rate of a certain bit island not being successfully recorded is relatively high and almost the same, when the bit island gets too close, e.g., less than θ/f_0 , ($\theta < 0.5$), to the previous/next write window. Apparently, there are about $\lceil (0.5 - \theta)f/\Delta_f \rceil$ bits before and after each synchronization error that seriously diverge from the center of their intended write windows and are hence subjected to burst substitution errors. Therefore, the maximum burst error lengths before and after each synchronization error are considered to be the same in this thesis. In addition, the overall BPMR system may fail if the length of the burst errors are too long. However, we note that on one hand, a faster accumulation of phase

3.1 Data-Dependent Characteristics of WIEs in BPMR

When $f < f_0$: Insertion occurs

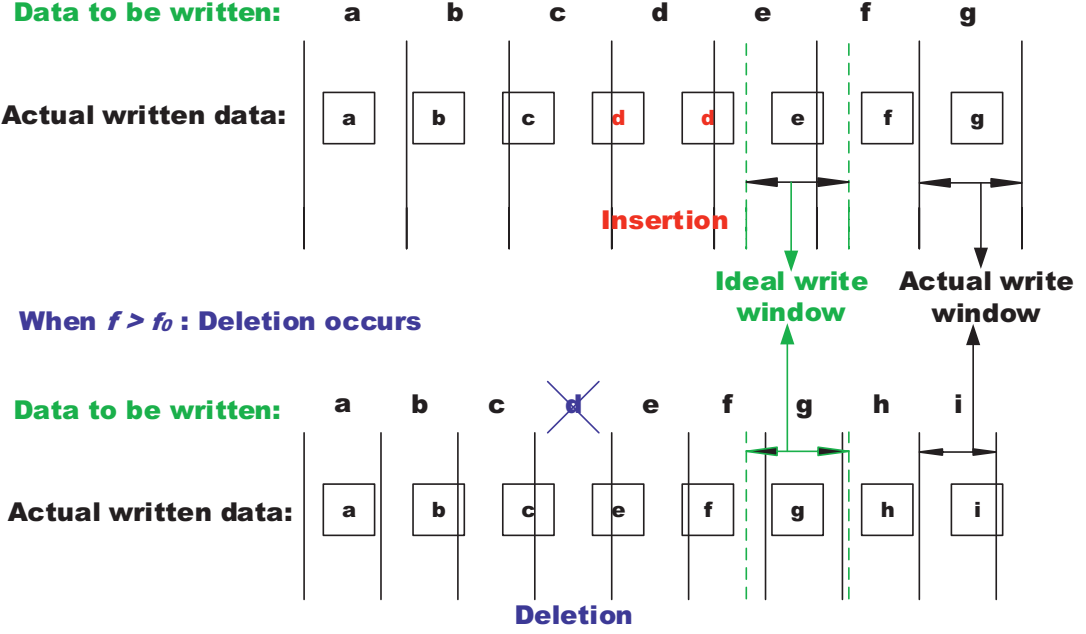


Figure 3.1: Modeling insertion and deletion errors that are surrounded by burst substitution errors.

drift leads to higher insertion/deletion rates as the number of bits needed to accumulate to the point of generating an insertion/deletion error is $\lceil 0.5f/\Delta_f \rceil$, which decreases in Δ_f . On the other hand, a faster accumulation of phase drift shortens the burst error length as $\lceil (0.5 - \theta)f/\Delta_f \rceil$, which also decreases in Δ_f . In other words, shorter burst error lengths may be traded for higher insertion/deletion rates, which implies that the ECCs developed for BPMR systems should expect relatively high insertion and deletion rates.

The DIDS channel model proposed to mimic the BPMR write process in the next section will capture all these aforementioned data-dependencies of WIEs.

3.2 The DIDS Channel Model

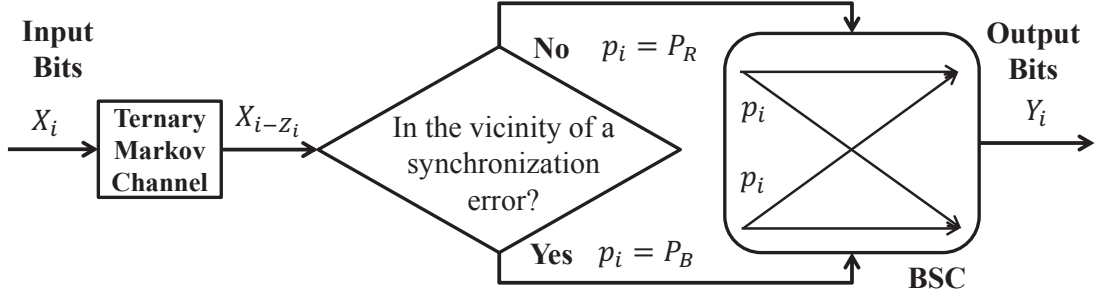


Figure 3.2: The DIDS channel model. The input is $\{X_i\}$ and the output from the ternary Markov channel model is $\{X_{i-Z_i}\}$ which feeds to the two-state BSC to yield the final output $\{Y_i\}$.

3.2 The DIDS Channel Model

Our DIDS channel model is a composite channel consisting of a ternary Markov state channel followed by a two-state BSC as shown in Fig. 3.2. The ternary Markov state channel produces insertions and deletions that occur in pairs such that the inserted bit is the same as the last input bit. The output of this channel is fed to the two-state BSC which models substitution errors that occur randomly, as well as in bursts of length at most L before and after each synchronization error. Throughout, let $\mathbf{X} = \{X_i\}$ be the binary input sequence to the DIDS channel, $\mathbf{Y} = \{Y_i\}$ the corresponding channel output, and $\mathbf{Z} = \{Z_i\}$ the state sequence of the ternary Markov state channel. We refer to $\{Z_i\}$ as the *channel state sequence* as in [30].

3.2.1 Modeling Insertion-Deletion & Deletion-Insertion Pairs

The ternary Markov channel in the DIDS channel model is an extension of the binary Markov state channel model of [30]. For the binary Markov state channel, the channel state sequence, which we denote by \mathbf{Z} , is a stationary first-order Markov state with

3.2 The DIDS Channel Model

$Z_i \in \{0, 1\}$ and initial state 0. Given the input-output relationship on this channel, i.e.,

$$Y_i = X_{i-Z_i}, \quad (3.1)$$

it is easy to see that an insertion at time i is induced by the state transition $Z_{i-1} = 0 \rightarrow Z_i = 1$ while a deletion at time i is induced by the state transition $Z_{i-1} = 1 \rightarrow Z_i = 0$. Moreover, the inserted bit is the same as the last input bit. More importantly, note that synchronization is lost due to an insertion and subsequently regained when a deletion occurs.

To allow for synchronization to be lost due to a deletion and subsequently regained when an insertion occurs, we take \mathbf{Z} to be a stationary Markov process with $Z_i \in \{-1, 0, 1\}$ and initial state 0. Then from (3.1), we see that two additional state transitions introduce synchronization errors. Specifically, a deletion at time i is induced by the state transition $Z_{i-1} = 0 \rightarrow Z_i = -1$, while an insertion at time i is induced by the state transition $Z_{i-1} = -1 \rightarrow Z_i = 0$. We will refer to an insertion-deletion (resp., deletion-insertion) pair as a *positive* (resp., *negative*) *cycle*.

Only one bit can be deleted at any one time in the DIDS channel model. Therefore we have $\Pr(Z_i = -1 | Z_{i-1} = 1) = 0$. Further, the inserted bit in the output of the ternary Markov channel is the same as the last input bit. We thus set $\Pr(Z_i = 1 | Z_{i-1} = -1) = 0$. We nevertheless do not allow the same bit to be inserted twice. Therefore, we also set $\Pr(Z_i = 1 | Z_{i-1} = 0, Z_{i-2} = -1) = 0$. Consequently, we let $\Pr(Z_i = 0 | Z_{i-1} = -1, Z_{i-2}) = \Pr(Z_i = 1 | Z_{i-1} = 0, Z_{i-2} \neq -1) = P_I$, $\Pr(Z_i = 0 | Z_{i-1} = 1, Z_{i-2}) = \Pr(Z_i = -1 | Z_{i-1} = 0, Z_{i-2}) = P_D$, where P_I and P_D are the insertion and deletion probabilities, respectively. Hence, \mathbf{Z} is a stationary second-order Markov process.

3.2 The DIDS Channel Model

3.2.2 Modeling Substitution Errors

Recall, the output of the ternary Markov channel feeds into a two-state BSC. The cross-over probability associated with the input X_{i-Z_i} to the BSC at time i is p_i . The two states of the BSC are specified by two different cross-over probabilities P_R and P_B . Strictly speaking, the BSC produces only random substitution errors. However, by taking P_R to be small (e.g. 10^{-3}) and P_B to be large (e.g. 10^{-1}), we assume that the two-state BSC produces random substitution errors when $p_i = P_R$ and *burst-like* substitution errors when $p_i = P_B$. Henceforth, we will simply write burst substitution errors instead of burst-like substitution errors for brevity. Note that the two-state BSC is similar to the Gilbert-Elliot channel model [96] in the sense that the cross-over probabilities of both channel models are dictated by a stationary Markov process. However, while the Markov process in the DIDS channel model is a ternary process, the Markov process in the Gilbert-Elliot channel is a binary process. Despite this difference, the two-state BSCs in both the DIDS channel and the Gilbert-Elliot channel can be used to model burst errors by choosing a suitably large cross-over probability for the “bad” state.

Whether the BSC produces random or burst substitution errors depends on the channel state sequence \mathbf{Z} . We are not aware of any paper in the literature that considers the length of the burst errors before and after a synchronization error. Thus, for simplicity, we model a burst of substitution errors of length at most L before and after a synchronization error at time i as follows. For an insertion at time i , let $p_{i'} = P_B$ for $i' \in \{i - L, \dots, i + L\}$. Similarly, for a deletion at time i , let $p_{i'} = P_B$ for $i' \in \{i - L, \dots, i + L - 1\}$. We refer to the set $\{i - L, \dots, i + L\}$ (resp., $\{i - L, \dots, i + L - 1\}$) as the *vicinity* of an insertion (resp., deletion) at time i . The apparent asymmetry in the definition of the vicinity of an insertion and the vicinity of a deletion is a direct consequence of the above assumption. Other bits that are not in the

3.3 Applying the DM Construction to the DIDS Channel Model

vicinity of any synchronization errors are transmitted through the BSC with $p_i = P_R$.

Unlike the binary Markov channel model of [30] wherein the inserted bit is identical to the last input bit with probability 1, the inserted bit in our channel model is identical to the last input bit with probability $1 - P_B$. Our rationale is as follows. In a BPMR system, an insertion is due to severe misalignment between the intended writing window and the actual switching position of each island. The burst errors occurring before and after an insertion, are similarly due to this severe misalignment. Since the inserted bit is at the center of the region of severe misalignment, we therefore subject the inserted bit to a substitution error probability of P_B in our channel model.

The (overall) substitution error rate P_S of the DIDS channel can be approximated as

$$P_S \approx P_R + \frac{8}{3} \cdot P_I(P_B - P_R)L - 2P_IP_B \sum_{i=1}^{2L} (1 - P_I)^{i-1} P_I(2L - i) + \frac{2}{3} P_IP_B \quad (3.2)$$

where the state transition $-1 \rightarrow 0 \rightarrow 1$ is assumed to be allowed to simplify the computation. In Fig. 3.3, we show that the approximation is very accurate for $L = 0, \dots, 5$ and $P_I \leq 2 \times 10^{-2}$.

An example for DIDS channel with $L = 1$ is illustrated in Fig. 3.4.

3.3 Applying the DM Construction to the DIDS Channel Model

In this section, we apply the DM construction to the DIDS channel model with a modified inner decoding scheme. The modified inner decoding scheme takes into account and takes advantages of the data-dependencies of errors introduced by the DIDS channel. It is also capable of taking in soft extrinsic information from the outer decoder to further improve the overall performance.

3.3 Applying the DM Construction to the DIDS Channel Model

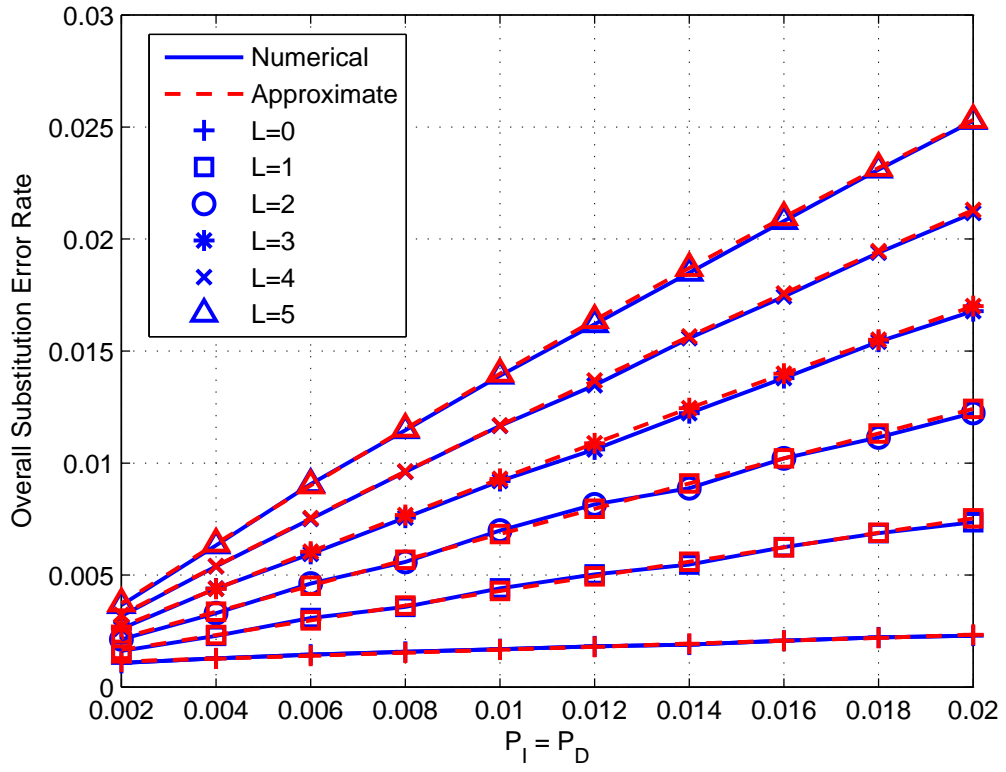


Figure 3.3: Numerical overall substitution error rates obtained via simulations and corresponding overall substitution error rates computed by (3.2).

3.3 Applying the DM Construction to the DIDS Channel Model

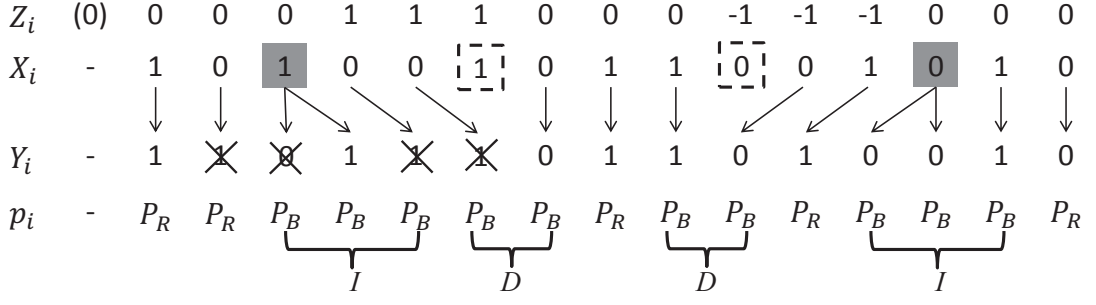


Figure 3.4: Illustration of the DIDS channel model. The arrow shows how the input bits map into the received sequence \mathbf{Y} according to the channel state sequence \mathbf{Z} . Inserted (resp., deleted) bits are indicated by gray (resp., dashed) square. Crosses in the figure denote the received bits resulting from substitution errors. The burst substitution errors in the vicinity of an insertion and vicinity of a deletion are indicated by I and D , respectively. The initial state of \mathbf{Z} is denoted by (0).

The DM coding scheme considered in this section is the same as that reviewed in Section 2.2. However, the overall codeword input to the DIDS channel is now denoted by $\mathbf{X} = \{X_i\}_{i=0}^{Nn-1}$ to be consistent with Fig. 3.2.

3.3.1 Modifying the Inner Decoder

Recall that the channel state sequence \mathbf{Z} in the DIDS channel is a second-order Markov process. The received sequence corresponding to the input bit X_i depends on

$$\{Z_{i-1}, Z_i, Z_{i+1}\}.$$

Further, in order to identify whether the received sequence is transmitted through the two-state BSC with cross-over probability P_R or P_B , L channel states before Z_{i-1} and after Z_{i+1} need to be considered. Therefore, we define

$$\mathbf{v}_i \triangleq (Z_{i-1-L}, \dots, Z_i, \dots, Z_{i+1+L})$$

3.3 Applying the DM Construction to the DIDS Channel Model

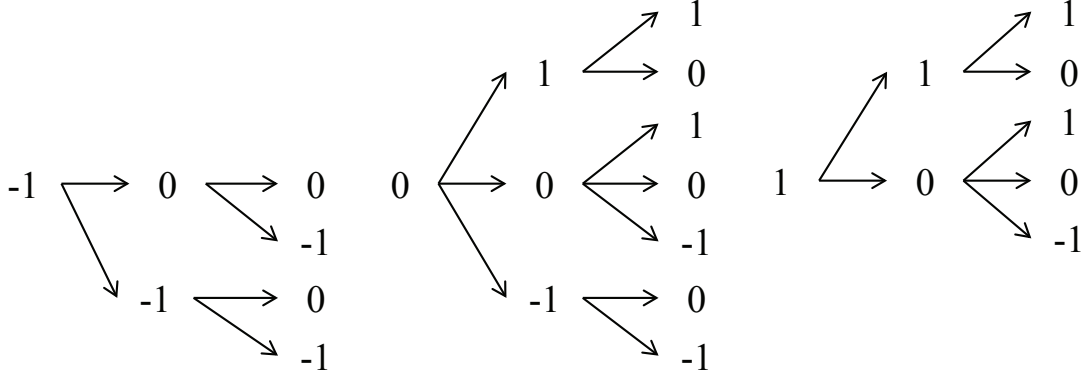


Figure 3.5: Illustration of the 16 valid SCSWs for $L = 0$.

and refer to \mathbf{v}_i as a *sliding channel state window* (SCSW). We say that \mathbf{v}_i is a valid SCSW if $\Pr(Z_{t+1}|Z_t, Z_{t-1}) \neq 0$, for $t = i - L, \dots, i + L$.

Fig. 3.5 shows three ternary trees for $L = 0$, where each node is a channel state and each tree follows the second-order Markov process \mathbf{Z} . Consequently, each root-to-leaf path corresponds to a valid SCSW and we have 16 valid SCSWs in total when $L = 0$. Moreover, we can generate all valid SCSWs for arbitrary L using those three basic ternary trees.

It is easy to see that $\mathbf{V} = \{\mathbf{v}_i\}$ is a stationary first-order Markov process such that

$$\Pr(\mathbf{v}_i|\mathbf{v}_{i-1}) = \Pr(Z_{i+L+1}|Z_{i+L}, Z_{i+L-1}). \quad (3.3)$$

The initial state of \mathbf{V} is set to be $(0, \dots, 0)$.

Further, let the subsequence $(Y_0, \dots, Y_{f_i(\mathbf{v}_i)})$ of \mathbf{Y} correspond to the input subsequence (X_0, \dots, X_i) . One checks that

$$f_i(\mathbf{v}_i) = \begin{cases} i + 1 & \text{if } Z_{i+1} = 1 \\ i - 1 & \text{if } Z_i = -1 \\ i & \text{otherwise.} \end{cases}$$

Thus, the difference between the number of bits that enter the channel, and the corresponding number of bits received, is either -1 , 0 or 1 . Consequently, to identify

3.3 Applying the DM Construction to the DIDS Channel Model

$$\begin{array}{cccccc}
 Z_{-1} & Z_0 & Z_1 & \cdots & Z_{Nn-1} & Z_{Nn} \\
 & X_0 & X_1 & \cdots & X_{Nn-1} & \\
 Y_{-1} & Y_0 & Y_1 & \cdots & Y_{Nn-1} & Y_{Nn}
 \end{array}$$

Figure 3.6: Illustration of the received bits needed by the inner decoder.

the boundaries of the received sequence corresponding to the codeword $\{X_i\}_{i=0}^{Nn-1}$, the inner decoder needs to take into account the received bits spanning Y_{-1} and Y_{Nn} , as illustrated in Fig. 3.6.

Denoting the subsequence (Y_a, \dots, Y_b) of \mathbf{Y} by \mathbf{Y}_a^b , the probability of receiving \mathbf{Y} given that X_i has entered the channel and the state transition $\mathbf{v}_{i-1} \rightarrow \mathbf{v}_i$, is given by:

$$\begin{aligned}
 & \Pr(\mathbf{Y}_{f_{i-1}(\mathbf{v}_{i-1})+1}^{f_i(\mathbf{v}_i)}, \mathbf{v}_i | X_i, \mathbf{v}_{i-1}) \\
 &= \Pr(\mathbf{v}_i | \mathbf{v}_{i-1}) \cdot \begin{cases} 1 & \text{if } u = 0 \\ \Pr(Y_{f_{i-1}(\mathbf{v}_{i-1})+1} | X_i) & \\ \cdot (\Pr(Y_{f_i(\mathbf{v}_i)} | X_i))^{u-1} & \text{if } u > 0, \end{cases} \quad (3.4)
 \end{aligned}$$

where $u = f_i(\mathbf{v}_i) - f_{i-1}(\mathbf{v}_{i-1})$ denotes the number of bits received due to X_i entering the channel and

$$\Pr(Y_j | X_i) = \begin{cases} p_j & \text{if } Y_j \neq X_i \\ 1 - p_j & \text{otherwise,} \end{cases} \quad (3.5)$$

where Y_j is the received version of X_i and p_j the corresponding cross-over probability of the two-state BSC. Given \mathbf{v}_i , Y_j can be easily located in \mathbf{Y} and the corresponding p_j determined by checking whether Y_j is in the vicinity of a synchronization error or not.

Then, the likelihood $\Pr(\mathbf{Y} | c_i)$, which will serve as input to the outer (i.e., LDPC)

3.3 Applying the DM Construction to the DIDS Channel Model

decoder, can be computed via a forward-backward algorithm using \mathbf{V} as follows:

$$\Pr(\mathbf{Y}|d_i) = \sum_{\rho_1, \rho_2} F_i(\rho_1) \cdot M_i(\rho_1, \rho_2, d_i) \cdot B_i(\rho_2), \quad (3.6)$$

where

$$F_i(\rho_1) = \Pr(\mathbf{Y}_{-1}^{f_{in-1}(\rho_1)}, \mathbf{v}_{in-1} = \rho_1) \quad (3.7)$$

$$B_i(\rho_2) = \Pr(\mathbf{Y}_{f_{(i+1)n-1}(\rho_2)+1}^{Nn} | \mathbf{v}_{(i+1)n-1} = \rho_2) \quad (3.8)$$

$$M_i(\rho_1, \rho_2, d_i) = \Pr(\mathbf{Y}_{f_{in-1}(\rho_1)+1}^{f_{(i+1)n-1}(\rho_2)}, \mathbf{v}_{(i+1)n-1} = \rho_2 | d_i, \mathbf{v}_{in-1} = \rho_1). \quad (3.9)$$

The likelihood functions $F_i(\rho_1)$, $B_i(\rho_2)$ and $M_i(\rho_1, \rho_2, d_i)$ are the forward, backward and middle metrics, respectively.

To compute the forward and backward metrics, we adopt the approach of [71, Section III] as it enables the inner decoder to admit soft information from the outer decoder for iterative decoding. Similar to [71, Equation (10)], the forward metric $F_i(\rho_1)$ can be computed using the following recursive formula:

$$F_i(\rho_1) = \sum_{\rho_0, d_{i-1}} [F_{i-1}(\rho_0) \cdot \Pr(d_{i-1}) \cdot M_{i-1}(\rho_0, \rho_1, d_{i-1})]. \quad (3.10)$$

The backward metric $B_i(\rho_2)$ can be recursively computed in like manner

$$B_i(\rho_2) = \sum_{\rho_3, d_{i+1}} [B_{i+1}(\rho_3) \cdot \Pr(d_{i+1}) \cdot M_{i+1}(\rho_2, \rho_3, d_{i+1})]. \quad (3.11)$$

Since the boundaries of the received version of the transmitted codeword is uncertain, the initial values for $F_0(\mathbf{v}_{-1})$ and $B_{N-1}(\mathbf{v}_{Nn-1})$ are set to be equal for all possible values of \mathbf{v}_{-1} and \mathbf{v}_{Nn-1} .

Finally, the middle metric $M_i(\rho_1, \rho_2, d_i)$ can be calculated by fixing

$$(X_{in}, \dots, X_{(i+1)n-1})$$

according to d_i and performing a forward pass between $\mathbf{v}_{in-1} = \rho_1$ and $\mathbf{v}_{(i+1)n-1} = \rho_2$

3.3 Applying the DM Construction to the DIDS Channel Model

as follows:

$$\begin{aligned}
M_i(\rho_1, \rho_2, c_i) &= \Pr(\mathbf{Y}_{f_{in-1}(\rho_1)+1}^{f_{(i+1)n-1}(\rho_2)}, \mathbf{v}_{(i+1)n-1} = \rho_2 | c_i, \mathbf{v}_{in-1} = \rho_1) \\
&= \Pr(\mathbf{Y}_{f_{in-1}(\rho_1)+1}^{f_{(i+1)n-1}(\rho_2)}, \mathbf{v}_{(i+1)n-1} = \rho_2 | \mathbf{X}_{in}^{(i+1)n-1}, \mathbf{v}_{in-1} = \rho_1) \\
&= \sum_{\mathbf{v}_{(i+1)n-2}=\rho_{i2}} \Pr(\mathbf{Y}_{f_{in-1}(\rho_1)+1}^{f_{(i+1)n-1}(\rho_2)}, \mathbf{v}_{(i+1)n-2} = \rho_{i2}, \mathbf{v}_{(i+1)n-1} = \rho_2 | \mathbf{X}_{in}^{(i+1)n-1}, \mathbf{v}_{in-1} = \rho_1) \\
&= \sum_{\mathbf{v}_{(i+1)n-2}=\rho_{i2}} \left\{ \Pr(\mathbf{Y}_{f_{(i+1)n-2}(\rho_{i2})+1}^{f_{(i+1)n-1}(\rho_2)}, \mathbf{v}_{(i+1)n-1} = \rho_2 | \mathbf{X}_{(i+1)n-1}, \mathbf{v}_{(i+1)n-2} = \rho_{i2}) \right. \\
&\quad \left. \cdot \Pr(\mathbf{Y}_{f_{in-1}(\rho_1)+1}^{f_{(i+1)n-2}(\rho_{i2})}, \mathbf{v}_{(i+1)n-2} = \rho_{i2} | \mathbf{X}_{in}^{(i+1)n-2}, \mathbf{v}_{in-1} = \rho_1) \right\}
\end{aligned}$$

Further, the LUT approach of [72] can be adopted to significantly reduce the computational-complexity of the modified inner decoder by computing and storing all possible middle metrics in a LUT, since they do not change for a fixed DIDS channel.

3.3.2 Reduced-Complexity Inner Decoding

The computational complexity of the inner decoder is $O(N_s^2)$ where N_s is the total number of valid SCSWs considered by the decoder. TABLE 3.1 summarizes N_s for $L = 0, 1, 2, 3, 4, 5$ in the second column. Evidently, for $L \geq 2$, the large number of valid SCSWs renders the complexity of the inner decoder too high for practical use.

Table 3.1: Number of valid SCSWs for $L = 0, 1, 2, 3, 4, 5$ with $T_{max} = 1, 2$.

L	N_s	N_s with $T_{max} = 1$	N_s with $T_{max} = 2$
0	16	11	16
1	85	19	52
2	447	29	112
3	2345	35	196
4	12291	43	304
5	64147	51	436

3.4 Simulation Results

To reduce the complexity of the inner decoder described in Section III-B, we first note that the probability of observing a valid SCSW with a state transitions, is given by $\binom{2L+2}{a} P_D^{\lceil a/2 \rceil} \cdot P_I^{\lfloor a/2 \rfloor}$ if a deletion occurs before an insertion, or $\binom{2L+2}{a} P_I^{\lceil a/2 \rceil} \cdot P_D^{\lfloor a/2 \rfloor}$ if an insertion occurs before a deletion. In either case, this probability decreases exponentially fast as a increases. Thus, the complexity of the inner decoder can be reduced by only considering the valid SCSWs that have a small number of state transitions.

To this end, let T_{max} denote the maximum number of state transitions contained in a valid SCSW to be considered by the inner decoder. The third and forth columns of TABLE I give the number of valid SCSWs to be considered by the inner decoder for $L = 0, 1, \dots, 5$ and $T_{max} = 1, 2$. Clearly, the complexity of the inner decoder is significantly reduced by setting T_{max} to be equal to 1 or 2. In Section IV, we will show that the performance degradation resulting from setting $T_{max} = 1$ is negligible for $L = 0, 1$ at least.

3.3.3 Iterative Decoding

The forward and backward metric recursive formulas enable the inner decoder to admit extrinsic information from the outer decoder to be fed back to the inner decoder to form an iterative decoder. Specifically, the extrinsic information will be used to improve the prior probability $\Pr(d_i)$ in (5) and (6). We compute the extrinsic information as prescribed by the iterative decoding structure in Fig. 2.4.

3.4 Simulation Results

In this section, we analyze the distribution of the length (in bits) of negative and positive cycles in the DIDS channel. We then investigate the frame error rate (FER) performance of the DM scheme with and without iterative decoding over the DIDS channel.

3.4 Simulation Results

Finally, the FER performance of applying reduced-complexity inner decoder for DIDS channels with $L > 0$ is illustrated.

Since the insertions and deletions occur in pairs in the DIDS channel, the insertion and deletion error rates should be the same after transmitting a large number of bits. Thus, we set $P_I = P_D$ in the following simulations.

3.4.1 Distribution of the Length of Negative/Positive Cycles

The respective length distributions of the negative and positive cycles with $P_I = P_D = 0.01$ are shown in Fig. 3.7 and Fig. 3.8. Since $P_I = P_D$, the two distributions are almost the same. In addition, the occurrence of negative and positive cycle decreases exponentially as the length increases. This coincides with the experimental data in [29, TABLE I].

3.4.2 FER Performance on the DIDS Channel

In the following simulations, we fix $P_R = 0.001$ and $P_B = 0.1$. Further, we use a fixed DM code for which the outer code is a (999,888) LDPC code over GF(16), and the rate for the inner code is 4/5. Thus, the overall codeword length (in bits) is 4995 and the overall code rate is 0.71. A BP decoder is used as the outer decoder. Under non-iterative decoding, the maximum number of BP iterations is set to 60. For the inner decoder, we switch between the modified inner decoder described in Section 3.3.1, the reduced-complexity variant described in Section 3.3.2, and the inner decoder of [71], which we refer to inner decoder A, inner decoder B and inner decoder C, respectively. As in Section 3.3.3, iterative decoding with the BP decoder and inner decoder C is realized using the iterative decoding structure in Fig. 2.4. Iterations between the inner and outer decoder stop when a valid codeword is found or the maximum number of iterations is reached. Henceforth, an iteration between the inner and outer decoder will

3.4 Simulation Results

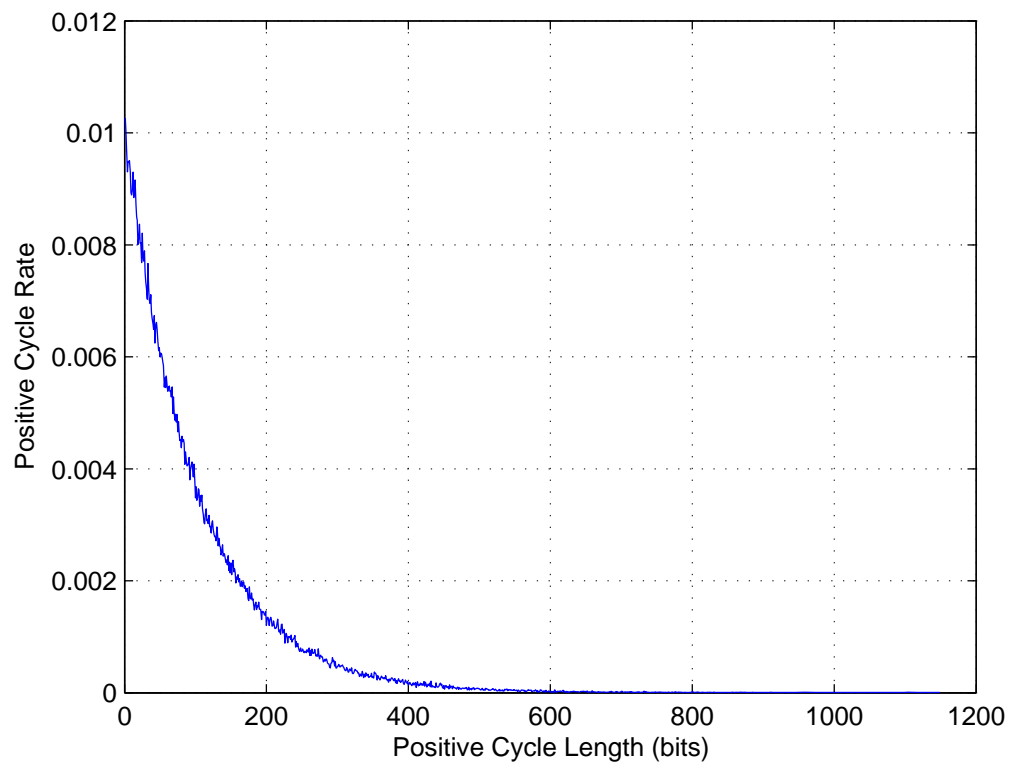


Figure 3.7: Positive cycle rate vs. Positive cycle length.

3.4 Simulation Results

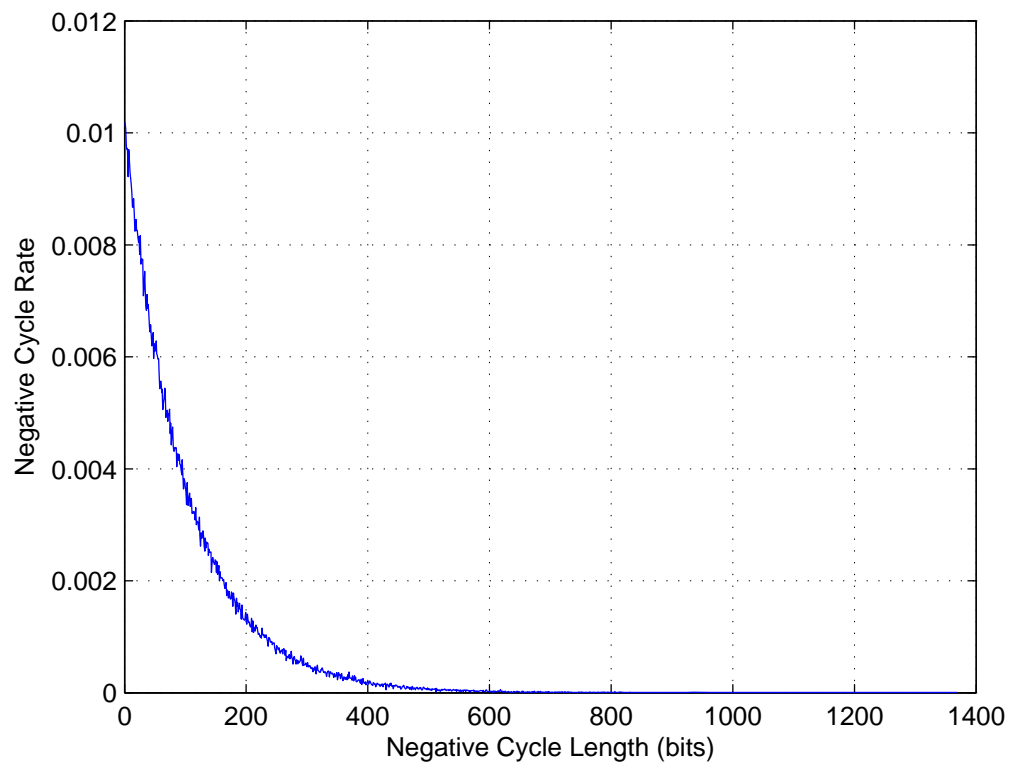


Figure 3.8: Negative cycle rate vs. Negative cycle length.

3.4 Simulation Results

be referred to as an outer iteration to distinguish it from the BP iterations of the outer decoder.

Fig. 3.9 shows the FER performance when inner decoder A is deployed, with and without iterative decoding for $L = 0$. Fig. 3.10 presents the FER performance when inner decoder C is deployed for the same value of L . For these simulations, the maximum number of BP iterations, β , and the maximum number of outer iterations, α , are varied such that $\alpha\beta = 60$. Clearly, inner decoder A yields superior performance compared to inner decoder C. For instance, with iterative decoding, a FER of 10^{-4} is achieved with inner decoder C when $P_I = P_D = 6.0 \times 10^{-3}$. Remarkably, for the same insertion/deletion rate, inner decoder A yields almost the same FER performance without iterative decoding. This outcome is as expected since inner decoder C ignores the dependencies between the synchronization errors. Fig. 3.9 also shows that iterative decoding provides substantial performance improvement, although there is hardly any improvement beyond 6 outer iterations. To understand why this is so, we plot in Fig. 3.11 histograms showing the number of codewords corrected as a function of the number of outer iterations performed for the three values of (α, β) shown in Fig. 3.9, when $P_I = P_D = 0.01$. As Fig. 3.11 shows, most codewords can be corrected within the first three outer iterations, indicating a fast convergence of the iterative decoder to a reliable codeword estimate.

Next, we switch to inner decoder B and vary T_{max} between 1 and $2L+2$ to demonstrate that the performance degradation resulting from setting $T_{max} = 1$ is negligible for $L = 0, 1$, as previously claimed. We are unable to do the same for $L \geq 2$ as the prohibitively large values of N_s corresponding to $T_{max} = 2L + 2$ (as shown in the second column of TABLE I), render the complexity of the inner decoder too high for simulations to be performed. Note that when $T_{max} = 2L + 2$, no valid SCSWs are ignored by inner decoder B and so this inner decoder is identical to inner decoder A in this case. Following [57, Section B of Appendix], we measure the quality of the

3.4 Simulation Results

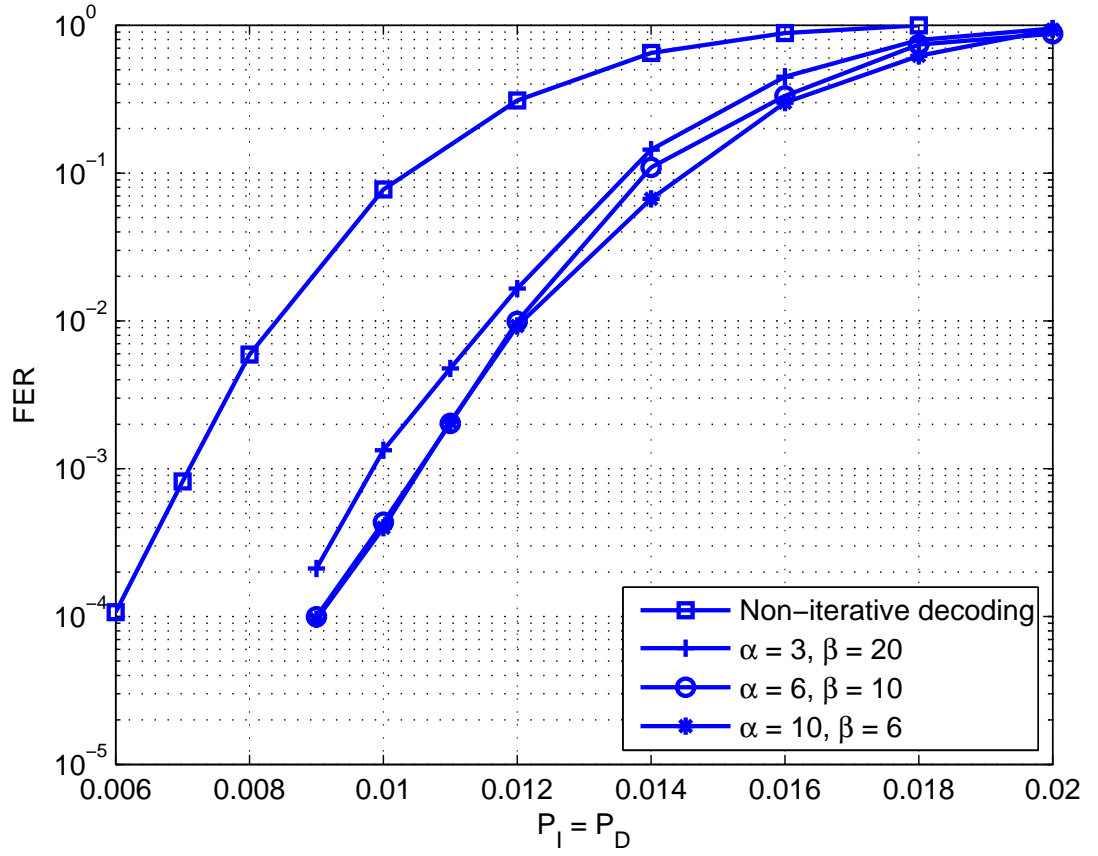


Figure 3.9: FER performance under iterative and non-iterative decoding over the DIDS channel with inner decoder A for $L = 0$.

3.4 Simulation Results

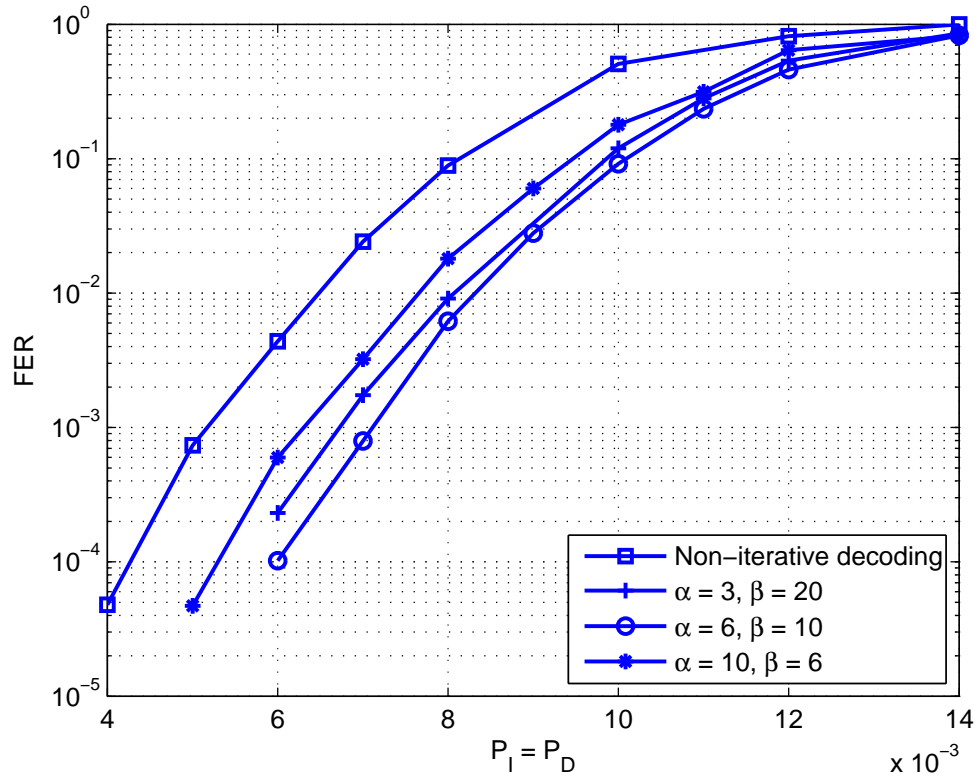


Figure 3.10: FER performance under iterative and non-iterative decoding over the DIDS channel with inner decoder C for $L = 0$.

3.4 Simulation Results

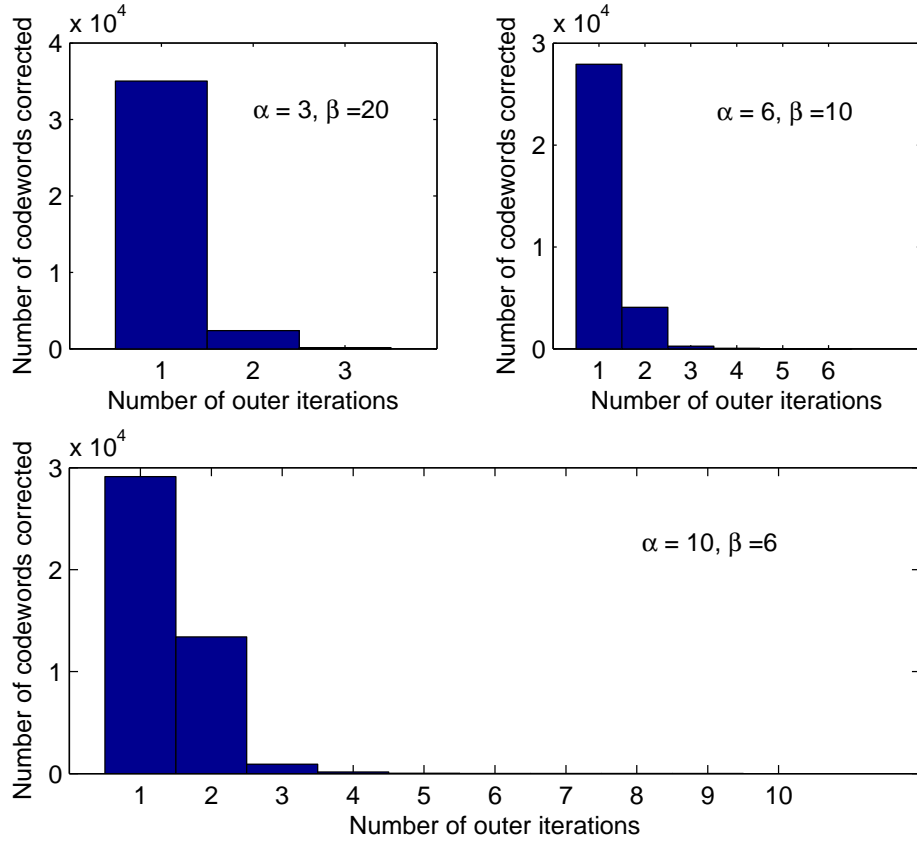


Figure 3.11: Number of codewords corrected vs. Number of outer iterations performed with inner decoder A for $P_I = P_D = 0.01$ and $L = 0$.

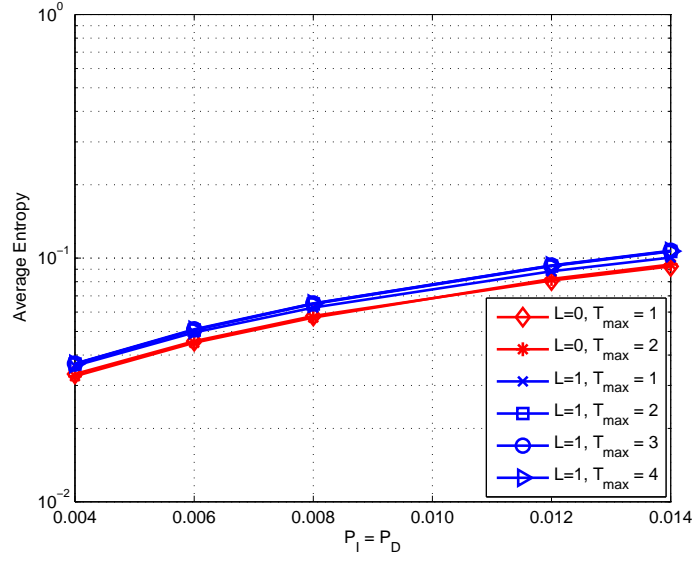
3.4 Simulation Results

estimates of the outer code symbols generated by inner decoder B by computing the average entropy of its output likelihoods $\Pr(\mathbf{Y}|c_i)$. Fig. 3.12(a) plots the average entropy of these likelihoods against $P_I = P_D$ for $1 \leq T_{max} \leq 2L + 2$ and $L = 0, 1$. As these plots show, setting $T_{max} = 1$ does not significantly affect the quality of the outer code symbols estimates. Fig. 3.12(b) shows the FER performance we obtained for $1 \leq T_{max} \leq 2L + 2$, $L = 0, 1$ and $(\alpha, \beta) = (1, 60)$. Evidently, setting $T_{max} = 1$ does not have a significant impact on performance. In view of Fig. 3.12(a), this is not surprising.

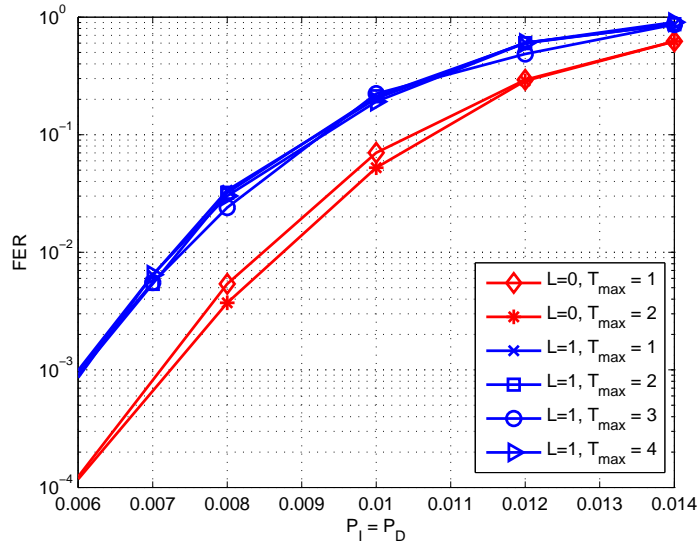
Since independent and uniformly distributed (i.u.d) input process is assumed in our simulations, we investigate the symmetric information rate (SIR) [30] of the DIDS channel, which is a channel capacity lower bound obtained by assuming i.u.d input to a channel. A detailed derivation and discussion on the lower and upper channel capacity bounds for the DIDS channel with stationary and ergodic (SaE) input processes is given in Appendix A. In Fig. 3.13, we present the SIR for the DIDS channel with $L = 0, 1$ and SIR upper and lower bounds for $L = 2$. As this figure shows, increasing L from 0 to 1 significantly reduces the SIR while further increasing L from 1 to 2 does not cause as significant a loss in SIR, which implies that further reduction in SIR due to the increase in L actually decreases for larger values of L . We also observe that the loss in SIR caused by increasing L is negligible when insertion/deletion error rates are small (e.g., $\leq 10^{-2}$), which implies that a large L may be efficiently handled by employing appropriate codes with only a slight reduction in the code rate especially when the insertion and deletion rates are relatively low. Further, we observe that the SIR for $L = 0, 1$ decreases dramatically by increasing $P_I = P_D$ from 0 to about 0.01. This coincides with the waterfall region for the performance of DM coding scheme shown in Fig. 3.12(b).

To conclude this section, we report in Fig. 11, the FER performance under iterative decoding with inner decoder B for $T_{max} = 1$, $L = 0, 1, \dots, 5$ and $(\alpha, \beta) =$

3.4 Simulation Results



(a)



(b)

Figure 3.12: (a) Average entropy of the likelihoods $\Pr(\mathbf{Y}|c_i)$ generated by inner decoder B, as a function of $P_I = P_D$, for $1 \leq T_{max} \leq 2L + 2$ and $L = 0, 1$; (b) FER performance under non-iterative decoding with inner B for the different values of T_{max} and L considered in part (a).

3.4 Simulation Results

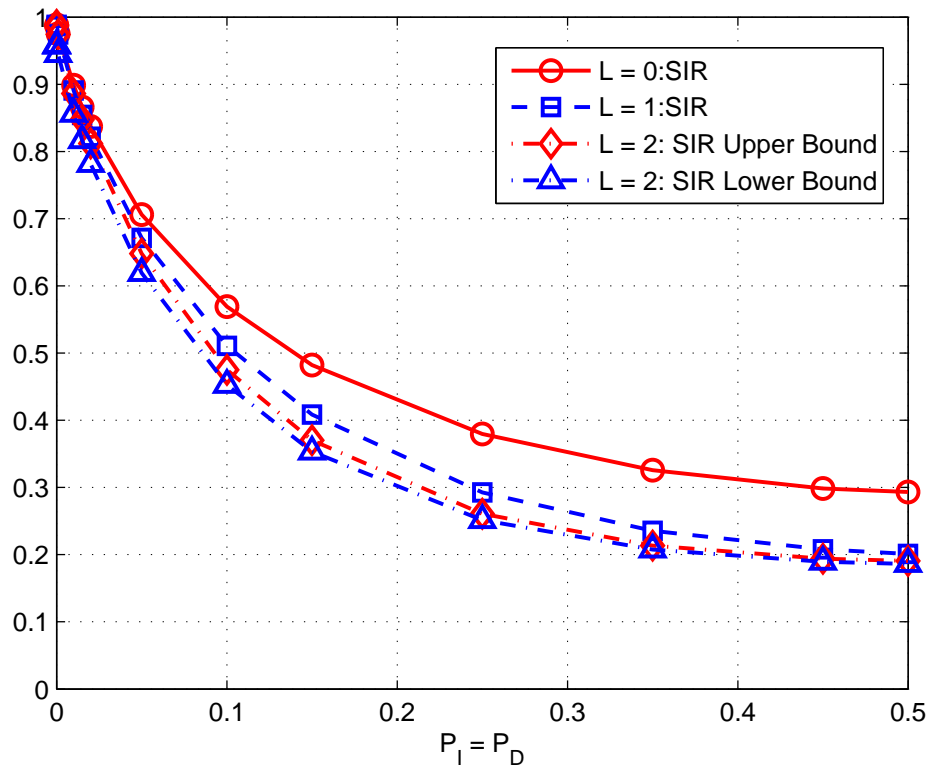


Figure 3.13: Symmetric information rate for the DIDS channel with independent and uniformly distributed input for $L = 0, 1, 2$.

3.5 Conclusion

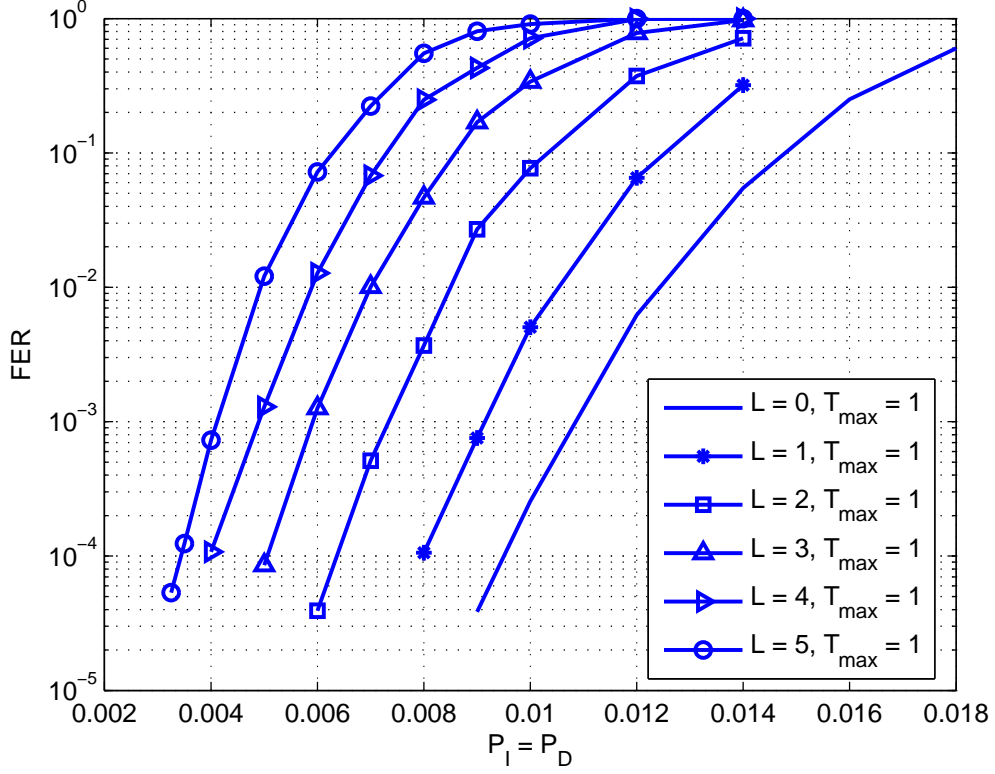


Figure 3.14: FER performance under iterative decoding with inner decoder B for $L = 0, 1, 2, 3, 4, 5$, $T_{\max} = 1$ and $(\alpha, \beta) = (10, 10)$.

(10, 10). Fig. 11 shows that for low insertion/deletion rates (e.g. $\leq 10^{-3}$) and short burst error lengths (i.e., ≤ 5) before and after a synchronization error, FERs below 10^{-5} are achievable with inner decoder B under iterative decoding.

3.5 Conclusion

We have proposed a DIDS channel model, which consists of a ternary Markov channel and a two-state BSC, to mimic the write channel of a BPMR system. The ternary Markov state channel produces insertions and deletions that occur in pairs such that the inserted bit is the same as the last input bit, while the two-state BSC generates substi-

3.5 Conclusion

tution errors that occur randomly, as well as in bursts in the vicinity of synchronization errors. We have further modified the inner decoder of the DM construction to make it applicable to our channel model. With the reduced-complexity variant of our modified inner decoder and its ability to accept soft information from the outer decoder, our investigations show that DM construction is a promising coding scheme for the DIDS channel where synchronization errors are relatively sparse and burst error lengths are relatively short. To complete the investigation, the channel capacity lower bounds of the DIDS channel are also investigated and shown.

Chapter 4

Detection-Decoding on Rectangular BPMR Channels with Written-In Error Correction and ITI Mitigation

Recall, a BPMR channel can be modeled as a concatenation of two independent sub-channels – a noisy write channel and a PR read channel. In Chapter 3, we have proposed the DIDS channel model to mimic the write process found in an actual BPMR system. To protect data from WIEs, the DM coding scheme was applied to the DIDS channel with a modified inner decoding algorithm. For simplicity, the read channel was assumed to have sufficiently high SNR such that the read channel detector can compensate for all impairments introduced in the readback process. In other words, the read channel was assumed to be perfect without any noise. However, this assumption is not realistic and raising the SNR alone does not necessarily reduce the effects of ISI, ITI and media noise [29, 34, 60]. In this chapter, we hence investigate the error performance of the DM coding scheme with various read channel detection schemes on BPMR write-read channels.

As very high areal densities require the track pitch to be very small, ITI arises as

4.1 Two-Dimensional Pulse response of Isolated Bit Island

another impairment besides ever-increasing ISI, which if not well compensated, will significantly degrade the performance of the readback process. ITI and ISI form the 2D interference in BPMR read process, hence the 2D response of an isolated bit island is required to model the 2D interference. Although the actual pulse response is only known by only a few HDD manufacturers, researchers have developed methods to obtain the numerical 2D pulse response by applying 3D reciprocity integral with respect to the magnetic potential of a magneto-resistive (MR) or giant magneto-resistive (GMR) head located directly over the center of an island [62, 63, 97].

Recall that ITI in staggered BPMR is reduced compared to that in rectangular BPMR at the same areal density, for the bits in staggered BPMR are not aligned with the bits in neighboring tracks. However, the presence of WIEs is a common challenge faced by both BPMR systems. For simplicity, we first investigate in this chapter the detection and decoding on rectangular BPMR channels with WIE correction and ITI mitigation. The investigation of detection and decoding on staggered BPMR channels with WIE correction and ITI mitigation will be presented in the next chapter.

The remainder of this chapter is organized as follows. First, the method to model the 2D pulse response of an individual bit island will be reviewed. Further, we will develop detection-decoding schemes to recover data encoded by the DM coding scheme on rectangular BPMR write-read channels, while the channel detection schemes considered range from SE detection to MTD with 2D equalization.

4.1 Two-Dimensional Pulse response of Isolated Bit Island

To obtain the 2D pulse response of an isolated island, we follow the method proposed in [63] and consider the 3D geometry of a GMR/MR read head being centered directly

4.1 Two-Dimensional Pulse response of Isolated Bit Island

over a square island of length a and thickness σ , as illustrated in Fig. 4.1. The perpendicular magnetization of the island is assumed to be uniform with strength M . The read head consists of two side shields and a sensing element of length L and width W . The sensing element is assumed to have semi-infinite height and unit magnetic potential. The flight height of the sensing element over the surface of the magnetic island is denoted by d . The two non-magnetic shields are placed at a distance of G from the sensing element and assumed to have semi-infinite dimensions in both along-track and across-track directions to completely shield the sensing element from stray magnetic flux. The SUL which was introduced in PMR to allow the use of a stronger write field is also considered for BPMR, which is assumed to have semi-infinite dimensions coupled with infinite magnetic permeability. As shown in Fig. 4.1, the influence of SUL in the magnetic flux can be modeled as a mirror image of the read sensor beneath the island [63]. In Fig. 4.1, x, y, z represent the along-track, perpendicular and across-track directions, respectively.

The voltage of the readback signal $V(x, z)$ yielded by the MR/GMR element sensing the magnetization of the individual island is proportional to the 2D magnetic flux $\phi(x, z)$ injected into the sensor at its air bearing surface (ABS), i.e., $V(x, z) = C\phi(x, z)$ where C is a constant.

The 2D magnetic flux $\phi(x, z)$ can be computed by a 3D evaluation of the reciprocity integral, such that

$$\phi(x, z) = \frac{\mu_0}{i} \int_{-\infty}^{\infty} d\tilde{x} \int_d^{d+\delta} d\tilde{y} \int_{-\infty}^{\infty} d\tilde{z} \left[\Psi(x, y, z) \frac{\partial M_y(\tilde{x} - x, \tilde{y}, \tilde{z} - z)}{\partial \tilde{y}} \right] \quad (4.1)$$

where μ_0 is the permeability of free space, i is the current in the imaginary coil, $\Psi(x, y, z)$ is the magnetic potential. The perpendicular magnetization of the medium M_y is limited to the areal of the island, i.e.,

$$M_y = \begin{cases} M, & \text{when } -0.5a \leq x, z \leq 0.5a, \sigma \leq y \leq \sigma + d \\ 0, & \text{otherwise.} \end{cases} \quad (4.2)$$

4.1 Two-Dimensional Pulse response of Isolated Bit Island

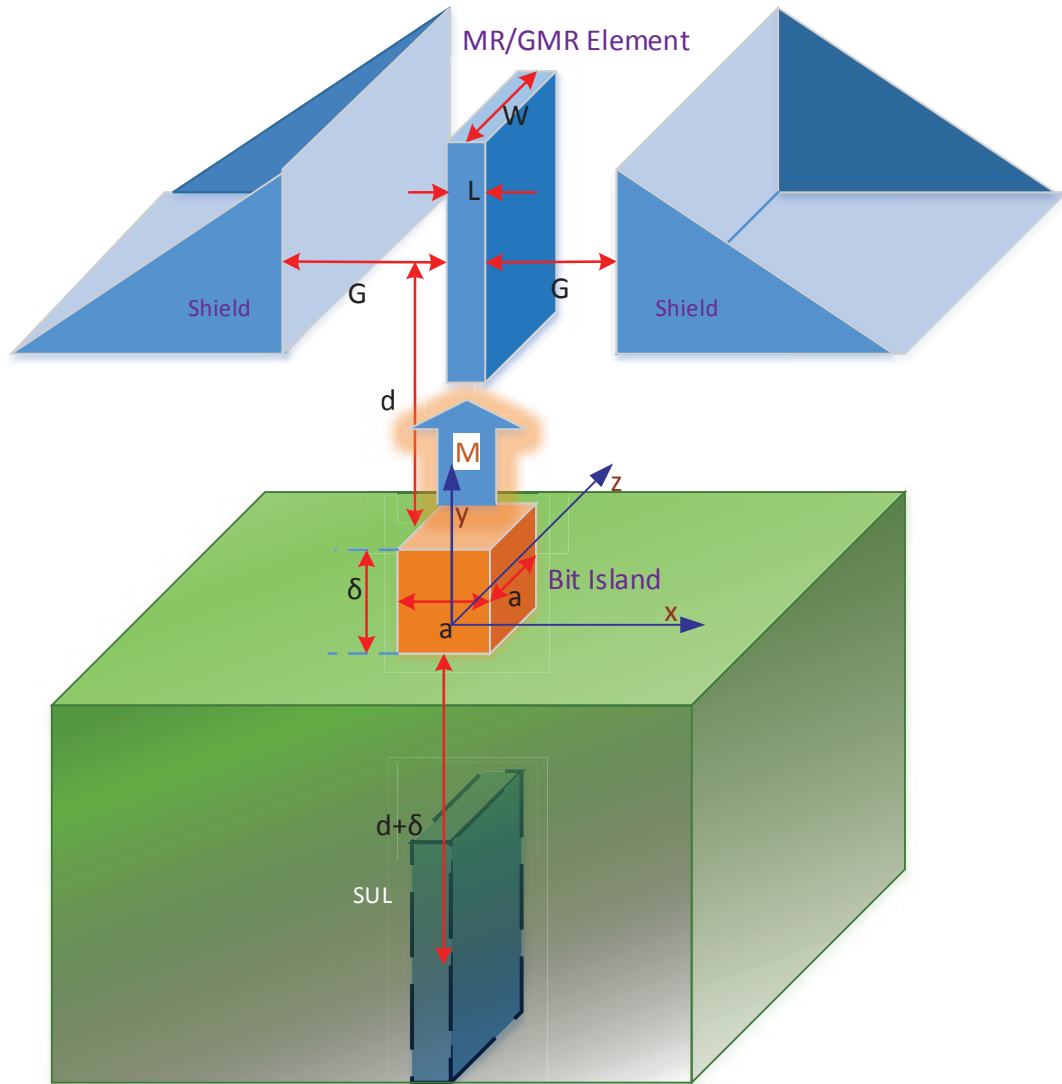


Figure 4.1: Geometry of MR/GMR read head sensing an individual square island of length a and thickness σ .

4.1 Two-Dimensional Pulse response of Isolated Bit Island

Hence, $\frac{\partial M_y(\tilde{x}-x, \tilde{y}, \tilde{z}-z)}{\partial \tilde{y}}$ in (4.1) is simply two impulse functions. Consider the counter affect caused by the mirror image of the read head, (4.1) can be computed as

$$\phi(x, z) = \frac{\mu_0}{i} \int_{-\infty}^{\infty} d\tilde{x} \int_{-\infty}^{\infty} d\tilde{z} \{ M(\tilde{x} - x, \tilde{z} - z) [\Psi(\tilde{x}, \tilde{y} = d, \tilde{z}) - \Psi(\tilde{x}, \tilde{y} = d + 2\delta, \tilde{z})] \} \quad (4.3)$$

According to [52], the magnetic potential $\Psi(x, y, z)$ is computed by

$$\Psi(x, y, z) = \frac{y}{2\pi} \int_{-\infty}^{\infty} \int_{-\infty}^{\infty} \frac{\Psi_s(\tilde{x}, \tilde{z})}{[(x - \tilde{x})^2 + y^2 + (z - \tilde{z})^2]^{1.5}} d\tilde{x} d\tilde{z} \quad (4.4)$$

where Φ_s is the magnetic potential on the head surface and can be approximated by [97]

$$\Psi_s(x, z) = \begin{cases} (G + 0.5L + x)/G & \text{if } -G - 0.5L \leq x < -0.5L, -0.5W \leq z < 0.5W \\ 1 & \text{if } -0.5L \leq x < -0.5L, -0.5W \leq z < 0.5W \\ (G + 0.5L - x)/G & \text{if } 0.5L \leq x < G + 0.5L, -0.5W \leq z < 0.5W \\ 0 & \text{elsewhere.} \end{cases} \quad (4.5)$$

Then, (4.4) has a closed form expression as follows [98]:

$$\begin{aligned} & \Psi(x, y, z) \\ = & \left(\left\{ \frac{y}{4\pi G} \log \left[\frac{R + (z - \tilde{z})}{R - (z - \tilde{z})} \right] + \frac{G + 0.5L + x}{2\pi G} \tan^{-1} \left[\frac{(z - \tilde{z})(x - \tilde{x})}{yR} \right] \right\} \Big|_{\tilde{x}=-G-0.5L}^{-0.5L} \right. \\ & + \frac{1}{2\pi} \tan^{-1} \left[\frac{(z - \tilde{z})(x - \tilde{x})}{yR} \right] \Big|_{\tilde{x}=-0.5L}^{0.5L} \\ & \left. + \left\{ -\frac{y}{4\pi G} \log \left[\frac{R + (z - \tilde{z})}{R + (z - \tilde{z})} \right] + \frac{G + 0.5L - x}{2\pi G} \tan^{-1} \left[\frac{(z - \tilde{z})(x - \tilde{x})}{yR} \right] \right\} \Big|_{\tilde{x}=0.5L}^{0.5L+G} \right) \Big|_{\tilde{z}=-0.5W}^{0.5W} \end{aligned} \quad (4.6)$$

where $R = \sqrt{(x - \tilde{x})^2 + y^2 + (z - \tilde{z})^2}$.

Substitute (4.6) into (4.1), we can compute the 2D magnetic flux $\phi(x, z)$ numerically for any head and medium configuration represented by Fig. 4.1.

It has been observed in [63] that the 2D pulse response for some head and medium configurations can be well fitted by a 2D Gaussian pulse

$$h(x, z) = A \exp \left(-\frac{1}{2} c^2 \left(\frac{x^2}{PW_{50-along}^2} + \frac{z^2}{PW_{50-across}^2} \right) \right) \quad (4.7)$$

4.2 Rectangular BPMR Channel Model

where A is the peak amplitude, $c = \sqrt{2 \ln 2}$, $PW_{50\text{-}along}$, $PW_{50\text{-}across}$ are the widths of the numerical replay response of each island at half the peak amplitude in the along-track and cross-track directions, respectively. This approximation can dramatically reduce the computational-complexity required for modeling the read channel.

4.2 Rectangular BPMR Channel Model

The BPMR channel model considered here is a composite channel consisting of a DIDS write channel introduced in Section 3.2 followed by a 2D-equalized read channel with 2D optimized GPR target, as shown in Figs. 4.2(a) and 4.2(b), respectively. In this thesis, we focus on the mitigation of 2D ISI in the presence of WIEs and electronic noise, hence we simplify our channel model by assuming that there is no track mis-registration (TMR) or media noise. In Fig. 4.2(a), $X_i \in \{-1, +1\}$ is the data intended to be recorded while a_i is the actual data written on the disk. In Fig. 4.2(b), $a_{j,k} \in \{-1, +1\}$ represents the k th bit recorded on track j with track 0 being the center track. Tracks $-2, -1, 0, 1$ and 2 are sensed with three read heads on tracks $-1, 0$ and 1 . In addition, \mathbf{f} , \mathbf{w}_0 (resp., \mathbf{g} , \mathbf{w}_1) are the optimized GPR target and equalizer for the center track (resp., sidetracks), respectively. The symmetry of the read channel is exploited to simplify the channel model whereby instead of considering each individual track, we consider the aggregation of tracks -1 and 1 , and -2 and 2 , by defining: $b_k = a_{-1,k} + a_{1,k}$ and $c_k = a_{-2,k} + a_{2,k}$, where $b_k, c_k \in \{-2, 0, +2\}$. We refer to tracks -1 and 1 as the *inner sidetracks* and tracks -2 and 2 as the *outer sidetracks*. Finally, r_k is the readback signal generated by the equalizer corresponding to the bit $a_{0,k}$ on the desired center track.

4.2 Rectangular BPMP Channel Model

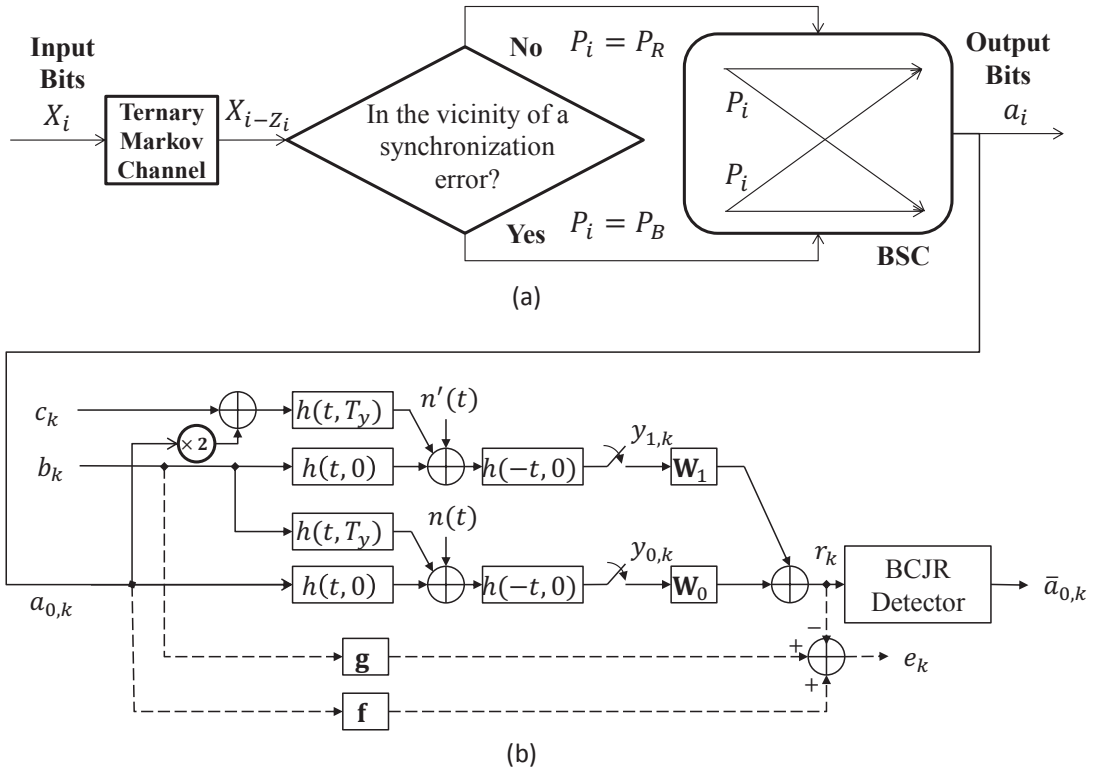


Figure 4.2: (a) DIDS write channel model; (b) Rectangular read channel model with MTD and 2D equalization.

4.3 Read Channel Equalization and Detection

For the read channel model, we adopt the same medium and head designs used in [63] and the pulse response of the length- l square island can be approximated very well by the 2D Gaussian response of (4.7). It has been shown in [63] that under the same medium and head designs, the peak amplitude A , $PW_{50\text{-along}}$ and $PW_{50\text{-across}}$ all increase with l . Further, according to [49], the response of tracks 1 and -1 that contributes to the ITI sensed during the detection of the center track is $h(t, T_y) = h(t, -T_y)$. When the size of the island is fixed, the level of ISI and ITI can be adjusted by varying island periods T_x in the along-track direction and T_y in the across-track direction, and different areal densities can be achieved in this way. Following [49], the level of ITI and ISI are measured by the side-track amplitude $A_s = h(0, T_y)$ and the normalized pulse width $PW_N = PW_{50\text{-along}}/T_x$, respectively.

The electronic noise in the read channel is modelled by AWGN $n(t) \sim N(0, \sigma^2)$ and A^2/σ^2 is defined as the SNR. To maximize the SNR, the matched filter $h(-t, 0)$ for the center track replay response is utilized. Since b_k represents the sum of two symmetric bits recorded on inner sidetracks, the electronic noise $n'(t)$ in the detection of b_k is actually the sum of two identical and independent copies of AWGN $n(t)$, i.e., $n'(t) \sim N(0, 2\sigma^2)$. Further, since each inner sidetrack is surrounded by the center track and one of the outer sidetracks, the ITI affecting the detection of b_k is produced by the convolution of the sum $2a_{0,k} + c_k$ and $h(t, \pm T_y)$, as indicated in Fig. 4.2(b).

Following [47], the causal optimized 2D GPR target \mathbf{f} , \mathbf{g} and the 2D equalizer components \mathbf{w}_0 and \mathbf{w}_1 can be jointly computed by minimizing the mean-squared error

$$E[e_k^2] = E[(\mathbf{y}_1^T \mathbf{w}_1 + \mathbf{y}_0^T \mathbf{w}_0 - \mathbf{b}^T \mathbf{g} - \mathbf{a}_0^T \mathbf{f})^2] \quad (4.8)$$

where

$$\mathbf{y}_1 = [y_{1,k+Lw1}, \dots, y_{1,k-Lw1}]^T, \quad \mathbf{y}_0 = [y_{0,k+Lw0}, \dots, y_{0,k-Lw0}]^T,$$

4.4 Channel Detection and Decoding

$$\begin{aligned}\mathbf{w}_1 &= [w_{1,-Lw1}, \dots, w_{1,Lw1}]^T, \quad \mathbf{w}_0 = [w_{0,-Lw0}, \dots, w_{0,Lw0}]^T, \\ \mathbf{b} &= [b_k, \dots, b_{k-L_g+1}]^T, \quad \mathbf{a}_0 = [a_{0,k}, \dots, a_{0,k-L_f+1}]^T, \\ \mathbf{g} &= [g_0, \dots, g_{L_g-1}]^T, \quad \mathbf{f} = [f_0, \dots, f_{L_f-1}]^T.\end{aligned}$$

Defining $\mathbf{w} = [\mathbf{w}_0^T \ \mathbf{w}_1^T]^T$, $\mathbf{y} = [\mathbf{y}_0^T \ \mathbf{y}_1^T]^T$, $\mathbf{t} = [\mathbf{f}^T \ \mathbf{g}^T]^T$, $\mathbf{a} = [\mathbf{a}_0^T \ \mathbf{b}^T]^T$, (4.8) can be expressed as $E[e_k^2] = E[(\mathbf{w}^T \mathbf{y} - \mathbf{t}^T \mathbf{a})^2]$. By minimizing $E[e_k^2]$ under the monic constraint $f_0 = 1$ [47], we have

$$\begin{aligned}\mathbf{t} &= \lambda(\mathbf{R}_a - \mathbf{R}_{\mathbf{y},\mathbf{a}}^T \mathbf{R}_{\mathbf{y}}^{-1} \mathbf{R}_{\mathbf{y},\mathbf{a}})^{-1} \mathbf{I} \\ \mathbf{w} &= \mathbf{R}_{\mathbf{y}}^{-1} \mathbf{R}_{\mathbf{y},\mathbf{a}} \mathbf{t}\end{aligned}$$

where $\mathbf{R}_a = E\{\mathbf{a}\mathbf{a}^T\}$, $\mathbf{R}_{\mathbf{y}} = E\{\mathbf{y}\mathbf{y}^T\}$, $\mathbf{R}_{\mathbf{y},\mathbf{a}} = E\{\mathbf{y}\mathbf{a}^T\}$ and $\mathbf{I} = [1, 0, \dots, 0]^T$, $\lambda = 1/\mathbf{I}^T(\mathbf{R}_a - \mathbf{R}_{\mathbf{y},\mathbf{a}}^T \mathbf{R}_{\mathbf{y}}^{-1} \mathbf{R}_{\mathbf{y},\mathbf{a}})^{-1} \mathbf{I}$.

The above 2D equalization with 2D optimized GPR target technique (which we refer to as 2D2D equalization as in [49]) cannot effectively remove the ITI on its own, as taking into account the unknown data on the sidetracks actually increases the amount of noise in the center track detector. MTD with 2D2D equalization, as proposed in [49], however avoids this problem. This scheme detects the inner sidetracks first and utilizes the resulting *a posteriori* information as *a priori* information in the 2D2D detection of the center track.

Note that the 2D2D equalization becomes joint-track equalization (JE) investigated in [49] when the channel is only equalized by a 1D GPR target \mathbf{w}_0 , i.e., setting $\mathbf{w}_1 = [0, \dots, 0]^T$. In addition, the JE will be further simplified to become SE when the channel is equalized by \mathbf{w}_0 to the 1D GPR target \mathbf{f} only, i.e., $\mathbf{g} = [0, \dots, 0]^T$.

4.4 Channel Detection and Decoding

In this section, we consider the problem of combining the read channel detector and the DM inner decoder. By interpreting the inner decoder as a detector for the write

4.4 Channel Detection and Decoding

channel, one approach is to detect the read and write channels sequentially. With this approach, there are two possibilities: the BCJR detector output could be quantized or left unquantized. Alternatively, the read and write channels could be jointly detected. We hence will consider three different read-write channel detection strategies below, starting with separate read-write channel detection with quantized BCJR detector outputs, followed by joint read-write channel detection, and finally, separate read-write channel detection with unquantized BCJR detector outputs. Applying iterative decoding to improve performance will also be discussed.

4.4.1 BCJR Detection with Binary-Input-Inner-Decoding

Since the components of the 2D GPR target \mathbf{f} and \mathbf{g} have binary input $a_{0,k}$ and ternary input b_k , respectively, the trellis on which the BCJR detector performs has in total $2^{L_f-1} \times 3^{L_g-1}$ states. Each state S_k corresponds to a unique combination of the two sequences $[a_{0,k-1}, \dots, a_{0,k-L_f+1}]$ and $[b_{k-1}, \dots, b_{k-L_g+1}]$, and is connected to six possible next states with each state transition corresponding to one of the six possible values of the pair $\{a_{0,k}, b_k\}$. Further, as noted in Section. 3.2, the maximum absolute difference between the number of bits leaving and entering the DIDS channel is 1. Thus, by taking the readback sequence $\mathbf{r} = [r_{-1}, \dots, r_{Nn}]$ into account in the BCJR detector, the need to identify the boundaries of consecutive readback sequences can be avoided.

The *a posteriori* probability of $\{a_{0,k}, b_k\}$ is computed by the BCJR algorithm as

$$P(a_{0,k}, b_k | \mathbf{r}) = \frac{1}{P(\mathbf{r})} \sum_{S_k} \alpha_k(S_k) \cdot \gamma(S_k, S_{k+1}) \cdot \beta_{k+1}(S_{k+1}) \quad (4.9)$$

where

$$\alpha_k(S_k) = \sum_{S_{k-1}} \alpha_{k-1}(S_{k-1}) \gamma(S_{k-1}, S_k) \quad (4.10)$$

$$\beta_k(S_k) = \sum_{S_{k+1}} \beta_{k+1}(S_{k+1}) \gamma(S_k, S_{k+1}) \quad (4.11)$$

4.4 Channel Detection and Decoding

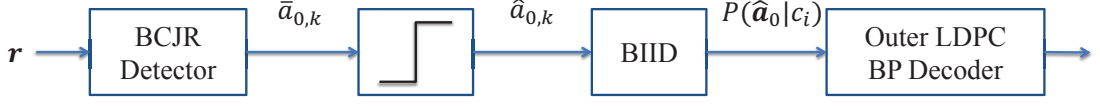


Figure 4.3: The BCJR-BIID detection-decoding scheme.

are the forward and backward state probabilities, respectively. The trellis state transition probability $\gamma(S_k, S_{k+1})$ is computed by

$$\gamma(S_k, S_{k+1}) = P(a_{0,k})P(b_k)P(r_k|a_{0,k}, b_k, S_k) \quad (4.12)$$

where $P(a_{0,k}) = 0.5$, $P(b_k)$ is the *a priori* information of the data on the sidetracks, and

$$P(r_k|a_{0,k}, b_k, S_k) = \frac{1}{\sqrt{2\pi\lambda}} \exp\left[-\frac{(r_k - \mathbf{b}^T \mathbf{g} - \mathbf{a}_0^T \mathbf{f})^2}{2\lambda}\right]. \quad (4.13)$$

The *a posteriori* probability of $a_{0,k}$ can then be computed as

$$P(a_{0,k}|\mathbf{r}) = \sum_{b_k} P(a_{0,k}, b_k|\mathbf{r}). \quad (4.14)$$

Similarly, $P(a_{0,k}|\mathbf{r})$ in SE can be obtained by ignoring b_k and \mathbf{g} in (4.9 – 4.13).

To deal with the errors remaining in the detector output, including substitution errors resulting from imperfect read channel detection and WIEs, we can employ the BIID to further process the detector output. Since the BIID can only take in binary input, the detector output first needs to be 1-bit quantized, as depicted in Fig. 4.3, where

$$\bar{a}_{0,k} = \log \frac{P(a_{0,k} = 1|\mathbf{r})}{P(a_{0,k} = -1|\mathbf{r})} \quad (4.15)$$

is the log-likelihood ratio (LLR) of $a_{0,k}$ and its corresponding quantized value is

$$\hat{a}_{0,k} = \begin{cases} -1 & \text{if } \bar{a}_{0,k} \leq 0 \\ 1 & \text{if } \bar{a}_{0,k} > 0. \end{cases}$$

4.4 Channel Detection and Decoding

The BIID is almost the same as the inner decoding algorithm proposed in Section 3.3.1 with input sequence \mathbf{Y} replaced by $\hat{\mathbf{a}}$, except that (3.5) is now computed as

$$P(\hat{a}_{0,j}|X_i) = \begin{cases} \mathcal{P}_j & \text{if } \hat{a}_{0,j} \neq X_i \\ 1 - \mathcal{P}_j & \text{otherwise} \end{cases} \quad (4.16)$$

where \mathcal{P}_j is the overall substitution error rate at the quantizer's output corresponding to the channel input X_j . Similar to [99, Equation (1)], \mathcal{P}_j is given by

$$\mathcal{P}_j = (1 - p_d)P_j + p_d(1 - P_j)$$

where P_j is the corresponding crossover probability of the two-state BSC in Fig. 4.2(a) and p_d is the bit error rate (BER) of the detector obtained via the simulations proposed in [49].

Obviously, quantization inevitably causes information loss. Moreover, it blindly eliminates the correlations among the BCJR output LLRs. Therefore, a significant performance degradation is expected, particularly at low SNRs when the soft output from the detector is highly unreliable. We nevertheless investigate the performance offered by this simple approach to provide a benchmark against which the performance of the detection-inner-decoding strategies presented in Sections 4.4.2 and 4.4.3 will be compared.

4.4.2 Joint Detection-Inner-Decoding

The sub-optimality of the BCJR-BIID motivates the development of the *joint* detection-inner-decoding (JDD) algorithm, which uses a single forward-backward algorithm to jointly detect the write and read channels. This algorithm simultaneously considers the SCSWs of the DIDS channel and the trellis of the read channel detection, and directly processes the output sequence \mathbf{r} from the equalizer, as shown in Fig. 4.4. Hence, quantization is avoided and the correlations among the BCJR output LLRs are preserved and exploited.

4.4 Channel Detection and Decoding

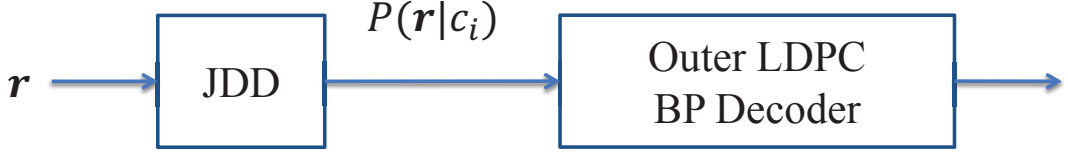


Figure 4.4: The JDD detection-decoding scheme.

With a slight abuse of notation, the forward, backward and middle metrics of the JDD are also denoted as $F_i(\cdot)$, $B_i(\cdot)$ and $M_i(\cdot)$, respectively. Then, $P(\mathbf{r}|c_i)$ is computed by

$$P(\mathbf{r}|c_i) = \sum_{\rho_1, \rho_2} F_i(\rho_1) M_i(\rho_1, \rho_2, c_i) B_i(\rho_2) \quad (4.17)$$

where

$$\begin{aligned} F_i(\rho_1) &= P(\mathbf{r}_{f-1(\mathbf{v}_{-1})}^{f_{in-1}(\rho_1)}, \mathbf{v}_{in-1} = \rho_1) \\ &= \sum_{\rho_0, c_{i-1}} F_{i-1}(\rho_0) M_{i-1}(\rho_0, \rho_1, c_{i-1}) P(c_{i-1}) \end{aligned} \quad (4.18)$$

$$\begin{aligned} B_i(\rho_2) &= P(\mathbf{r}_{f(i+1)n-1(\rho_2)+1}^{f_{Nn-1}(\mathbf{v}_{Nn-1})}, \mathbf{v}_{(i+1)n-1} = \rho_2, \mathbf{r}_{-1}^{f(i+1)n-1(\rho_2)}) \\ &= \sum_{\rho_3, c_{i+1}} B_{i+1}(\rho_3) M_{i+1}(\rho_2, \rho_3, c_{i+1}) P(c_{i+1}) \end{aligned} \quad (4.19)$$

Denoting $\mathbf{r}_{f-1(\mathbf{v}_{-1})}^{f_{in-1}(\rho_1)}$, $\mathbf{r}_{f(i+1)n-1(\rho_2)+1}^{f(i+1)n-1(\rho_2)}$ and the possible bit sequence $\mathbf{a}_{f_{in-1}(\rho_1)+1}^{f(i+1)n-1(\rho_2)}$ recorded on the center track corresponding to $\mathbf{r}_{f_{in-1}(\rho_1)+1}^{f(i+1)n-1(\rho_2)}$ by \mathbf{r}_{F_i} , \mathbf{r}_{M_i} and \mathbf{a}_{M_i} , respectively, the middle metric $M_i(\rho_1, \rho_2, c_i)$ can be computed as

$$\begin{aligned} &M_i(\rho_1, \rho_2, c_i) \\ &= P(\mathbf{r}_{M_i}, \mathbf{v}_{(i+1)n-1} = \rho_2 | \mathbf{r}_{F_i}, \mathbf{v}_{in-1} = \rho_1, c_i) \\ &= \sum_{\mathbf{a}_{M_i}} P(\mathbf{r}_{M_i}, \mathbf{a}_{M_i}, \mathbf{v}_{(i+1)n-1} = \rho_2 | \mathbf{r}_{F_i}, \mathbf{v}_{in-1} = \rho_1, c_i) \\ &= \sum_{\mathbf{a}_{M_i}} \left[\begin{aligned} &P(\mathbf{r}_{M_i} | \mathbf{a}_{M_i}, \mathbf{r}_{F_i}, \mathbf{v}_{in-1} = \rho_1, \mathbf{v}_{(i+1)n-1} = \rho_2) \\ &\cdot P(\mathbf{a}_{M_i}, \mathbf{v}_{(i+1)n-1} = \rho_2 | \mathbf{v}_{in-1} = \rho_1, c_i) \end{aligned} \right] \end{aligned} \quad (4.20)$$

4.4 Channel Detection and Decoding

where

$$\begin{aligned}
 & P(\mathbf{r}_{M_i} | \mathbf{a}_{M_i}, \mathbf{r}_{F_i}, \mathbf{v}_{in-1} = \rho_1, \mathbf{v}_{(i+1)n-1} = \rho_2) \\
 &= \sum_{S_{f_{in-1}(\rho_1)+1}} \left[\begin{array}{c} P(\mathbf{r}_{M_i} | S_{f_{in-1}(\rho_1)+1}, \mathbf{a}_{M_i}) \\ \cdot P(S_{f_{in-1}(\rho_1)+1} | \mathbf{r}_{F_i}) \end{array} \right] \quad (4.21)
 \end{aligned}$$

The probability $P(S_{f_{in-1}(\rho_1)+1} | \mathbf{r}_{F_i})$ in (4.21) can be computed using the BCJR forward state probability of (4.10), such that

$$P(S_{f_{in-1}(\rho_1)+1} | \mathbf{r}_{F_i}) = \frac{\alpha_{f_{in-1}(\rho_1)+1}(S_{f_{in-1}(\rho_1)+1})}{\sum_{S_{f_{in-1}(\rho_1)+1}} \alpha_{f_{in-1}(\rho_1)+1}(S_{f_{in-1}(\rho_1)+1})}.$$

Note that the probability $P(\mathbf{a}_{M_i}, \mathbf{v}_{(i+1)n-1} = \rho_2 | \mathbf{v}_{in-1} = \rho_1, c_i)$ of (4.20) resembles (3.9) with $\mathbf{Y}_{f_{in-1}(\rho_1)+1}^{f_{(i+1)n-1}(\rho_2)}$ being replaced by \mathbf{a}_{M_i} , thus it can be computed using the approach described in Section 3.3.1 for computing middle metric in the DM inner decoder modified for the DIDS channel. Further, as there exists a finite number of possible $P(\mathbf{a}_{M_i}, \mathbf{v}_{(i+1)n-1} = \rho_2 | \mathbf{v}_{in-1} = \rho_1, c_i)$ for a given write channel, a considerable amount of computational savings can be achieved by storing all the possible values in a LUT as in [72].

So far, the only term left undetermined is $P(\mathbf{r}_{M_i} | S_{f_{in-1}(\rho_1)+1}, \mathbf{a}_{M_i})$ in (4.21). For SE, this probability can be efficiently obtained by performing a BCJR forward pass from $S_{f_{in-1}(\rho_1)+1}$ to $S_{f_{(i+1)n-1}(\rho_2)+1}$ according to \mathbf{a}_{M_i} , since the number of states in the trellis for SE is relatively small and each trellis state transition only depends on $a_{0,k}$.

However, this probability cannot be computed in exactly the same way when JE or 2D2D detection scheme is employed, for each trellis transition now depends on the pair of inputs $\{a_{0,k}, b_k\}$ instead of just $a_{0,k}$ when SE is employed. Nevertheless, we may still mimick the same method, taking into account this difference, to compute this probability as

$$P(\mathbf{r}_{M_i} | S_{f_{in-1}(\rho_1)+1}, \mathbf{a}_{M_i}) \quad (4.22)$$

$$= \sum_{\mathbf{b}_{M_i}} P(\mathbf{b}_{M_i}) P(\mathbf{r}_{M_i} | S_{f_{in-1}(\rho_1)+1}, \mathbf{a}_{M_i}, \mathbf{b}_{M_i}) \quad (4.23)$$

4.4 Channel Detection and Decoding

where $\mathbf{b}_{M_i} = \mathbf{b}_{f_{in-1}(\rho_1)+1}^{f_{(i+1)n-1}(\rho_2)}$ is the data sequence on the inner sidetracks corresponding to \mathbf{r}_{M_i} , and $P(\mathbf{r}_{M_i} | S_{f_{in-1}(\rho_1)+1}, \mathbf{a}_{M_i}, \mathbf{b}_{M_i})$ can be obtained by setting $S_{f_{in-1}(\rho_1)+1}$ to $S_{f_{(i+1)n-1}(\rho_2)+1}$ according to $\{\mathbf{a}_{M_i}, \mathbf{b}_{M_i}\}$. It seems to be quite straightforward to compute $P(\mathbf{r}_{M_i} | S_{f_{in-1}(\rho_1)+1}, \mathbf{a}_{M_i})$ in this manner. However, we note that there are in total $6^{f_{(i+1)n-1}(\rho_2)-f_{in-1}(\rho_1)}$ possible $\{\mathbf{a}_{M_i}, \mathbf{b}_{M_i}\}$ in (4.23). Therefore, the computation of the middle metric in the JDD using (4.23) has a complexity of $O(6^n)$, which increases exponentially in n and can be prohibitively high for even a small value of n . For instance, if $n = 5$, the number of possible combinations of \mathbf{a}_{M_i} and \mathbf{b}_{M_i} that needs to be considered for each $M_i(\rho_1, \rho_2, c_i)$ ranges from 6^3 to 6^7 .

We therefore propose an alternative method to compute (4.22) with relatively lower complexity by taking advantage of the fact that \mathbf{a}_{M_i} and \mathbf{b}_{M_i} are independent of each other. Firstly, we decompose the trellis for MTD into two sub-trellises. One sub-trellis corresponds to \mathbf{f} and has 2^{L_f-1} states S_k^f , each having two outgoing branches corresponding to $a_{0,k}$, while the other corresponds to \mathbf{g} and has 3^{L_g-1} states S_k^g , each having three outgoing branches corresponding to b_k . Then, (4.22) can be computed as

$$\begin{aligned} P(\mathbf{r}_{M_i} | S_{f_{in-1}(\rho_1)+1}, \mathbf{a}_{M_i}) &= P(\mathbf{r}_{M_i} | S_{f_{in-1}(\rho_1)+1}^g, S_{f_{in-1}(\rho_1)+1}^f, \mathbf{a}_{M_i}) \\ &= P(\tilde{\mathbf{r}}_{M_i} = \mathbf{r}_{M_i} - \tilde{\mathbf{a}}_{M_i} | S_{f_{in-1}(\rho_1)+1}^g) \end{aligned} \quad (4.24)$$

where $\tilde{\mathbf{a}}_{M_i}$ is the output from the center track target \mathbf{f} with respect to the input \mathbf{a}_{M_i} and initial state $S_{f_{in-1}(\rho_1)+1}^f$. Now, we proceed to compute (4.24) via a short backward pass on the sub-trellis corresponding to \mathbf{g} , such that

$$\begin{aligned} &P(\mathbf{r}_{M_i} | \mathbf{a}_{M_i}, S_{f_{in-1}(\rho_1)+1}) \\ &= P(\tilde{\mathbf{r}}_{M_i} | S_{f_{in-1}(\rho_1)+1}^g) \\ &= \sum_{S_{f_{in-1}(\rho_1)+2}^g} \left[\begin{aligned} &P(\tilde{\mathbf{r}}_{f_{in-1}(\rho_1)+2}^{f_{(i+1)n-1}(\rho_2)} | S_{f_{in-1}(\rho_1)+2}^g) \\ &\cdot P(\tilde{\mathbf{r}}_{f_{in-1}(\rho_1)+1} | S_{f_{in-1}(\rho_1)+1}^g, S_{f_{in-1}(\rho_1)+2}^g) \\ &\cdot P(S_{f_{in-1}(\rho_1)+2}^g | S_{f_{in-1}(\rho_1)+1}^g) \end{aligned} \right] \end{aligned}$$

4.4 Channel Detection and Decoding

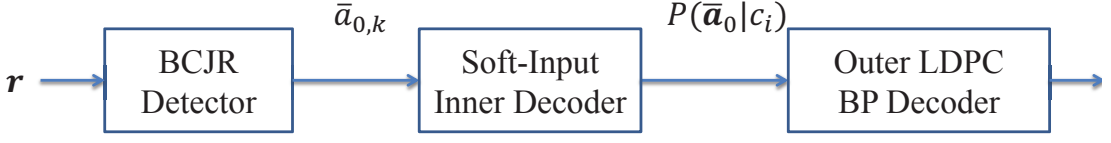


Figure 4.5: The BCJR-SIID detection-decoding scheme.

As no information is lost in the derivation of the JDD algorithm, it is expected to have an edge over the BCJR-BIID algorithm. However, this performance gain comes at the cost of relatively high computational-complexity. This motivates the detection-inner-decoding strategy described in Section 4.4.3.

4.4.3 BCJR Detection with Soft-Input-Inner-Decoding

To achieve better performance than the BCJR-BIID without the computational cost of the JDD, we propose to use a soft-input-inner-decoder (SIID) to dispense with the quantizer in the BCJR-BIID, as shown in Fig. 4.5.

With the unquantized BCJR detector output $\bar{\mathbf{a}}_0 = (\bar{a}_{-1}, \dots, \bar{a}_{N_n})$ as input, the SIID uses a similar forward-backward algorithm to that used by the BIID to compute the likelihood $P(\bar{\mathbf{a}}_0 | c_i)$ via (3.6). While (3.7) through to (3.9) remain applicable besides minor changes in notation, the conditional probability density function (PDF) $p(\bar{a}_{0,j} | X_i)$ cannot be computed in the same way that $P(\hat{a}_{0,j} | X_i)$ is computed in (3.4). For simplicity, we ignore the correlations among the soft output from the detector and compute $p(\bar{a}_{0,j} | X_i)$ using Bayes' law as

$$p(\bar{a}_{0,j} | X_i) = \frac{p(\bar{a}_{0,j}) \cdot p(X_i | \bar{a}_{0,j})}{P(X_i)}. \quad (4.25)$$

Since the LLR $\bar{a}_{0,j}$ contains the probability $P(a_{0,j} | \mathbf{r})$, we can compute $p(X_i | \bar{a}_{0,j})$ by

$$\begin{aligned} p(X_i | \bar{a}_{0,j}) &= \sum_{a_{0,j}=\pm 1} P(X_i | a_{0,j}) P(a_{0,j} | \mathbf{r}) \\ &= \sum_{a_{0,j}=\pm 1} \frac{P(X_i) P(a_{0,j} | X_i)}{P(a_{0,j})} P(a_{0,j} | \mathbf{r}). \end{aligned} \quad (4.26)$$

4.4 Channel Detection and Decoding

Substituting (4.26) into (4.25), we have

$$p(\bar{a}_{0,j}|X_i) = p(\bar{a}_{0,j}) \sum_{a_{0,j}=\pm 1} \frac{P(a_{0,j}|\mathbf{r})P(a_{0,j}|X_i)}{P(a_{0,j})} \quad (4.27)$$

where the PDF $p(\bar{a}_{0,j})$ can be determined via Monte Carlo simulation, $P(a_{0,j}) = 0.5$, and $P(a_{0,j}|\mathbf{r})$ can be obtained from (4.15). The probability $P(a_{0,j}|X_i)$ is computed in similar fashion to $P(\hat{a}_{0,j}|X_i)$ in (4.16), i.e.,

$$P(a_{0,j}|X_i) = \begin{cases} P_j & \text{if } a_{0,j} \neq X_i \\ 1 - P_j & \text{otherwise} \end{cases} \quad (4.28)$$

where P_j is the cross-over probability of the two-state BSC in Fig. 4.2(a).

Obviously, the complexity of the BCJR-SIID is slightly higher than the BCJR-BIID, but much lower than the JDD. However, this reduction in complexity does not translate into a significant performance degradation. Simulation results in Section 4.5 will show that the performance of the BCJR-SIID and the JDD are very close, and both schemes significantly outperform the BCJR-BIID, particularly at low SNRs.

4.4.3.1 Iterative Decoding

Recall that the iterative decoding framework of [72], which iteratively utilizes the extrinsic information computed by the soft-input, soft-output outer decoder to improve the *a priori* probability $P(c_i)$ involved in the computation of the forward and backward metrics of the inner decoder, was applied in Section 3.3.3 to enhance the BIID's performance on the DIDS channel. Since the BIID and SIID have essentially the same forward-backward algorithm, the same framework can be applied to the SIID to improve its performance. Further, as the JDD is also based on a forward-backward algorithm with $P(c_i)$ being used in (4.18) and (4.19), a similar iterative decoding structure can be adopted by the JDD. These facts are summarized in Fig. 4.6, where \mathbf{q} denotes the input sequence to the inner decoder or JDD, i.e., $\hat{\mathbf{a}}_0$ for the BIID, or \mathbf{r} for the JDD, and $\bar{\mathbf{a}}_0$ for the SIID.

4.4 Channel Detection and Decoding

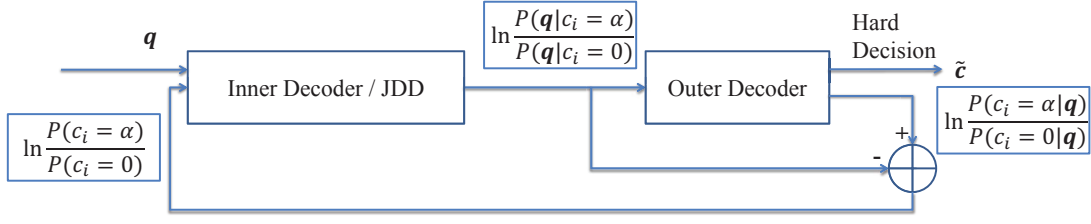


Figure 4.6: Iterative decoding framework for the BIID, JDD and SIID..

It is interesting to note that each additional iteration (after the first) between the outer decoder and inner decoder or JDD incurs the same increase in computational cost, as (i) only the forward and backward metrics $F_i(\cdot)$, $B_i(\cdot)$ are updated in each additional iteration, and (ii) the computation of these metrics in the BIID, SIID and JDD are identical. This is a plus point for iterative decoding because it is the middle metric computations, rather than the forward and backward metrics, that dominate the complexity of each detection-inner-decoding scheme.

To show that the middle metric computations dominate the complexity, we take the BIID as an example for it has the simplest middle metric computations. From (3.7) and (3.8), it can be seen that each forward and backward metric requires $q \cdot N_s$ additions and $2q \cdot N_s$ multiplications. As the middle metric is obtained via a forward pass between \mathbf{v}_{in-1} and $\mathbf{v}_{(i+1)n-1}$ while Fig. 3.5 indicates that each SCSW can lead to at least two possible SCSWs depending on the next term in the channel state sequence and current SCSW, the computation of each middle metric needs at least $2n$ additions and $4n$ multiplications. The total number of additions and multiplications needed to compute all forward and backward metrics are $2(N-1) \cdot q \cdot N_s^2$ and $4(N-1) \cdot q \cdot N_s^2$, while computing all likelihoods $P(\hat{\mathbf{a}}_0|c_i)$ of (3.6), (given the components of each summand), requires $N \cdot q \cdot N_s^2$ additions and $2N \cdot q \cdot N_s^2$ multiplications. On the other hand, the total number of additions and multiplications required to compute all middle metrics are at least $2N \cdot n \cdot q \cdot N_s^2$ and $4N \cdot n \cdot q \cdot N_s^2$.

4.5 Simulation Results and Discussions

Thus, it is easy to see that the middle metric computations dominate the complexity of the BIID. Obviously, these computations will become even more dominant in the SIID and JDD.

4.5 Simulation Results and Discussions

In all the computer simulations reported here, the LDPC codes used are constructed using the PEG algorithm [94]. The BP decoder serves as the outer LDPC decoder and performs a maximum of 60 iterations for non-iterative decoding. For iterative decoding, the maximum number of iterations between the outer decoder and the inner decoder or JDD is 6 while at most 10 BP iterations are performed. To speed up our simulations for $L > 2$ when there exists an huge number of valid SCSWs, we adopt the reduced-complexity approach of 3.3.2 to reduce the complexity for all three proposed algorithms on the BPMR channel by only considering those valid SCSWs that have at most one DIDS channel state transition. Throughout, we will take P_I and P_D to be equal.

For simplicity, we will start with single-track equalized rectangular BPMR write-read channel, on which the performance of those three detection-decoding schemes are investigated. As previously stated, the probability $P(\mathbf{r}_{M_i} | S_{f_{in-1}(\rho_1)+1}, \mathbf{a}_{M_i})$ in (4.21) for JDD with SE is obtained by performing a BCJR forward pass from $S_{f_{in-1}(\rho_1)+1}$ to $S_{f_{(i+1)n-1}(\rho_2)+1}$ according to \mathbf{a}_{M_i} . Since SE is unable to mitigate ITI, we then employ MTD and 2D2D equalization on the rectangular BPMR channel and investigate the performance gain achieved due to the mitigation of ITI.

MTD relies heavily on the reliability of the *a priori* information corresponding to the recorded bits on the inner sidetracks. MTD with 2D2D equalization applied to tracks -1 , 0 and 1 , a scheme proposed in [49] and referred to as M-2D2D, does not achieve the aforementioned performance bound, as 2D2D equalization cannot provide

4.5 Simulation Results and Discussions

reliable *a priori* information of the recorded bits on the inner sidetracks [49]. To improve the quality of the sidetrack detection and avoid implementing a hybrid system that utilizes another detection technique on the sidetracks, a simple extension of M-2D2D was proposed in [49]. This scheme, which we refer to as M-2D2D (5 tracks) as in [49], detects all 5 tracks $-2, 1, 0, 1, 2$ using M-2D2D, such that $a_{0,k}$, c_k are first detected with no *a priori* information, then b_k is detected with *a priori* information corresponding to the center track data $a_{0,k}$ and aggregated outer sidetrack data c_k and finally, the detection of $a_{0,k}$ is assisted with *a priori* information corresponding to the aggregated inner sidetrack data b_k . It was shown in [49] that M-2D2D (5 tracks) can achieve the performance bound therein in the presence of strong ITI and ISI. For this reason, we adopt this scheme in our simulations to effectively mitigate the ITI.

Further, it is easy to see that the use of M-2D2D (5 tracks) does not change the mathematics in the preceding sections, since the center track is still detected by 2D2D with improved *a priori* information through sidetrack detection. We choose $L_f = 3$, $L_g = 2$ and $Lw0 = Lw1 = 10$ for 2D2D equalization, since longer targets and equalizers significantly increase the detection complexity but provide only negligible performance improvements [49]. For a fair comparison, we also set $L_f = 3$ and $Lw0 = 10$ for the SE.

4.5.1 Performance Comparison of the BCJR-BIID, JDD and BCJR-SIID with SE

In this section, we investigate and compare the performance of the BCJR-BIID, JDD and BCJR-SIID on the single-track equalized BPMR channel. As in Chapter 3, the outer code is a (999, 888) GF(16) LDPC code. The inner code has rate $4/5$ and maps each LDPC code symbol into one of the 16 length-5 binary string of lowest weight. The substitution error rates of the DIDS channel are $P_R = 0.001$ and $P_B = 0.1$. For the

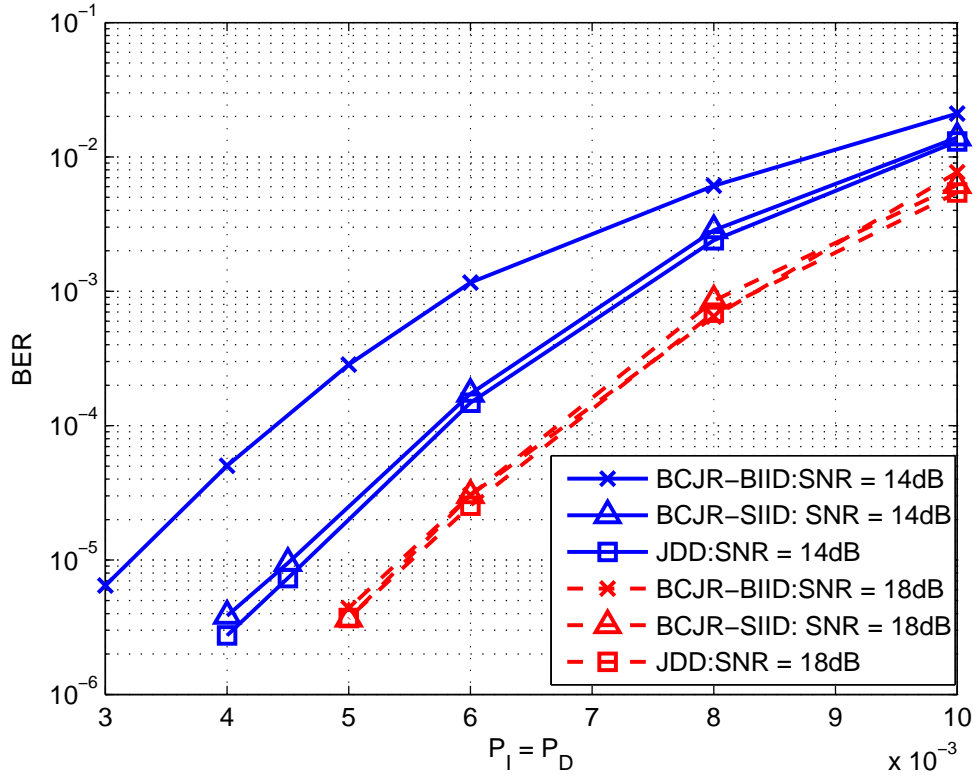
4.5 Simulation Results and Discussions

read channel, we adopt the configuration of [49], i.e., length-11 nm square islands are distributed on rectangular grids with $T_x = 13$ nm, $T_y = 18.82$ nm. Consequently, the symbol areal density is 2.64 Tb/inch² and $PW_{50-long} = 19.5$ nm, $PW_{50-across} = 24.7$ nm, which indicate strong ISI and ITI for $PW_N = 1.5$ and $A_S = 0.2$.

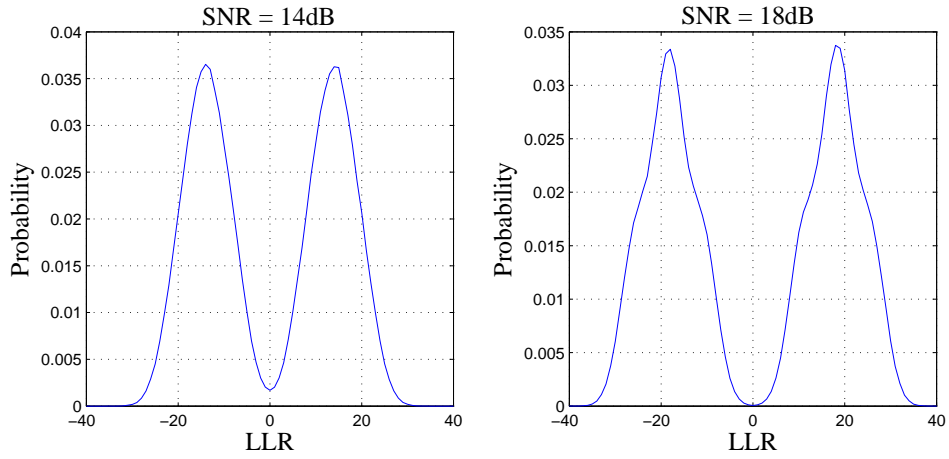
Fig. 4.7(a) shows the BER performance of the BCJR-BIID, JDD and BCJR-SIID under non-iterative decoding on the BPMR channel with $L = 1$ for different SNRs. Fig. 4.7(b) plots $P(\bar{a}_k)$ for SNR=14 dB and 18 dB, which are used in (4.25) of the BCJR-SIID. As shown in Fig. 4.7(a), at SNR=14 dB, JDD yields significant and modest performance improvements over the BCJR-BIID and BCJR-SIID, respectively. Fig. 4.7(a) shows that at an SNR of 18 dB, there is little difference in performance between the three detection-decoding strategies. This implies that at this SNR value, the impairments of the BPMR channel are dominated by the WIEs

In Figs. 4.8 and 4.9, we plot the BER performance of the BCJR-BIID, BCJR-SIID and JDD for $L = 5$ under non-iterative and iterative decoding, respectively. Evidently, at SNR=14 dB, the BCJR-SIID yields almost the same BER performance as the JDD and superior performance compared to the BCJR-BIID, under iterative and non-iterative decoding. Further, at SNR=18 dB, the BER performance of the BCJR-BIID, BCJR-SIID and JDD are once again almost the same. Comparing Figs. 4.8 and 4.9 indicates that iterative decoding provides significant performance improvements over non-iterative decoding for all these three proposed detection-decoding schemes as one might expect. We also observe that at SNR=14 dB, applying iterative decoding to the JDD and BCJR-SIID yields larger performance improvements than when it is applied to the BCJR-BIID.

4.5 Simulation Results and Discussions



(a)



(b)

Figure 4.7: (a) BER under non-iterative decoding with the proposed BCJR-BIID, JDD and BCJR-SIID on the single-track equalized BPMR channel with $L = 1$ for different SNR values; (b) The distribution of LLRs generated by the BCJR detector for different SNRs considered in part (a).

4.5 Simulation Results and Discussions

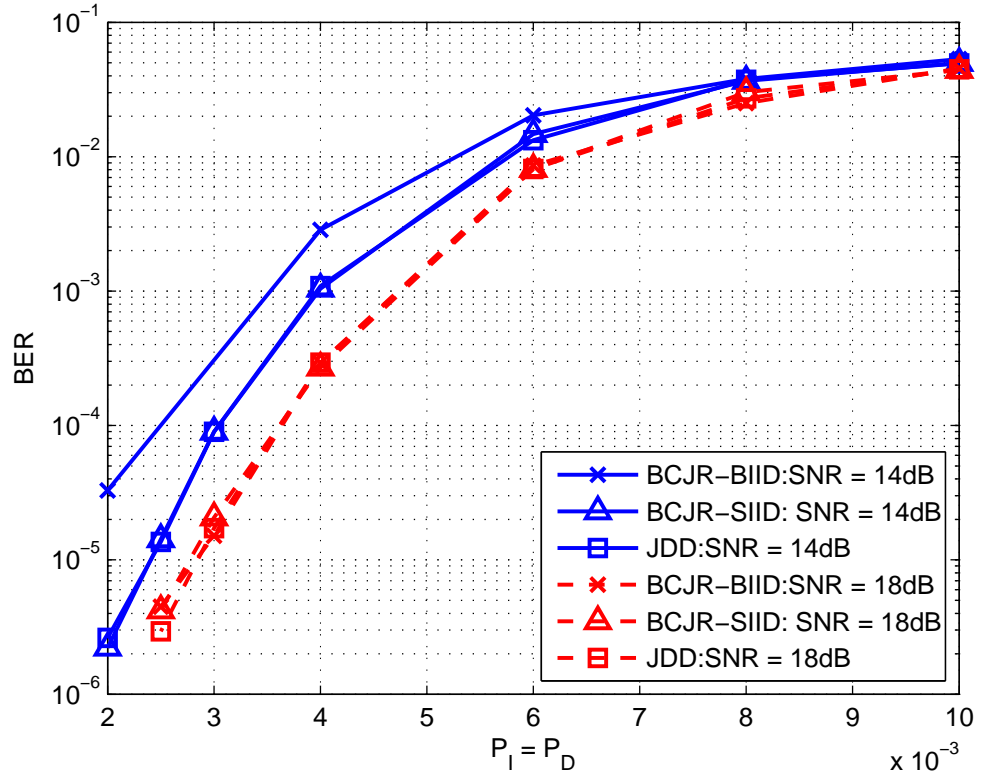


Figure 4.8: BER under non-iterative decoding with the proposed BCJR-BIID, JDD and BCJR-SIID on the BPMR channel with $L=5$ for different SNR values.

4.5 Simulation Results and Discussions

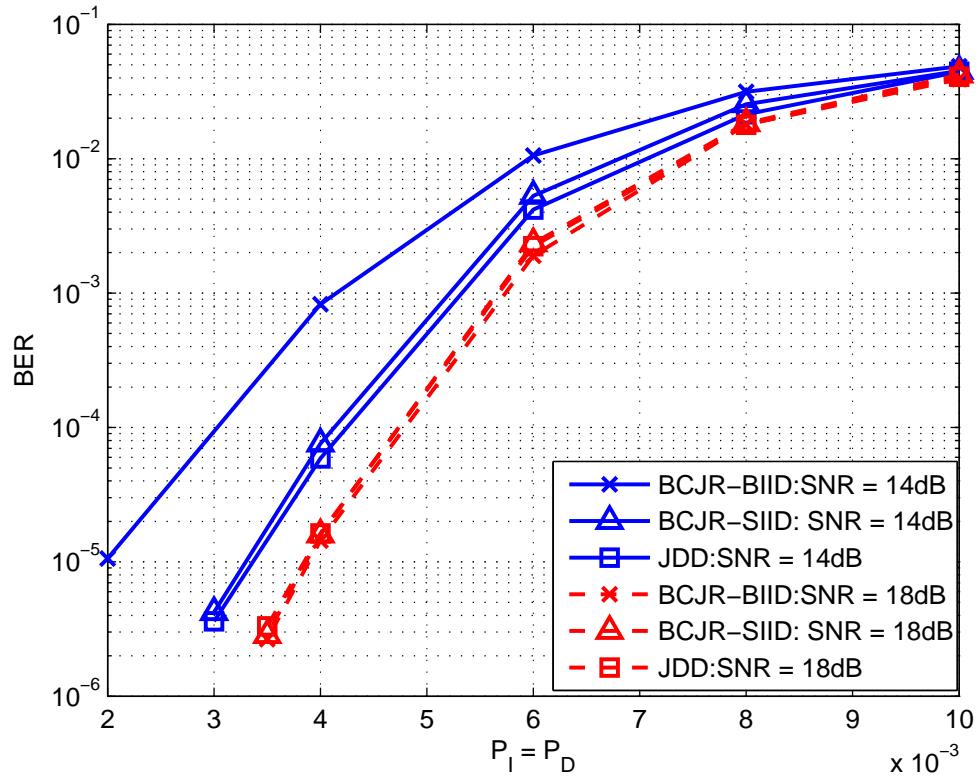


Figure 4.9: BER under iterative decoding with the proposed BCJR-BIID, JDD and BCJR-SIID on the BPMR channel with $L=5$ for different SNR values.

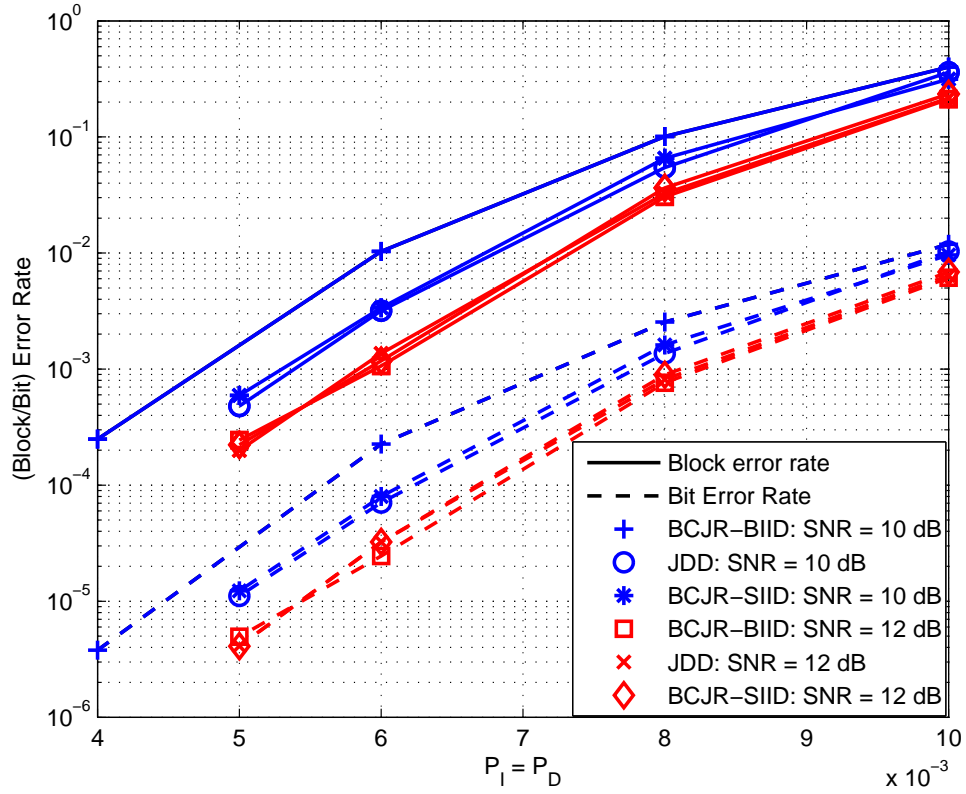
4.5.2 Performance Comparison of the BCJR-BIID, JDD and BCJR-SIID with M-2D2D (5 tracks)

In this section, we investigate and compare the performance of the BCJR-BIID, JDD and BCJR-SIID on the equalized BPMR channel with ITI being mitigated by M-2D2D (5 tracks) detection scheme. The DM code and BPMR channel model are the same as those considered in Section 4.5.1.

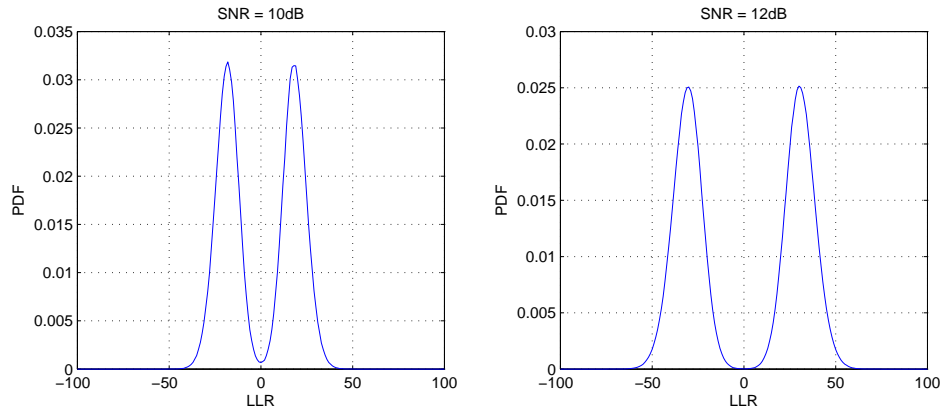
Fig. 4.10(a) shows the block error rate (BLER) and BER performance of the BCJR-BIID, JDD and BCJR-SIID against the insertion/deletion error rates on the BPMR channel with $L = 1$, while Fig. 4.10(b) presents the corresponding $p(\bar{a}_{0,k})$ used by the BCJR-SIID. As shown in Fig. 4.10(a), the JDD has a modest performance improvement over the BCJR-SIID while both schemes significantly outperform the BCJR-BIID at SNR = 10 dB. As the SNR increases to 12 dB, hardly any performance difference between those three strategies can be observed. This is expected since when SNR increases, the BCJR detector alone provides reliable estimates of the data recorded on the disk and hence the dominant channel impairments are those introduced by the write channel. This can be seen from the BCJR output LLR PDFs in Fig. 4.10(b), which shows that the probability of obtaining an LLR of small magnitude (e.g., ≤ 15) is less at SNR = 12 dB than at SNR = 10 dB. Consequently, there will be less erroneous hard-decision values that the quantizer generates at higher SNR.

Next, Fig. 4.11 presents the BLER and BER performance of the BCJR-BIID, JDD and BCJR-SIID for $L = 1$ under iterative decoding. Once again, the performance of the BCJR-BIID, JDD and BCJR-SIID at SNR = 12 dB are almost the same, while JDD and BCJR-SIID yield very close performance and both significantly outperform the BCJR-BIID when SNR = 10 dB. By comparing Figs. 4.10(a) and 4.11, we observe that iterative decoding significantly improves the performance for all three detection-inner-decoding schemes, as expected. We further observe from Figs. 4.10(a) and 4.11

4.5 Simulation Results and Discussions



(a)



(b)

Figure 4.10: (a) BER and BLER under non-iterative decoding with the proposed BCJR-BIID, JDD and BCJR-SIID on the BPMP channel with $L = 1$ for different SNR values; (b) The PDF of LLRs generated by the BCJR detector for different SNRs considered in part (a).

4.5 Simulation Results and Discussions

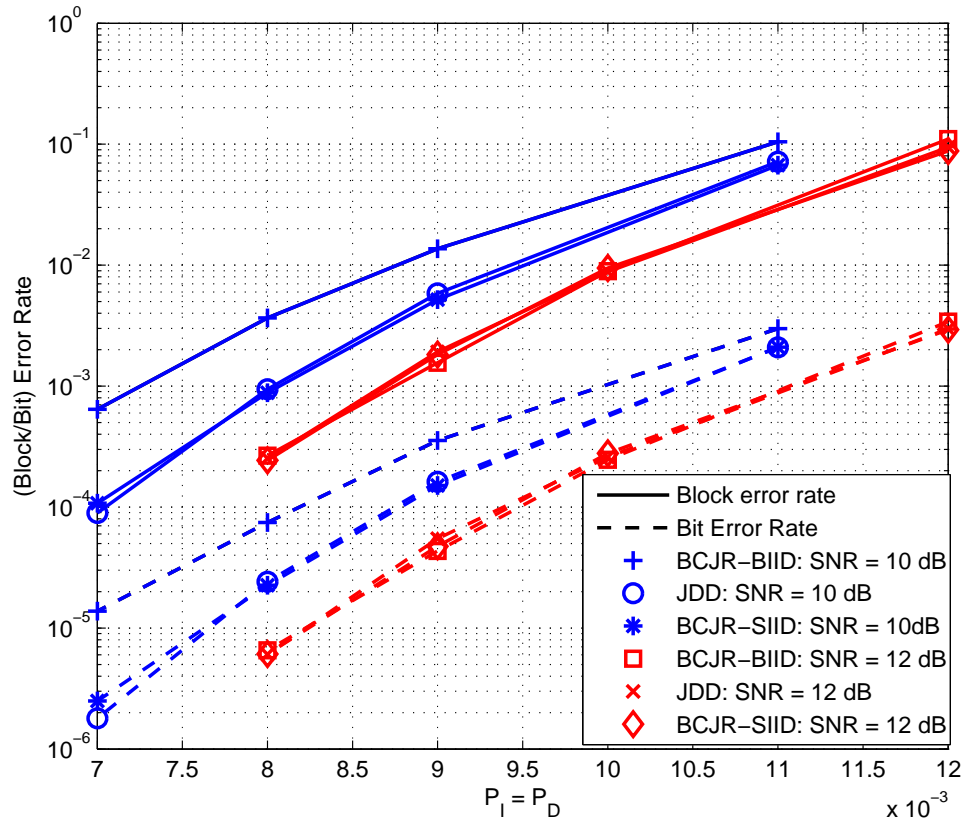


Figure 4.11: BER and BLER under iterative decoding with the proposed BCJR-BIID, JDD and BCJR-SIID on the BPMR channel with $L = 1$ for different SNR values.

4.5 Simulation Results and Discussions

that the BLER and BER performance curves both show how the BCJR-BIID, JDD and BCJR-SIID measure up against one another. Henceforth, we will only use the BER to measure error performance.

As the output from the BCJR-BIID, JDD and BCJR-SIID are the likelihoods initializing the outer LDPC decoder, a more rigorous comparison of the performance of these three schemes can be obtained by removing the influence of the outer code and measuring the quality of these likelihoods. We show in Fig. 4.12 the average entropy of the output likelihoods computed by these three schemes against the insertion/deletion error rates for $L = 1$. Observe that when $\text{SNR} = 10$ dB, the average entropy of the output from the JDD and BCJR-SIID are very close while they are lower than that of the BCJR-BIID. As the SNR increases to 12 dB, the curves corresponding to these three strategies overlap. Evidently, these results agree with the error performance shown in Fig. 4.10(a).

Therefore, we conclude that on the BPMR channel with M-2D2D (5 tracks), the BCJR-SIID (resp., BCJR-BIID) provides good performance-complexity trade-offs at low to moderate (resp., high) SNRs. This conclusion is similar to that made in Section 4.5.1. However, the performance improvement due to the use of M-2D2D (5 tracks) is remarkable, which can be easily observed by comparing Fig. 4.10(a) and Fig. 4.7(a) which presents the BER performance of the three single-track-detection-decoding counterparts with the same channel code, outer decoder (with the same limit on the number of iterations), and channel parameters. Specifically, when $P_I = P_D = 5 \times 10^{-3}$, the lowest BER obtained in Fig. 4.7(a) with SE at $\text{SNR} = 18$ dB is 3.45×10^{-6} while Fig. 4.10(a) indicates that a BER equal to 4.11×10^{-6} can be easily obtained with M-2D2D (5 tracks) detection at $\text{SNR} = 12$ dB. This indicates that the use of M-2D2D (5 tracks) leads to about 6 dB improvement in SNR compared to the single-track detection.

Since the BCJR-SIID comes very close to the JDD in error performance yet has

4.5 Simulation Results and Discussions

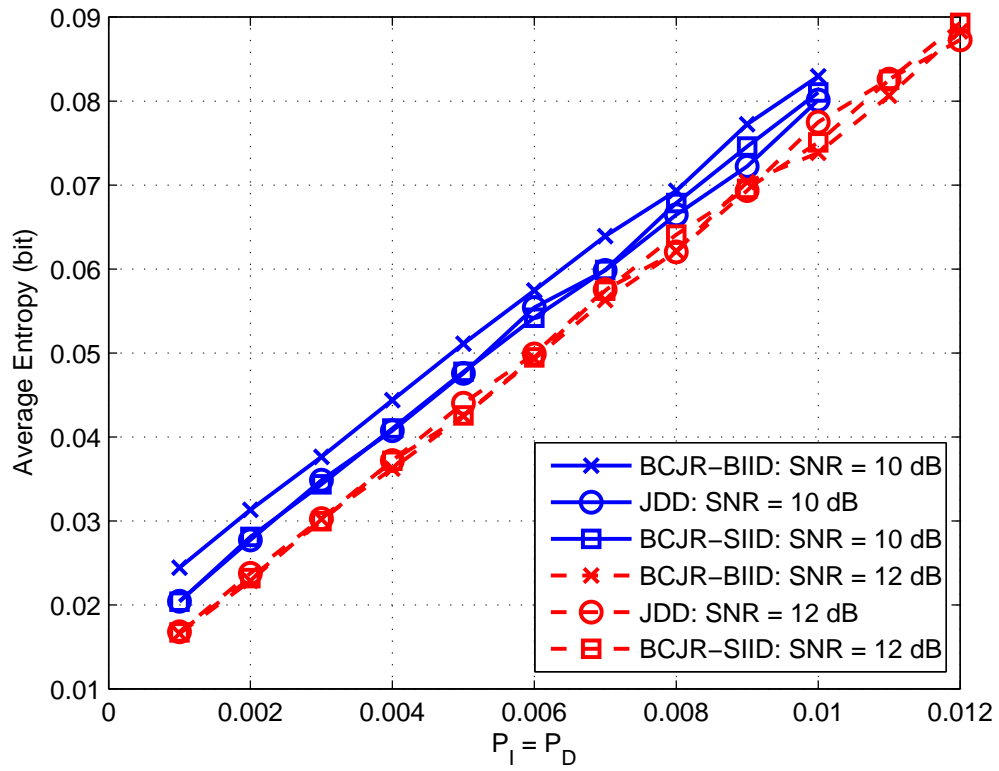


Figure 4.12: Average entropy of the likelihoods generated by the BCJR-BIID, JDD and BCJR-SIID of Fig. 4.10(a).

4.5 Simulation Results and Discussions

substantially lower complexity and M-2D2D (5 tracks) significantly improves the performance by mitigating ITI, we will focus on BCJR-SIID with M-2D2D (5 tracks) in our remaining simulations.

4.5.2.1 Performance Degradation Due to the Length of Burst Substitution Errors

Besides the insertion/deletion error rates, the maximum number L of burst errors preceding and following each insertion/deletion error, is another write channel performance-limiting factor. To investigate the performance degradation resulting from increasing L , we repeat the simulations for the BCJR-SIID reported in Fig. 4.11 for $L = 0, \dots, 5$. The case when the channel is least adversarial (in terms of the burst error length), i.e., $L = 0$, is presented as a benchmark against which the performance for $L > 0$ is compared. The simulations results are shown in Fig. 4.13. Clearly, increasing the maximum burst error length dramatically degrades the overall BER performance for both SNRs considered. By comparing the performance between SNR = 10 dB and SNR = 12 dB for a fixed $P_I = P_D$, we see that the performance gap between SNR = 10 dB and SNR = 12 dB narrows as L increases. This suggests that for a given $P_I = P_D$, the quality of the BPMR channel is, to a great extent, determined by L , as it only takes a modest value of L to cause an otherwise reliable readback signal when the read channel SNR is large, to be severely corrupted.

4.5.3 Performance of Increased Code Rate and Higher Areal Density

Here, we consider a higher overall code rate of 0.8 by concatenating a (568, 512) LDPC code over GF(256) to a rate-8/9 inner code which maps each outer code symbol to one of the 256 length-9 binary strings of lowest weight. The increase in complexity of

4.5 Simulation Results and Discussions

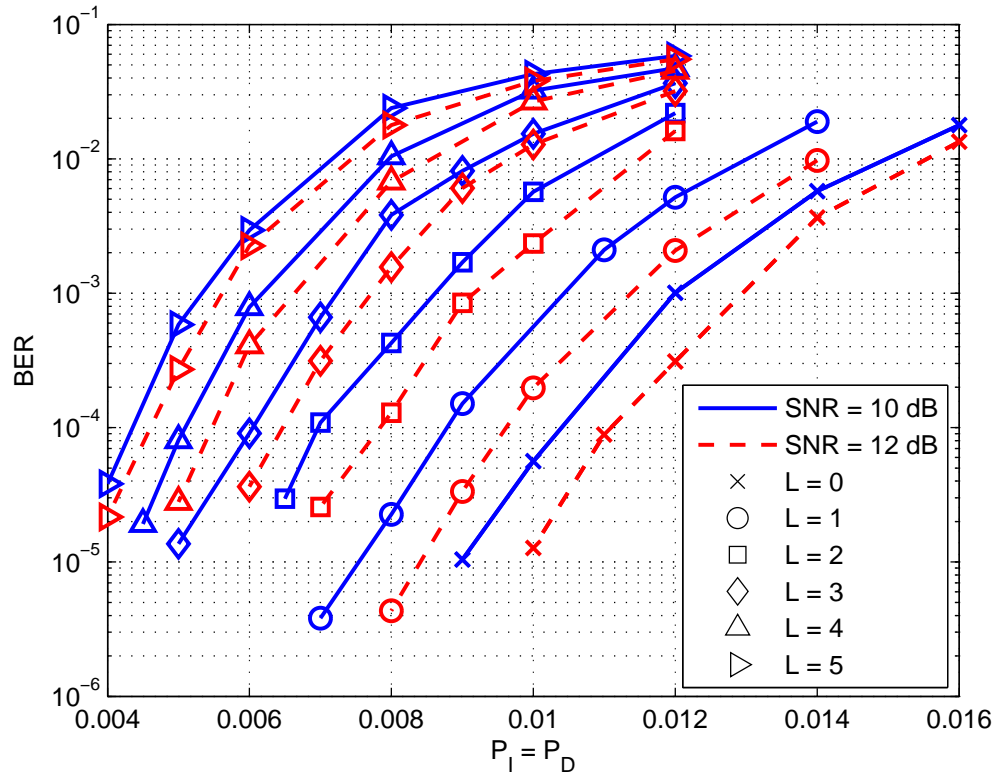


Figure 4.13: BER performance of BCJR-SIID under iterative decoding on the BPMR channels with $L = 0, \dots, 5$ for different SNRs.

4.5 Simulation Results and Discussions

the BP decoder owing to the larger LDPC code alphabet size, is compensated by applying the fast Fourier transform approach of [75] to computing the check-to-variable node messages. To achieve a higher areal density such as 4 Tb/inch², we cautiously choose a media configuration where the length of each square island is 5 nm, since shrinking the islands further renders the replay response signal too weak while the corresponding reduction in $PW_{50\text{--}along}$ and $PW_{50\text{--}across}$ is negligible [63]. Fig. 4.14 shows the normalized 2D pulse response of an isolated island obtained numerically and Fig. 4.15 presents the numerically computed and Gaussian fitted normalized pulse response of an island in both the along-track and cross-track directions. The numerical pulse response is obtained by applying the head potential distribution of [40] while the analytical pulse response is computed using (4.7). The $PW_{50\text{--}along}$ and $PW_{50\text{--}across}$ of the pulse response are 18.136 nm and 19.832 nm, respectively. In order to maintain the extent of the ISI to be $PW_N = 1.5$ at an areal density of 4 Tb/inch², we arrange the islands on a rectangular grid with $T_x = 12.09$ nm and $T_y = 13.34$ nm, which results in severe ITI with $A_s = 0.2852$.

Fig. 4.16 shows the simulated error performance of the BCJR-SIID in conjunction with the above rate-0.8 DM coding scheme under iterative decoding at areal densities of 4 Tb/inch² and 2.64 Tb/inch². For both cases, the read channel SNR is 12 dB, the maximum burst error length L is varied from 0 to 5, while the substitution error rates are fixed at $P_R = 0.001$ and $P_B = 0.1$. Fig. 4.17 presents the PDFs of the BCJR detector output LLRs for the two areal densities considered.

As Fig. 4.16 shows, for a fixed L (including $L = 0$), increasing the areal density from 2.64 Tb/inch² to 4 Tb/inch² only has a modest impact on BER performance. Moreover, Fig. 4.17 shows a slight contraction of the BCJR detector's output LLR density towards the origin, as the areal density is increased, thus reflecting a slight decrease in reliability in the BCJR output. We conjecture that the slight degradation in error performance and reliability of the BCJR detector output is mainly due to the

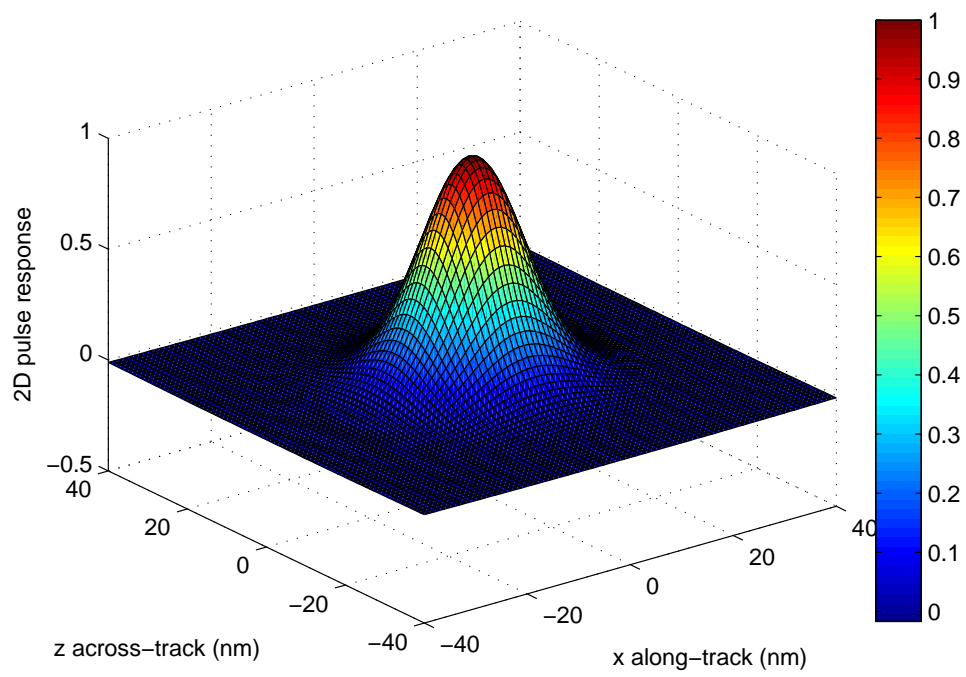
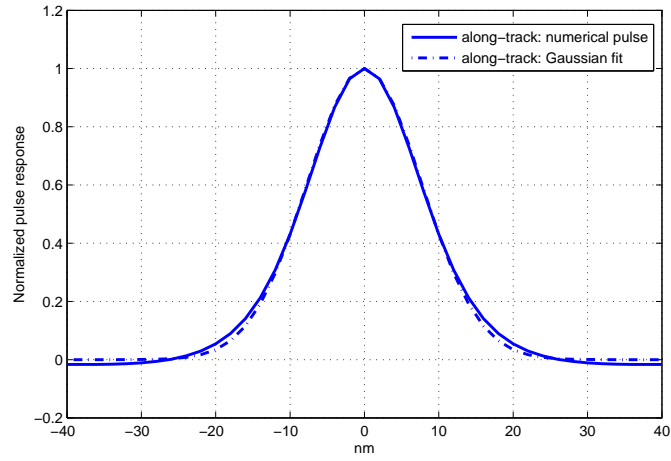
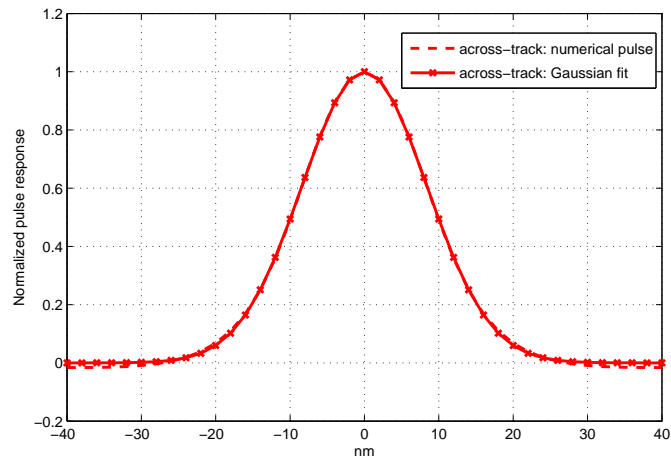


Figure 4.14: Normalized 2D pulse response of a length-5 nm square island.

4.5 Simulation Results and Discussions



(a)



(b)

Figure 4.15: Normalized pulse response for numerical and Gaussian fitted analytical pulses in the (a) along-track and (b) cross-track directions of a length-5 nm square island.

4.5 Simulation Results and Discussions

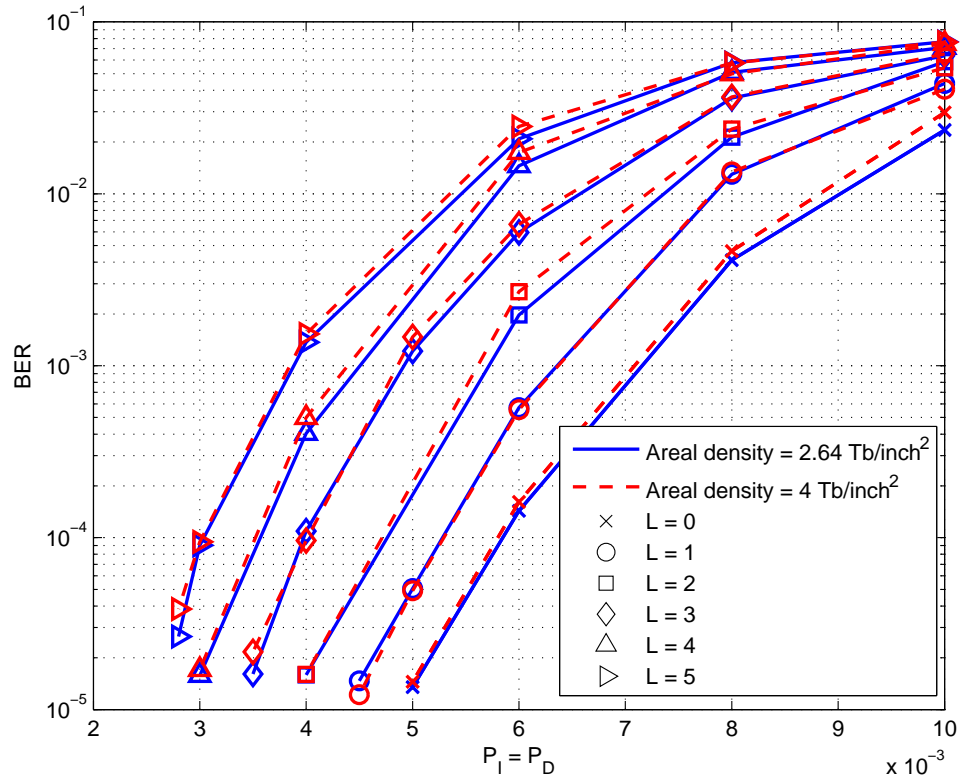


Figure 4.16: BER performance of the BCJR-SIID under iterative decoding on the BPMR channel with different areal density and $L = 0, \dots, 5$, when $\text{SNR} = 12 \text{ dB}$.

4.5 Simulation Results and Discussions

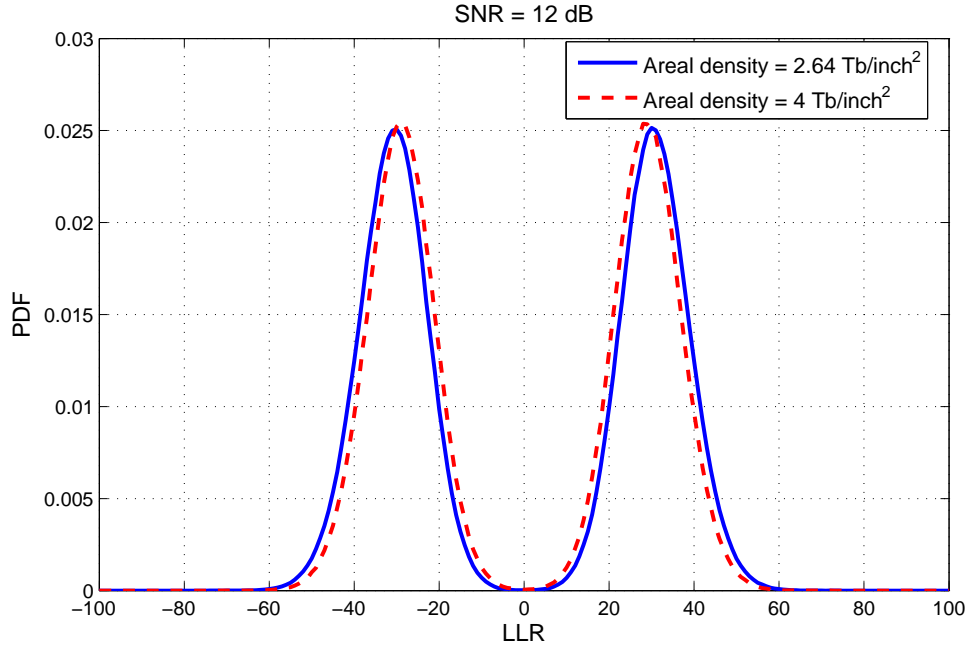


Figure 4.17: PDF of LLRs generated by the BCJR detector with the read channel of different areal densities considered in Fig. 4.16.

increase in ITI, since the sidetrack amplitude A_s increases from 0.2 to 0.2852 as the areal density increases from 2.64 Tb/inch² to 4 Tb/inch². On the other hand, for a fixed insertion/deletion rate, the deterioration in error performance as L increases is significant. This reinforces the conclusion drawn from Fig. 4.13 that the quality of the BPMP channel is to a large extent determined by L . Finally, Fig. 4.16 shows that at an areal density of 4 Tb/inch², with low to moderate insertion/deletion rates (e.g., $P_I = P_D \leq 10^{-3}$) and short burst errors (i.e., $L \leq 5$), BERs lower than 10^{-5} are attainable with the BCJR-SIID in conjunction with a rate-0.8 DM coding scheme.

4.6 Conclusion

In summary, we have investigated the problem of data recovery on rectangular BPMR channels modelled as a serial concatenation of the DIDS write channel model and a rectangular BPMR read channel model. MTD and 2D equalization techniques are employed to mitigate ISI and ITI while the DM coding scheme corrects WIEs as well as errors resulting from imperfect read channel detection. Three ways of combining the read channel detector and inner decoder modified for the DM construction on the BPMR channel are proposed and investigated, namely the BCJR-BIID algorithm, the JDD algorithm and the BCJR-SIID algorithm.

On the rectangular BPMR channel, media configurations leading to areal densities of 2.64 Tb/inch^2 and 4 Tb/inch^2 with comparable ISI but significantly higher ITI in the latter case are considered. Computer simulations show that at low to moderate (resp., high) SNRs, BCJR-SIID (resp., BCJR-BIID) provides good performance-complexity trade-offs. Further, increasing the areal density from 2.64 Tb/inch^2 to 4 Tb/inch^2 while the IDS error rates remain fixed, does not significantly affect error performance on the BPMR channel. Rather, it is the length of burst errors preceding and following an insertion/deletion that severely impacts performance.

Chapter 5

Detection-Decoding on Staggered BPMR Channels with Written-In Error Correction and ITI Mitigation

In Chapter 4, we have observed that the areal density under the media configuration considered there, i.e., squared islands distributed on rectangular grids, cannot be further increased by simply shrinking the island size and/or reducing the track pitch and the along-track island period. The reason is that doing so will result in weak replay response signal and/or severe ITI and ISI [63].

To achieve even higher areal densities, e.g., 10 Tb/inch², staggered BPM is a promising solution as the distribution of islands on a hexagonal array reduces ITI at the expense of enhanced ISI which, however, can be effectively mitigated by utilizing longer optimized GPR targets [51]. Motivated by this fact, we investigate in this chapter the performance of the DM coding scheme on staggered BPMR channels at an areal density of 6 Tb/inch². BCJR-BIID and BCJR-SIID that achieve good performance-complexity tradeoffs on rectangular BPMR channels are employed.

5.1 BPMR Channel Model with JE

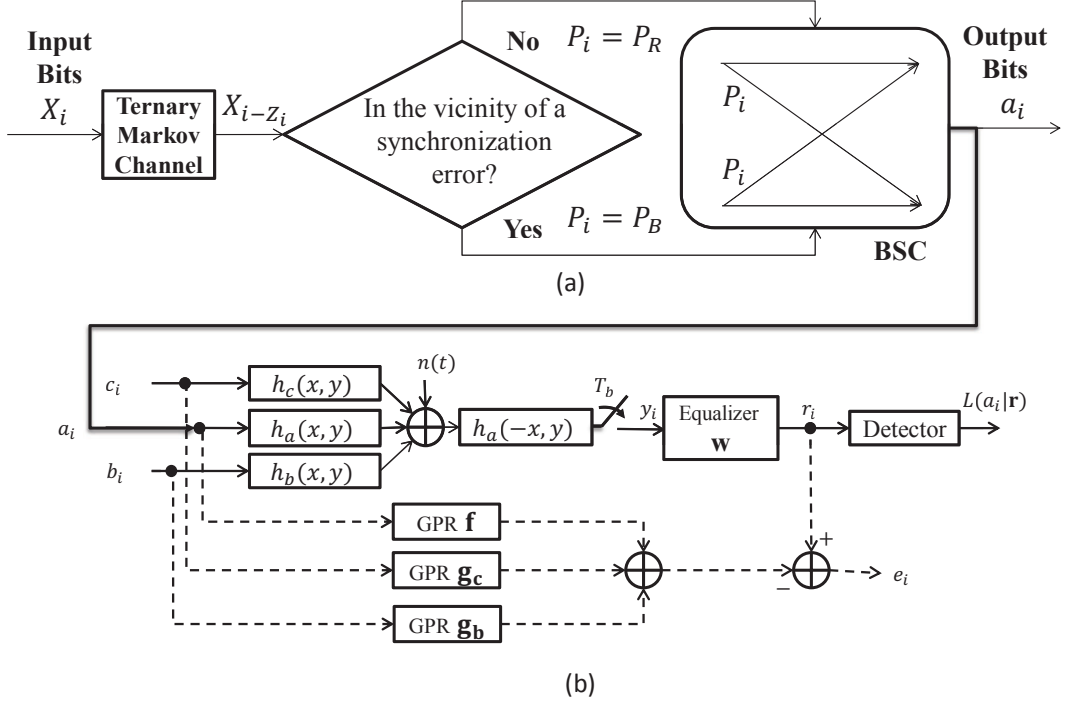


Figure 5.1: (a) DIDS write channel model; (b) Read channel model with joint-track equalization.

5.1 BPMR Channel Model with JE

Similar to the channel model considered in Section 4.2, the BPMR channel model considered in this section is a composite channel consisting of a DIDS write channel followed by a joint-track equalized read channel, as shown in Fig 5.1. In Fig. 5.1(a), $X_i \in \{-1, +1\}$ is the data intended to be recorded while $a_i \in \{-1, +1\}$ is the actual data written on the disk. The read channel presented in Fig. 5.1(b) is still characterized by the replay response of an isolated island, which is well fitted by (4.7).

The read channel model shown in Fig. 5.1(b) is a generalized read channel model which can be used to model rectangular BPMR as well as single-track and double-

5.2 Channel Detection and Decoding

track staggered BPMP read channels [51]. The three recording strategies with equal areal densities are illustrated in Fig. 5.1, where island period and array pitch in all three recording strategies are set to T_x and T_y , respectively.

To model rectangular BPMP, we set: $h_a(t, y) = h(t, 0)$, $h_b(t, y) = h_c(t, y) = h(t, T_y)$, and $b_i, c_i \in \{-1, +1\}$. As in [51], single-track staggered BPMP with one array per track can be modeled by setting: $h_a(t, y) = h(t, 0)$, $h_b(t, y) = h(t - T_x/2, T_y)$, $h_c(t, y) = h(t, 2T_y)$. In this case, $b_i, c_i \in \{-2, 0, +2\}$ are aggregated data on the side-tracks, i.e., $b_i = a_{-1,i} + a_{1,i}$ and $c_i = a_{-2,i} + a_{2,i}$ where $a_{m,i}$ represents the i th bit on the m th track with $a_{0,i} = a_i$ on the center track. Further, the double-track staggered BPMP with two arrays per track can be modeled by setting: $h_a(t, y) = h(t, T_y/2)$, $h_b(t, y) = h(t, 1.5T_y)$, $h_c(t, y) = h(t, 2.5T_y)$, and $b_i, c_i \in \{-1, +1\}$.

Note that only one read head is used to detect the waveform from the center track as shown in Fig. 5.1(b).

5.2 Channel Detection and Decoding

In Section 4.4, three detection-decoding schemes have been developed to work with an outer decoder to recover data encoded by the DM coding scheme on rectangular BPMP channels, i.e., the JDD algorithm, the BCJR-BIID algorithm and the BCJR-SIID algorithm. It has been verified that the BCJR-SIID (resp., BCJR-BIID) provides good performance-complexity trade-offs at low to moderate (resp., high) SNRs. Hence, we apply them to staggered BPMP channels in this paper.

In addition, MTD is employed to effectively mitigate ITI. Although MTD is applied with 2D equalization on the rectangular BPMP channel in Section. 4.4, it has been reported in [49] that MTD with JE (M-JE) exhibits similar performance as MTD with 2D equalization while requiring fewer track readings and lower complexity. Hence, we will only employ M-JE to mitigate ITI in this section. In M-JE, the signal

5.2 Channel Detection and Decoding

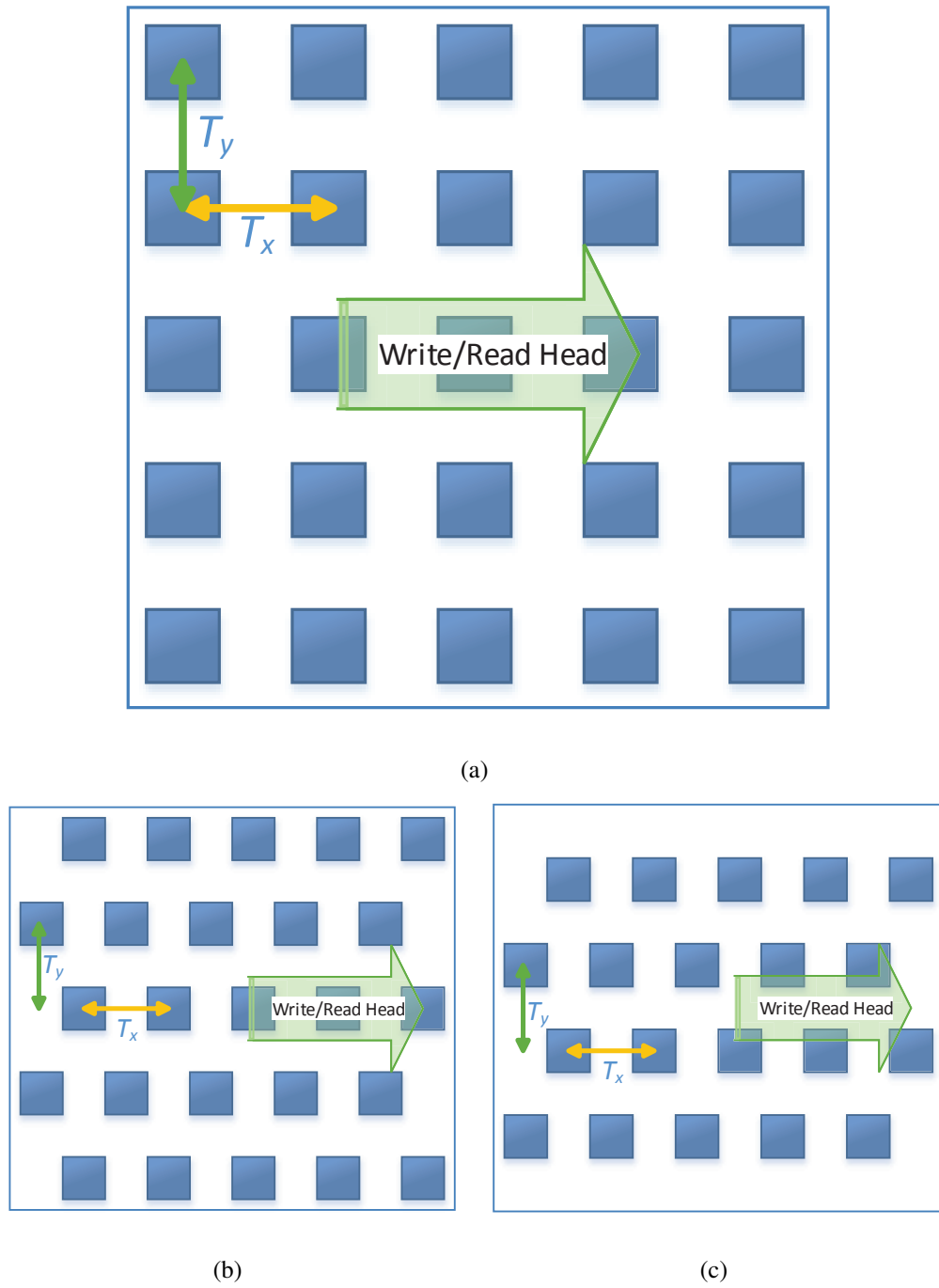


Figure 5.2: (a) Rectangular BPMR; (b) single-track staggered BPMR; (c) double-track staggered BPMR.

5.3 Simulation Results and Discussions

sequence read from the center track has to be equalized to 2D GPR targets as shown in Fig. 5.1(b), while the sidetracks can be detected with any detection scheme. We nevertheless utilize SE for sidetrack detection to reduce the complexity of M-JE. A detailed description of MTD can be found in [49].

5.3 Simulation Results and Discussions

We consider a square island of length 5 nm and thickness 10 nm, and a GMR read head of width 10 nm and thickness 4 nm. The fly height is 10 nm and shield to sensor spacing is 6 nm. Consequently, the 2D numerical pulse response obtained using the method reviewed in Section 4.1 is presented in Fig. 5.3, which has $PW_{50-long} = 17.91$ nm and $PW_{50-across} = 17.38$ nm. Fig. 5.4 verifies that the 2D pulse response can be well fitted by the 2D Gaussian pulse response of (4.7). Further, we set $T_x = 10.7$ nm and $T_y = 10$ nm to achieve an areal density of 6 Tb/inch². Following [51], the single-track and double-track staggered media are denoted by *Hex1* and *Hex2*, respectively.

We note that at 10 Tb/inch², the WIE rate is expected to be of the order of 10^{-3} . Consequently, for the DIDS write channel, we set $P_R = 10^{-3}$ so that the substitution error rate of the channel computed via (3.2) is $O(10^{-3})$ when $L > 0$. The BP decoder serves as the outer LDPC decoder, and the maximum number of iterations performed between the outer and inner decoders is 6 while at most 10 BP iterations are performed. As the complexity of the BIID increases exponentially with L , we adopt the reduced-complexity approach of Section. 3.3.2 to reduce the complexity of BIID and SIID, and speed up our simulations for $L > 2$.

5.3 Simulation Results and Discussions

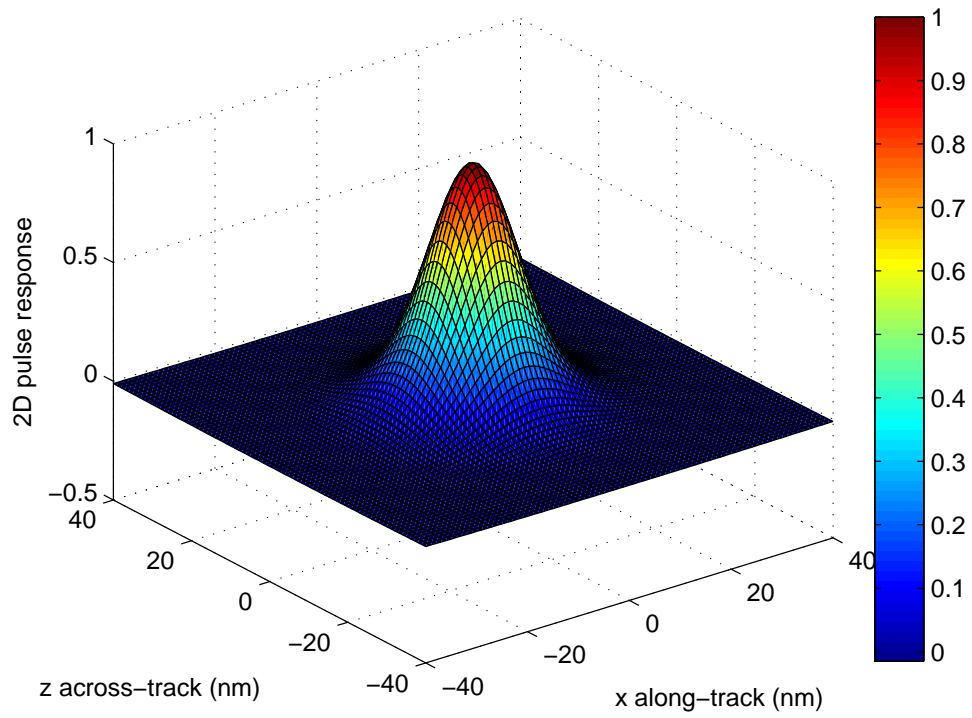
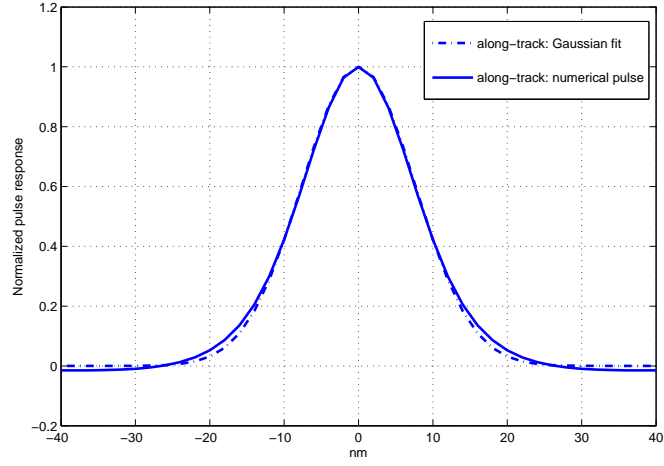
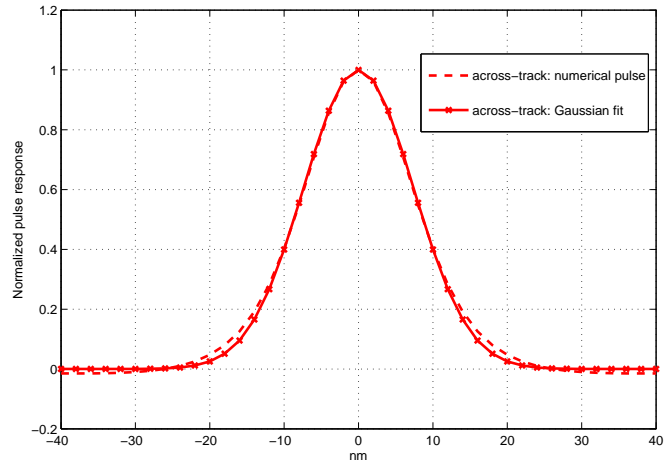


Figure 5.3: Normalized 2D pulse response of an isolated square island, which has length of 5 nm and thickness of 10 nm. The GMR read head is of width 10 nm and thickness 4 nm. The fly height is 10 nm and shield to sensor spacing is 6 nm.

5.3 Simulation Results and Discussions



(a)



(b)

Figure 5.4: Normalized pulse response for numerical and Gaussian fitted analytical pulses in the (a) along-track and (b) cross-track directions of Fig. 5.3.

5.3 Simulation Results and Discussions

5.3.1 Performance Comparison of M-JE on Rectangular and Staggered BPMR Read Channels

We present in Fig. 5.5 the BER performance of M-JE on single-track staggered, double-track staggered and rectangular BPMR systems at an areal density of 6 Tb/inch². Since M-JE is incapable of correcting WIEs, we assume a noiseless write channel and only consider data recovery of uncoded bits on the read channel shown in Fig. 5.1(b). The lengths of the 2D GPR targets \mathbf{f} , \mathbf{g}_b and \mathbf{g}_c are denoted by L_a , L_b and L_c , respectively. Evidently, double-track staggered BPMR with M-JE has the best performance when $\text{SNR} < 16$ dB. The performance of extended M-JE (EM-JE) on the single-track and double-track staggered BPMR read channels are also shown in Fig. 5.5. This scheme detects all sidetracks using M-JE instead of SE, hence ITI can be better mitigated with more reliable *a priori* information from sidetrack detection. Evidently, in exchange for the increase in complexity, performance is substantially improved for single-track staggered BPMR while there is limited amount of performance improvement for double-track staggered BPMR at high SNRs. This is expected since EM-JE is designed to thrive in high ITI settings but ITI on double-track staggered media is reduced [51]. Hence, we will focus on single-track staggered BPMR with EM-JE in Section 5.3.2, where the SNR is fixed at 12 dB.

5.3.2 Performance of DM Construction on Single-Track Staggered BPMR Channels

We first consider the rate-0.71 DM employed in Chapter 3, which we refer to as DM-0. It consists of a 16-ary (999, 888) LDPC code concatenated with a rate-4/5 inner code. Fig. 5.6 presents the performance of BCJR-BIID and BCJR-SIID on the single-track staggered BPMR write-read channel for various values of L and insertion/deletion

5.3 Simulation Results and Discussions

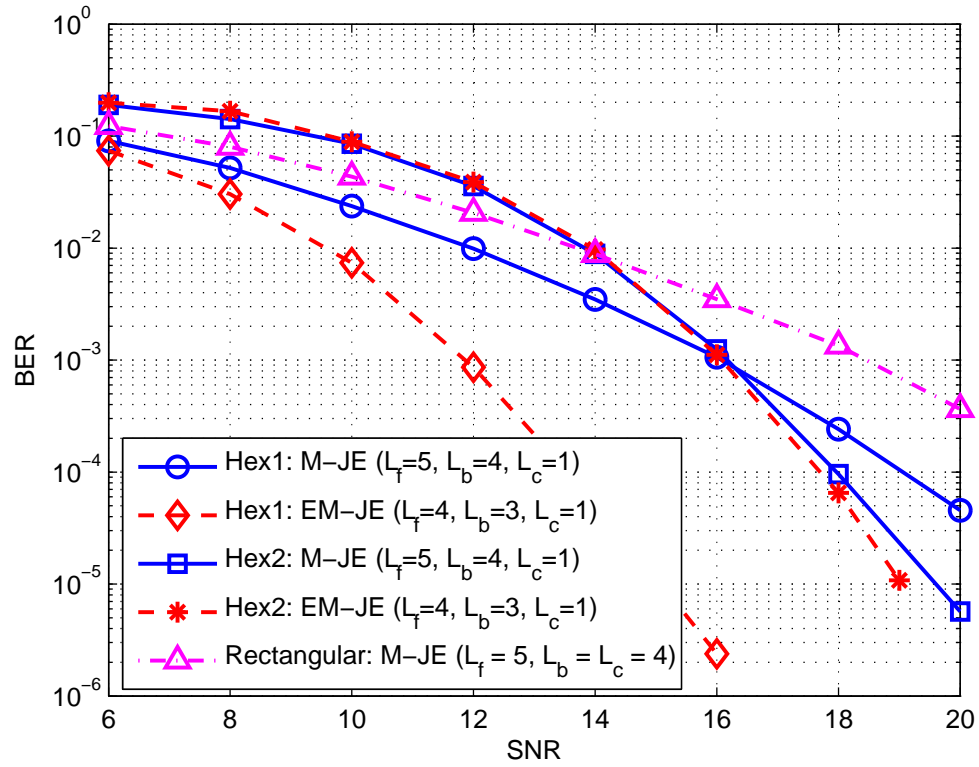


Figure 5.5: BER performance of M-JE on single-track staggered, double-track staggered and rectangular BPMR read channels at an areal density of 6 Tb/in².

5.3 Simulation Results and Discussions

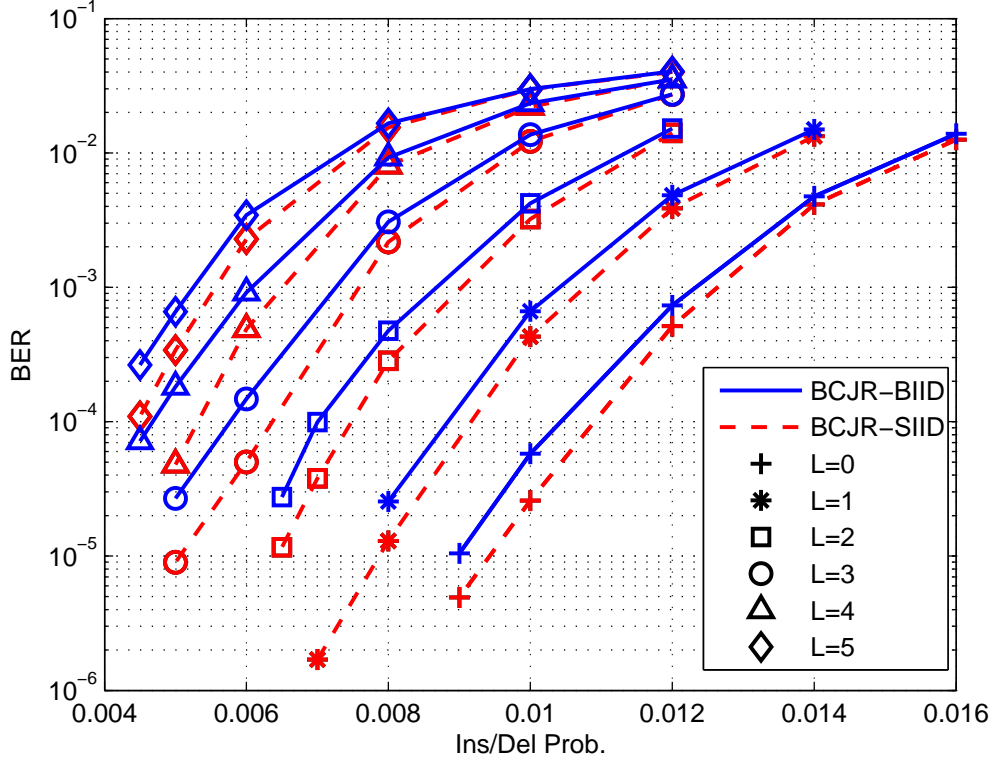


Figure 5.6: BER of rate-0.71 DM code with BCJR-BIID and BCJR-SIID under iterative decoding on the single-track staggered BPMR channel for $L = 0, \dots, 5$.

error rates. As expected, BCJR-SIID outperforms BCJR-BIID while increasing L dramatically degrades the performance of both detection-decoding schemes. We nevertheless observe that the performance loss induced by increasing L by 1 decreases as L increases. Thus, the deterioration in error performance as L is increased from 5 to 10, for example, will not be as dramatic as that when L is increased from 0 to 5. In other words, the sensitivity of system performance on L actually decreases for larger values of L .

Fig. 5.7 presents the performance of two other rate-0.71 DM codes, DM-1 and DM-2 with BCJR-BIID and BCJR-SIID. DM-1 consists of an outer 256-ary (495,440) LDPC code and a rate-8/10 inner code, while DM-2 consists of an outer 256-ary

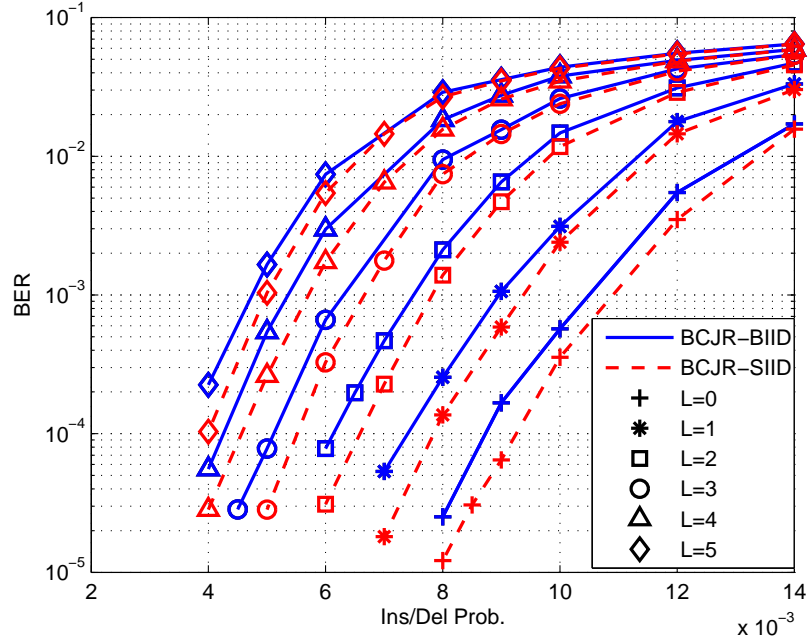
5.3 Simulation Results and Discussions

(500,400) LDPC code and a rate-8/9 inner code. Comparing Figs. 5.6 and 5.7, we observe that the performance of DM-1 is worse than that of DM-0. This may be because the outer LDPC code of DM-1 is inferior to that of DM-0 as the performance of LDPC code does not monotonically improve with the order of Galois field [81]. Further, DM-2 has a more powerful outer code and significantly outperforms DM-0 and DM-1, which suggests that the overall performance of a DM code on the single-track staggered BPMR channel is to a large extent determined by the error correction capability of the outer code. We also observe from Fig. 5.7(b) that a powerful outer code enables the BCJR-BIID and BCJR-SIID to yield similar performance, particularly when $L \geq 1$.

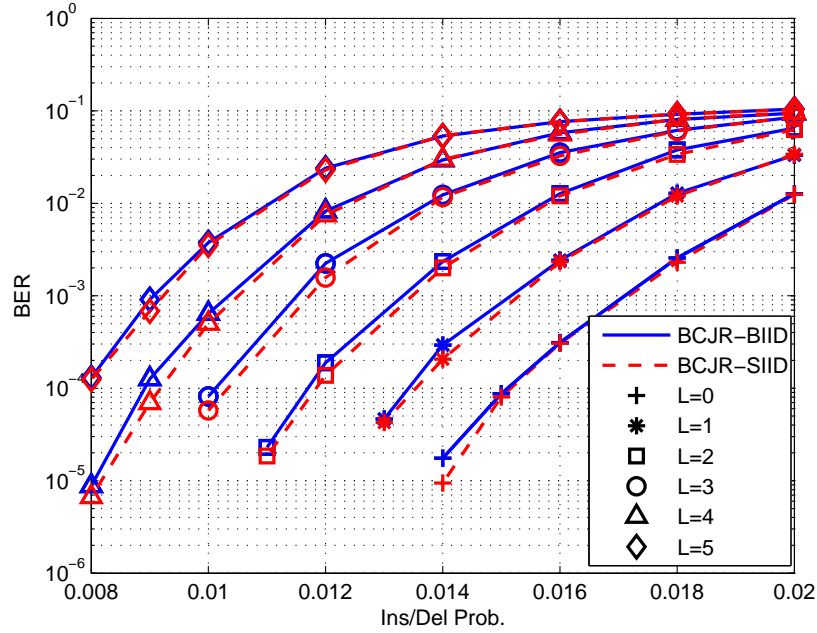
To have a more rigorous performance comparison between the BCJR-BIID and BCJR-SIID with DM-0 on the single-track staggered BPMR write-read channel, we eliminate the influence of the outer code and measure the quality of the likelihoods generated by the two detection-decoding schemes by computing the average entropy of these likelihoods following the approach of [57, Appendix B]. We plot in Fig. 5.8, the average entropy under non-iterative decoding against the inner code rate for various insertion/deletion probabilities and $L = 3, 4, 5$. As Fig. 5.8 shows, the average entropy for the BCJR-SIID is lower than that for the BCJR-BIID for a given channel setting, and the average entropy of both schemes reduces as channel conditions improve and/or the inner code rate decreases. Further, we observe that when the insertion/deletion probabilities drop to 0.002, the average entropy for the BCJR-SIID when $L = 5$ (resp., $L = 4$) is even lower than that for the BCJR-BIID when $L = 4$ (resp., $L = 3$). This suggests that at sufficiently low insertion/deletion probabilities, switching from the BCJR-BIID to the BCJR-SIID can yield better error performance even if the burst errors were to be slightly longer.

Fig. 5.9 shows the performance of the rate-0.8 DM code, i.e., a 256-ary (568, 512) LDPC outer code concatenated to a rate-8/9 inner code. As expected, the performance

5.3 Simulation Results and Discussions



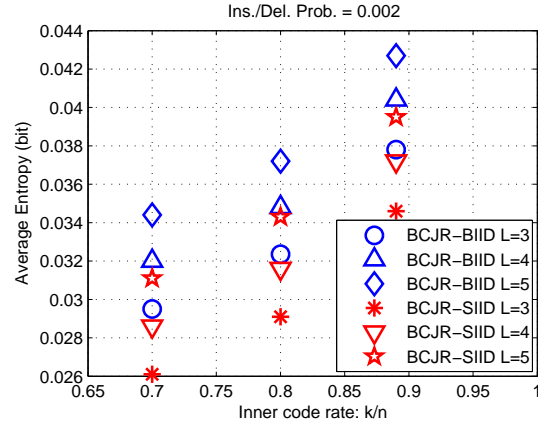
(a)



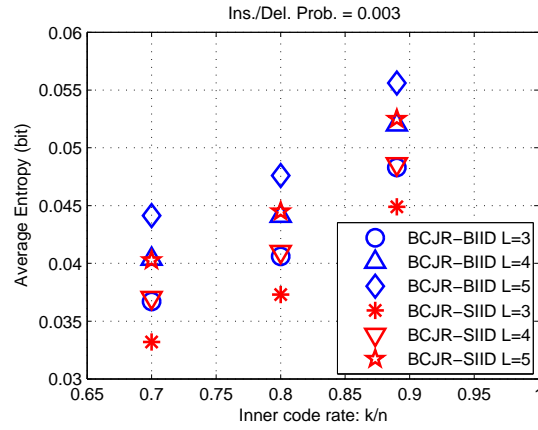
(b)

Figure 5.7: BER of BCJR-BIID and BCJR-SIID under iterative decoding on the single-track staggered BPMR channel with two rate-0.71 DM codes: a) DM-1 and b) DM-2.

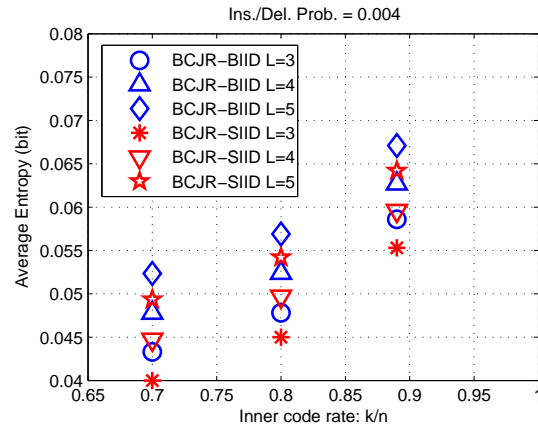
5.3 Simulation Results and Discussions



(a)



(b)



(c)

Figure 5.8: Average entropy of the likelihoods generated by BCJR-BIID and BCJR-SIID under non-iterative decoding against inner code rate for $L = 3, 4, 5$ and $P_I = P_D = 0.002, 0.003, 0.004$.

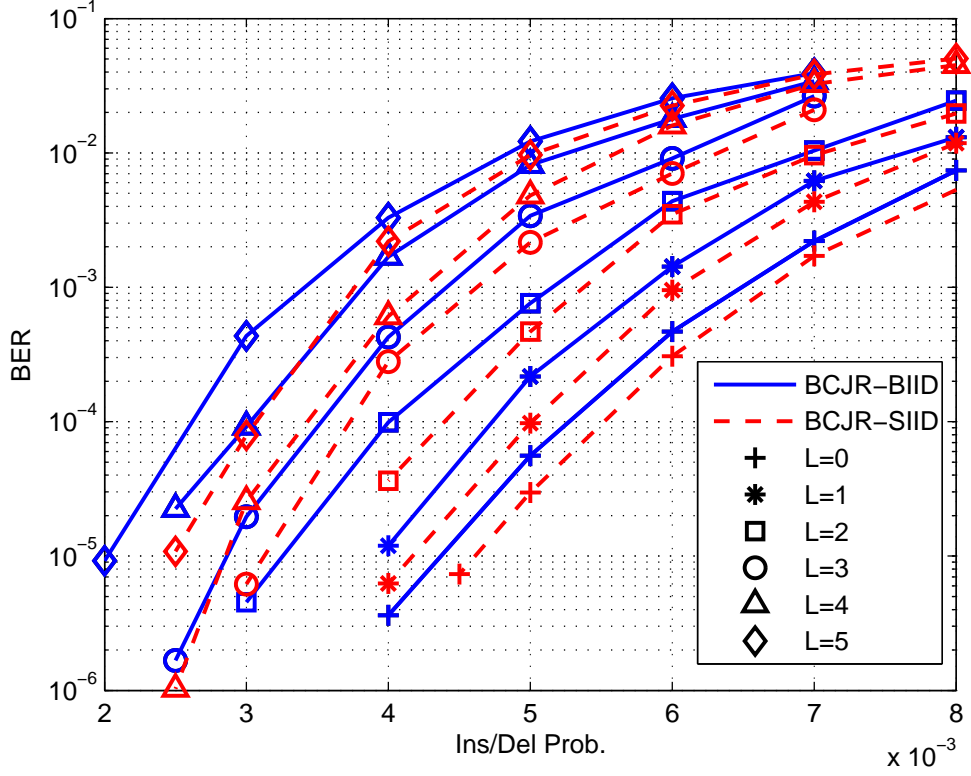


Figure 5.9: BER of rate-0.8 DM code with BCJR-BIID and BCJR-SIID under iterative decoding on the single-track staggered BPMR channel for $L = 0, \dots, 5$

of BCJR-SIID when $L = 5$ (resp., $L = 4$) is superior to that of the BCJR-BIID when $L = 4$ (resp., $L = 3$) for deletion/insertion probabilities not exceeding 0.003 (resp., 0.0027). Fig. 5.9 also shows that at a code rate of 0.8 and at low to moderate insertion/deletion probabilities (e.g., $< 2 \times 10^{-3}$), BERs below 10^{-5} are attainable with the BCJR-BIID provided the burst errors are short (i.e., $L \leq 5$).

5.4 Conclusion

In this chapter, we have investigated and compared the performance of M-JE on single-track staggered, double-track staggered and rectangular BPMR read channels at an

5.4 Conclusion

areal density of 6 Tb/inch². We find that M-JE exhibits the best performance on double-track staggered BPMR while EM-JE enables single-track staggered BPMR to outperform double-track staggered BPMR due to the ISI in the latter case being relatively more severe.

We also considered the DM coding scheme for single-track staggered BPMR. Our computer simulations show that at a code rate of 0.8, substitution error rate below 3.6×10^{-3} , insertion/deletion error rate at most 10^{-3} , a read channel SNR of 12 dB and an areal density of 6 inch², BERs below 10^{-5} are attainable provided the burst errors centered at a synchronization error are short (e.g., ≤ 10). Moreover, BCJR-SIID provides significantly better robustness against burst errors compared to BCJR-BIID at low insertion/deletion probabilities.

Chapter 6

Summary of Contributions and Suggestions for Future Work

In this thesis, we investigated and addressed some technical challenges in the development of BPMR from the signal processing and coding perspective. In this chapter, we summarize the investigation and highlight the contributions of this thesis. In the end, suggestions for future work are given.

6.1 Summary of Contributions

In BPMR, the presence of WIEs in the recording process is a unique and key challenge which can dramatically limit the overall performance. WIEs manifest as IDS errors in the recorded data sequence, which cannot be corrected by conventional substitution ECCs. Further, ultra-high areal densities in BPMR are achieved at the expense of reduced intervals between adjacent islands. As a consequence, ITI arises as a new performance limiting factor in addition to the conventional and ever-increasing ISI, which can significantly degrade the readback performance if not well compensated. Hence, the recovery of data written to the BPMR is a challenging task that requires

6.1 Summary of Contributions

significant progress made in the area of signal processing and coding.

In this thesis, we first investigated the DM concatenated coding schemes developed for channels with IIDS errors. The outer code used in the original DM coding scheme is a non-binary LDPC code. Motivated by the fact that RS codes are still considered for BPMR systems and powerful iterative soft-decision decoding schemes have been developed for RS codes, we hence investigated the performance improvements RS codes employed as the outer code in the DM coding scheme could bring. To this end, we first investigated the influence of the alphabet size of outer code and the length of each inner binary sparse string on the average uncertainty of the output from the DM inner decoder and the effective substitution error rate of the IIDS channel. Based on these discussions and in view of the fact that the code alphabet size of practical interest for RS codes are larger than that for LDPC codes, we considered two realizations of the DM coding scheme having the same length and same code rate: one employed a q -ary $(2(q^2 - 1), 2(q^2 - 1)R)$ LDPC code as the outer code while the other one used a q^2 -ary $(q^2 - 1, (q^2 - 1)R)$ RS code as the outer code. We showed that when insertion and deletion probabilities were sufficiently small, the latter offered better FER performance for moderate to high-rate applications involving relatively short blocklengths.

Experiments and simulations in the literature revealed that WIEs are data-dependent and the write channel introduces memories. Although many write channel models have been used to mimic the BPMR write process, they have their limits in capturing some of the characteristics of the WIEs. Therefore, we proposed a DIDS channel to mimic the impairments of the write process found in practical BPMR systems. This channel model consists of a ternary Markov state channel producing paired insertion and deletion errors, followed by a two-state BSC introducing burst-like substitution errors in the vicinity of each insertion and deletion error and random substitution error elsewhere. Further, we applied the DM coding scheme on this channel model with a modified inner decoder, which takes into account all the data-dependencies of the

6.1 Summary of Contributions

channel and delivers superior FER performance compared to that when the original symbol-level inner decoder is employed. We also proposed a scheme to efficiently reduce the complexity required by the modified inner decoder in dealing with burst-like substitution errors around each synchronization error. Computer simulation results on the DIDS channel had been presented, which were indicative of how well the DM coding scheme with the modified inner decoding algorithm will performance in an actual BPMR system, when the SNR is sufficiently high to enable the channel detector to compensate for all impairments of the read channel.

Further, we proceeded to investigate the problem of data recovery on rectangular and staggered BPMR write-read channels, which were modeled as a serial concatenation of the DIDS write channel and a partial response rectangular or staggered BPMR read channel with the addition of ITI. SE, JE, MTD and 2D equalization were considered for the read channel detection while the DM coding scheme combated WIEs as well as errors resulting from imperfect read channel detection.

Three detection-decoding schemes of combining the read channel detection and the modified DM inner decoder were first proposed and investigated on rectangular BPMR channel, namely the BCJR-BIID algorithm, the JDD algorithm and the BCJR-SIID algorithm. Computer simulations revealed that JDD provided the best performance at the expense of relatively high computational complexity, while BCJR-SIID (resp., BCJR-BIID) provided good performance-complexity trade-offs at low to moderate (resp., high) SNRs. It was also shown that increasing the areal density from 2.64 Tb/inch² to 4 Tb/inch² while the IDS error rates remained fixed in the recording process, did not significantly affect error performance on the rectangular BPMR channels. Rather, it was the burst errors preceding and following an insertion or deletion that had a significant impact on performance.

Since staggered BPMR can effectively reduce ITI at the expense of enhanced ISI which can nevertheless be effectively dealt with longer GPR targets, we inves-

6.2 Proposals for Future Research

tigated the data-recovery on staggered BPMR channels with areal density increased to 6 Tb/inch². We found that M-JE exhibited the best performance on double-track staggered BPMR while EM-JE enabled single-track staggered BPMR to outperform double-track staggered BPMR due to the ISI in the latter case being relatively more severe. Therefore, BCJR-BIID and BCJR-SIID that achieved good performance-complexity trade-offs on rectangular BPMR channels were employed for data recovery on single-track staggered BPMR with EM-JE. We observed that BCJR-SIID outperformed BCJR-BIID while increasing the length of burst errors preceding and following an insertion or deletion dramatically degraded the performance of both detection-decoding schemes. However, we also observed that the sensitivity of system performance on the length of burst errors actually decreased for longer length. Furthermore, we found that BCJR-SIID provided significantly better robustness against burst errors compared to BCJR-BIID at low insertion/deletion probabilities.

6.2 Proposals for Future Research

6.2.1 Efficiently Handle Relatively Long Burst Errors

In our investigation, we have identified that the overall performance of BPMR is highly dependent on the length of burst errors in the vicinity of each synchronization error. We have shown in this thesis the performance of DM coding scheme with a modified inner decoder for burst errors of length up to 10 bits. In an actual BPMR system, the burst error length may be longer. Although the modified DM inner decoder can theoretically handle burst errors of arbitrary length, its computational complexity increases exponentially in the length of burst errors.

Therefore, it would be of practical interest to develop new coding schemes or improve the modified inner DM decoding algorithm to efficiently handle burst errors

6.2 Proposals for Future Research

of relatively longer length.

6.2.2 Improving the DM Coding Scheme for DIDS Channel

In this thesis, we mainly use the original DM coding scheme to protect data on the DIDS channel. In Section 5.3.2, we show that the choice of outer LDPC code can significantly influence the overall performance of DM coding scheme employed on a single-track staggered BPMR channel. The outer LDPC codes used in this thesis are constructed using the PEG algorithm, and are therefore not optimized for the effective channel seen by the outer encoder and decoder, i.e., the serial concatenation of the inner encoder, DIDS channel and inner decoder. It has been reported in [38] that LDPC codes designed for IDS channels offer better performance when utilized as outer codes in marker codes. Therefore, it would be an interesting topic to construct LDPC outer codes specifically for the effective channel.

In addition, it has been reported in [70] that constructing the watermark string based on a certain probability metric can yield remarkable improvements over the randomly constructed watermark string. Further, it has been reported in [71] that the inner code in the DM coding scheme does not have to be sparse when symbol-level inner decoder is employed. Recently, we have optimized the DM inner code for the DIDS channel, which gets rid of the watermark string and significantly improves the performance of DM coding scheme on the BPMR channels [100]. Therefore, jointly optimizing the inner code and watermark string should further enhance the performance of the DM coding scheme when employed on the DIDS channel. This is an interesting pursuit.

6.2 Proposals for Future Research

6.2.3 Applying Marker Codes to the DIDS Channels

Like the DM coding scheme, marker code which was first introduced in [101] is also a promising concatenated coding scheme for channels with IDS errors [38, 39]. It can be interpreted as a special case of DM codes, where marker bits are inserted periodically into the transmitted sequence instead of uniformly distributed throughout the codeword. Hence, the inner decoder could similarly be modified to enable marker codes to be applied to make it applicable to the DIDS channel. It has been reported in [69] that replacing the inner watermark codes by marker codes with best markers of different size can offer significant performance improvement on the IIDS channel with low insertion/deletion error rates. Therefore, it would be interesting to investigate the performance of marker codes on the BPMR write-read channels considered in this thesis.

As highlighted in the first paragraph of Section 5.3.2, the sensitivity of the system performance on L actually decreases for larger values of L . In addition, according to Fig. 3.1, we note that shorter burst error lengths can be traded for higher insertion/deletion rates. Fortunately, the impact that higher insertion/deletion rates have on the performance of our detection-decoding schemes is less than that of longer burst errors. Thus, there may exist a threshold value whereby for insertion/deletion rates above this threshold, the burst errors are short enough to be efficiently dealt with.

Further, in view of the fact that the maximum inner code rate of the DM construction is limited by the code alphabet size of the outer code and prohibits the use of more powerful outer LDPC codes when the overall code rate is fixed, the synchronization error correction capability of the inner code may be more than necessary to handle the synchronization errors when the insertion/deletion error rates are relatively low while the outer code may be too weak to handle the relatively long burst of substitution errors. Marker codes on the other hand, do not have this limitation and so one has more

6.2 Proposals for Future Research

flexibility in choosing the inner and outer code rates. Since the markers, which serve as the inner code, can only correct synchronization errors while the substitution errors are entirely corrected by the outer code, the overall code structure can be optimized according to a particular BPMR channel for a fixed overall code rate, i.e., the inner (resp., outer) code rate can be reduced when the synchronization (resp., substitution) errors dominate the written-in errors. Further, since the markers are separated from each other, they will be affected by burst substitution errors to a lesser extent so that mis-synchronizations by the inner decoder are less likely compared to that in the DM construction. Moreover, a mis-synchronization in the DM inner decoder may propagate through the entire codeword and lead to more substitution errors that are too many to be corrected by the outer LDPC code. Therefore, marker codes may actually be a better choice to be used in a BPMR system when the burst substitution errors are long.

6.2.4 Detection-Decoding on BPMR Channels with Media Noise

Besides 2D interference and WIEs, media noise including island size and location variations is another critical and challenging issue that needs to be considered. Although the proposed DIDS channel mimicks the effects of media noise in the write channel, the WIE rates considered in this thesis have not been linked to the statistics of the media noise as well as other factors that contribute to WIEs such as mechanical disturbance, motor speed variation and so on. Improving our DIDS channel by establishing this link is clearly desirable. The computation of WIE rates based on the statistics of the media noise and other contributing factors have been considered in [12], however, the computation is only for a single island while ignoring the data-dependencies introduced by the write process. Therefore, establishing the aforementioned link by building on the results of [12] should take into account these dependencies.

On the other hand, media noise also significantly degrades the readback perfor-

6.2 Proposals for Future Research

mance and exacerbates the 2D interference. Since we focus on mitigating 2D interference in the presence of WIEs, the read channel detection techniques discussed in this thesis do not consider the effect of media noise. We nevertheless note that SE detection has been improved in [102] to take into account the effect of media noise in the read-back process. The modified SE detection yields superior performance compared to the original approach on the BPMR read channel with media noise. Another technique that has been widely used to mitigate data-dependent noise is pattern-dependent noise-prediction (PDNP) technique [103]. In [62], it was shown that applying PDNP to SE also yields significant performance improvements. However, SE cannot effectively mitigate ITI. Therefore, combining PDNP with MTD and/or 2D equalization that are designed with media noise considerations should effectively improve the performance of BPMR.

Appendix A

Channel Capacity Bounds for DIDS Channel

A.1 Channel Capacity Bounds for DIDS Channel with Stationary and Ergodic Input Process

Recall that the DIDS channel proposed in Chapter 3 is stationary and ergodic (SaE) as the channel state sequence \mathbf{Z} is a second order stationary process while all channel states can be reached within a finite number of steps from any channel state at any time with strictly positive probability [104]. Therefore, its channel capacity C can be defined as the information rate between the channel input sequence $\mathbf{X}_0^{+\infty}$ and the corresponding channel output sequence \mathbf{Y}_0^n following [105] as

$$C \triangleq \lim_{n \rightarrow +\infty} \sup_{\mathcal{P}(\mathbf{X}_0^{+\infty})} \frac{1}{n} I(\mathbf{X}_0^{+\infty}, \mathbf{Y}_0^n).$$

where $\mathcal{P}(\mathbf{X}_0^{+\infty})$ represents the channel input distribution.

Lemma A.1. *The channel capacity of the DIDS channel can be computed as*

$$C = \lim_{n \rightarrow +\infty} \sup_{\mathcal{P}(\mathbf{X}_0^{n+1})} \frac{1}{n} I(\mathbf{X}_0^{n+1}, \mathbf{Y}_0^n) \quad (\text{A.1})$$

A.1 Channel Capacity Bounds for DIDS Channel with Stationary and Ergodic Input Process

$$= \lim_{n \rightarrow +\infty} \sup_{\mathcal{P}(\mathbf{X}_0^{n+1})} \frac{1}{n} (H(\mathbf{Y}_0^n) - H(\mathbf{Y}_0^n | \mathbf{X}_0^{n+1})) \quad (\text{A.2})$$

Proof. Recall that the difference between the number of bits entering the DIDS channel and the corresponding number of bits received is either -1, 0 or 1. Therefore, when \mathbf{Y}_0^n is received, the input sequence could be either \mathbf{X}_{n-1} , \mathbf{X}_n or \mathbf{X}_{n+1} .

Since

$$\frac{1}{n} I(\mathbf{X}_0^{n+1}, \mathbf{Y}_0^n) = \frac{1}{n} I(\mathbf{X}_0^n, \mathbf{Y}_0^n) + \frac{1}{n} I(X_{n+1}; \mathbf{Y}_0^n | \mathbf{X}_0^n) \quad (\text{A.3})$$

and

$$\begin{aligned} I(X_{n+1}; \mathbf{Y}_0^n | \mathbf{X}_0^n) &\leq H(X_{n+1} | \mathbf{X}_0^n) \\ &\leq H(X_{n+1}) \\ &\leq 1, \end{aligned}$$

we have

$$\lim_{n \rightarrow +\infty} \frac{1}{n} I(X_{n+1}; \mathbf{Y}_0^n | \mathbf{X}_0^n) = 0$$

and

$$\lim_{n \rightarrow +\infty} \frac{1}{n} I(\mathbf{X}_0^{n+1}, \mathbf{Y}_0^n) \rightarrow \lim_{n \rightarrow +\infty} \frac{1}{n} I(\mathbf{X}_0^n, \mathbf{Y}_0^n)$$

Similarly, we can prove

$$\lim_{n \rightarrow +\infty} \frac{1}{n} I(\mathbf{X}_0^{n+1}, \mathbf{Y}_0^n) \rightarrow \lim_{n \rightarrow +\infty} \frac{1}{n} I(\mathbf{X}_0^{n-1}, \mathbf{Y}_0^n)$$

Therefore, without loss of generality, the DIDS channel capacity can be computed using (A.1). \square

As the DIDS channel is very complicated and introduces memory, it is impractical to find the optimal input distribution that maximizes the information rate. Therefore, we will shed some light on the DIDS channel capacity by deriving its lower bounds with typical SaE input processes, e.g., i.i.d input process and first-order Markov input process.

A.1 Channel Capacity Bounds for DIDS Channel with Stationary and Ergodic Input Process

Obviously, the channel output sequence \mathbf{Y} is SaE when both the channel input sequence and channel itself are SaE. Then, we have the following lemma.

Lemma A.2. *With a certain SaE input process \mathcal{X} , the SaE channel capacity of the DIDS channel is given by*

$$C_{SaE}(\mathcal{X}) = \lim_{n \rightarrow +\infty} \frac{1}{n} (H(\mathbf{Y}_0^n) - H(\mathbf{Y}_0^n | \mathbf{X}_0^{n+1})) \quad (\text{A.4})$$

$$= \lim_{n \rightarrow +\infty} (H(Y_n | \mathbf{Y}_0^{n-1}) - H(Y_n | \mathbf{X}_0^{n+1}, \mathbf{Y}_0^{n-1})) \quad (\text{A.5})$$

Proof. Since the channel output \mathbf{Y} is a SaE process, we follow the similar method proposed in [106] and have

$$\begin{aligned} \lim_{n \rightarrow +\infty} \frac{1}{n} H(\mathbf{Y}_0^n) &= \lim_{n \rightarrow +\infty} \frac{1}{n} (H(\mathbf{Y}_0^{2n}) - \sum_{i=n+1}^{2n} H(Y_i | \mathbf{Y}_0^i)) \\ &= 2 \lim_{n \rightarrow +\infty} \frac{1}{2n} H(\mathbf{Y}_0^{2n}) - \lim_{n \rightarrow +\infty} \frac{1}{n} \sum_{i=n+1}^{2n} H(Y_i | \mathbf{Y}_0^i) \\ &= 2 \lim_{n \rightarrow +\infty} \frac{1}{n} H(\mathbf{Y}_0^n) - \lim_{n \rightarrow +\infty} H(Y_n | \mathbf{Y}_0^{n-1}). \end{aligned}$$

Therefore,

$$\lim_{n \rightarrow +\infty} \frac{1}{n} H(\mathbf{Y}_0^n) = \lim_{n \rightarrow +\infty} H(Y_n | \mathbf{Y}_0^{n-1}). \quad (\text{A.6})$$

Similarly, we can prove that

$$\lim_{n \rightarrow +\infty} \frac{1}{n} H(\mathbf{Y}_0^n | \mathbf{X}_0^{n+1}) = \lim_{n \rightarrow +\infty} H(Y_n | \mathbf{X}_0^{n+1}, \mathbf{Y}_0^{n-1}). \quad (\text{A.7})$$

with the help of the fact that

$$\lim_{n \rightarrow +\infty} H(Y_i | \mathbf{X}_0^{2n+1}, \mathbf{Y}_0^{i-1}) = \lim_{n \rightarrow +\infty} H(Y_i | \mathbf{X}_0^{i+1}, \mathbf{Y}_0^{i-1})$$

since Y_i depends on up to X_{i+1} .

Then, substituting (A.6) and (A.7) into (A.4) implies the claim. \square

The actual $C_{SaE}(\mathcal{X})$ is still hard to compute, we hence derive its lower and upper bounds by evaluating each term in (A.5). Since conditioning reduces entropy, both

A.1 Channel Capacity Bounds for DIDS Channel with Stationary and Ergodic Input Process

terms can be upper-bounded as

$$\lim_{n \rightarrow +\infty} H(Y_n | \mathbf{Y}_0^{n-1}) \leq \lim_{n \rightarrow +\infty} H(Y_n | \mathbf{Y}_{n-M}^{n-1}) \quad (\text{A.8})$$

$$= H(Y_n | \mathbf{Y}_{n-M}^{n-1}) \quad (\text{A.9})$$

$$\lim_{n \rightarrow +\infty} H(Y_n | \mathbf{X}_0^{n+1}, \mathbf{Y}_0^{n-1}) \leq \lim_{n \rightarrow +\infty} H(Y_n | \mathbf{X}_{n-M}^{n+1}, \mathbf{Y}_{n-M}^{n-1}) \quad (\text{A.10})$$

$$= H(Y_n | \mathbf{X}_{n-M}^{n+1}, \mathbf{Y}_{n-M}^{n-1}) \quad (\text{A.11})$$

where $M \geq 0$. Equalities in (A.8, A.10) are achieved when $M = n$ and the equalities in (A.8, A.10) are due to the fact that \mathbf{X}, \mathbf{Y} are SaE. Further, the following lower bounds of both terms in (A.5) can be obtained with the help of the SCSW \mathbf{v}_i and the function $f_i(\mathbf{v}_i)$ defined in Chapter 3:

$$\lim_{n \rightarrow +\infty} H(Y_n | \mathbf{Y}_0^{n-1}) \geq \lim_{n \rightarrow +\infty} H(Y_n | \mathbf{Y}_0^{n-1}, \mathbf{v}_{n-M}) \quad (\text{A.12})$$

$$= \lim_{n \rightarrow +\infty} H(Y_n | \mathbf{Y}_{f_{n-M}(\mathbf{v}_{n-M})+1}^{n-1}, \mathbf{v}_{n-M}) \quad (\text{A.13})$$

$$= H(Y_n | \mathbf{Y}_{M_y+1}^{n-1}, \mathbf{v}_{n-M})$$

$$\lim_{n \rightarrow +\infty} H(Y_n | \mathbf{X}_0^{n+1}, \mathbf{Y}_0^{n-1}) \geq \lim_{n \rightarrow +\infty} H(Y_n | \mathbf{X}_0^{n+1}, \mathbf{Y}_0^{n-1}, \mathbf{v}_{n-M}) \quad (\text{A.14})$$

$$= \lim_{n \rightarrow +\infty} H(Y_n | \mathbf{X}_{n-M}^{n+1}, \mathbf{Y}_{f_{n-M}(\mathbf{v}_{n-M})+1}^{n-1}, \mathbf{v}_{n-M}) \quad (\text{A.15})$$

$$= H(Y_n | \mathbf{X}_{n-M}^{n+1}, \mathbf{Y}_{M_y}^{n-1}, \mathbf{v}_{n-M})$$

where $M_y = f_{n-M}(\mathbf{v}_{n-M}) + 1$. Equalities hold in (A.12, A.14) when $M = n$. The equalities in (A.13, A.15) are due to the fact that the sequence of \mathbf{v}_i 's is a first-order stationary Markov process.

Then, by defining

$$C_{SaE}^{lb}(\mathcal{X}) \triangleq H(Y_n | \mathbf{Y}_{M_y}^{n-1}, \mathbf{v}_{n-M}) - H(Y_n | \mathbf{X}_{n-M}^{n+1}, \mathbf{Y}_{n-M}^{n-1}) \quad (\text{A.16})$$

$$C_{SaE}^{ub}(\mathcal{X}) \triangleq H(Y_n | \mathbf{Y}_{n-M}^{n-1}) - H(Y_n | \mathbf{X}_{n-M}^{n+1}, \mathbf{Y}_{M_y}^{n-1}, \mathbf{v}_{n-M}) \quad (\text{A.17})$$

we have

$$C_{SaE}^{lb}(\mathcal{X}) \leq C_{SaE}(\mathcal{X}) \leq C_{SaE}^{ub}(\mathcal{X})$$

A.1 Channel Capacity Bounds for DIDS Channel with Stationary and Ergodic Input Process

Hence, $C_{SaE}^{lb}(\mathcal{X})$ and $C_{SaE}^{ub}(\mathcal{X})$ give the lower and upper bounds of $C_{SaE}(\mathcal{X})$, respectively. The accuracy of both bounds improves as M increases, which will be verified in the next section of the appendix.

The four conditional entropies in (A.16, A.17) can be computed as follows:

$$\begin{aligned}
H(Y_n | \mathbf{Y}_{M_y}^{n-1}, \mathbf{v}_{n-M}) &= \sum_{\mathbf{Y}_{M_y}^n, \mathbf{v}_{n-M}} P(\mathbf{Y}_{M_y}^n, \mathbf{v}_{n-M}) \log \frac{P(\mathbf{Y}_{M_y}^{n-1}, \mathbf{v}_{n-M})}{P(\mathbf{Y}_{M_y}^n, \mathbf{v}_{n-M})} \\
H(Y_n | \mathbf{X}_{n-M}^{n+1}, \mathbf{Y}_{M_y}^{n-1}, \mathbf{v}_{n-M}) &= \sum_{\mathbf{Y}_{M_y}^n, \mathbf{X}_{n-M}^{n+1}, \mathbf{v}_{n-M}} \left(P(\mathbf{Y}_{M_y}^n, \mathbf{X}_{n-M}^{n+1}, \mathbf{v}_{n-M}) \right. \\
&\quad \left. \cdot \log \frac{P(\mathbf{Y}_{M_y}^{n-1}, \mathbf{X}_{n-M}^{n+1}, \mathbf{v}_{n-M})}{P(\mathbf{Y}_{M_y}^n, \mathbf{X}_{n-M}^{n+1}, \mathbf{v}_{n-M})} \right) \\
H(Y_n | \mathbf{Y}_{n-M}^{n-1}) &= \sum_{\mathbf{Y}_{n-M}^n} P(\mathbf{Y}_{n-M}^n) \log \frac{P(\mathbf{Y}_{n-M}^{n-1})}{P(\mathbf{Y}_{n-M}^n)} \\
H(Y_n | \mathbf{X}_{n-M}^{n+1}, \mathbf{Y}_{n-M}^{n-1}) &= \sum_{\mathbf{X}_{n-M}^{n+1}, \mathbf{Y}_{n-M}^n} P(\mathbf{X}_{n-M}^{n+1}, \mathbf{Y}_{n-M}^n) \log \frac{P(\mathbf{X}_{n-M}^{n+1}, \mathbf{Y}_{n-M}^{n-1})}{P(\mathbf{X}_{n-M}^{n+1}, \mathbf{Y}_{n-M}^n)}
\end{aligned}$$

Obviously, only $P(\mathbf{Y}_{M_y}^n, \mathbf{X}_{n-M}^{n+1}, \mathbf{v}_{n-M})$ needs to be computed while other probabilities can be obtained through marginalization of $P(\mathbf{Y}_{M_y}^n, \mathbf{X}_{n-M}^{n+1}, \mathbf{v}_{n-M})$. As the input sequence is independent of the channel, this probability can be computed as

$$P(\mathbf{Y}_{M_y}^n, \mathbf{X}_{n-M}^{n+1}, \mathbf{v}_{n-M}) = P(\mathbf{Y}_{M_y}^n | \mathbf{X}_{n-M}^{n+1}, \mathbf{v}_{n-M}) P(\mathbf{X}_{n-M}^{n+1}) P(\mathbf{v}_{n-M}) \quad (\text{A.18})$$

$$\begin{aligned}
&= P(\mathbf{X}_{n-M}^{n+1}) P(\mathbf{v}_{n-M}) \sum_{\mathbf{v}_{n+1}} P(\mathbf{Y}_{M_y}^n, \mathbf{v}_{n+1} | \mathbf{X}_{n-M}^{n+1}, \mathbf{v}_{n-M}) \\
&\quad (\text{A.19})
\end{aligned}$$

where $P(\mathbf{X}_{n-M}^{n+1})$ is given by the channel input distribution and

$$P(\mathbf{Y}_{M_y}^n, \mathbf{v}_{n+1} | \mathbf{X}_{n-M}^{n+1}, \mathbf{v}_{n-M})$$

can be calculated by performing a forward pass between \mathbf{v}_{n-M} and \mathbf{v}_{n+1} using (3.4).

Denoting the space of all valid SCSWs as $\{S_k\}_{k=0}^{N_s-1}$, the *a priori* probability $P(\mathbf{v}_{n-M} = S_k)$ can be obtained by solving the following linear programming problem:

$$\mathbf{P}_T \mathbf{S}_p^T = \mathbf{S}_p$$

A.2 Symmetric Information Rate Lower and Upper Bounds of the DIDS Channel

$$\text{subject to : } \sum_{k=0}^{N_s-1} P(S_k) = 1 \quad (\text{A.20})$$

$$P(S_k) \geq 0, k = 0, 1, \dots, N_s - 1 \quad (\text{A.21})$$

where $\mathbf{S}_p = [P(S_0), P(S_1), \dots, P(S_{N_s-1})]^T$ and the element in the probability transfer matrix \mathbf{P}_T are given by

$$(\mathbf{P}_T)_{ij} = P(\mathbf{v}_t = S_i | \mathbf{v}_{t-1} = S_j)$$

Although increasing M improves the accuracy of both lower and upper bounds approximating $C_{SaE}(\mathcal{X})$, the computational complexity of (A.18) grows exponentially in M which prevents the use of relatively large M . Fortunately, we will show in the next section that both capacity bounds converge very fast even for small M when the length L of burst errors preceding and following each synchronization error is relatively short, i.e., $L \leq 2$.

A.2 Symmetric Information Rate Lower and Upper Bounds of the DIDS Channel

In this section, we consider the same DIDS channel as that considered in Section 3.4.2, i.e., the random and burst substitution rates are $P_R = 0.001$ and $P_B = 0.1$, respectively. We also consider equal insertion and deletion rates, i.e., $P_I = P_D$. Note that since

$$P(Z_i = 1 | Z_{i-1} = 0, Z_{i-2} = 0) + P(Z_i = -1 | Z_{i-1} = 0, Z_{i-2} = 0) = P_I + P_D \leq 1$$

we have $P_I = P_D \leq 0.5$. Since the DIDS channel is a binary system, we assume that \mathcal{X} is a i.u.d process, i.e., $P(X_i = 0) = P(X_i = 1) = 0.5$, and focus on the SIR of the DIDS channel. Note that the method derived in this appendix can also be used to estimate the lower and upper bounds of $C_{SaE}(\mathcal{X})$ for other SaE input processes, for an example, the first-order Markov input process considered in [30].

A.2 Symmetric Information Rate Lower and Upper Bounds of the DIDS Channel

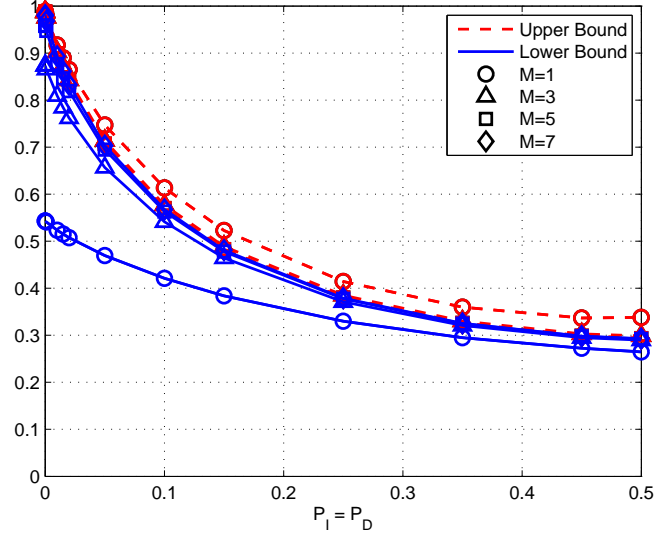


Figure A.1: Symmetric information rate lower and upper bounds for DIDS channel with $L = 0$.

In Figs. A.1 and A.2, we plot the upper and lower bounds of the SIR for the DIDS channel with $L = 0$ and $L = 1$, respectively. As expected, increasing M significantly improves the accuracy of both lower and upper bounds while $M = 5$ is sufficient for both bounds to converge to the actual SIR for both DIDS channels.

Further, we consider the SIR for the DIDS channel with $L = 2$. As shown in Table 3.1, we note that there is a large number of valid SCSWs for $L \geq 2$. Since the computational complexity of (A.18) increases exponentially in N_s and M , we only show the SIR upper and lower bounds for $L = 2$ with $M = 1, 3, 5$ in Fig. A.3. Compared to Figs. A.1 and A.2, we observe that the gap between SIR lower and upper bounds for $L = 2$ with $M = 3$ is wider than that for $L = 0, 1$. This is because the memory of the DIDS channel also increases in L . Therefore, a larger M is required to better estimate the SIR of the DIDS channel with longer burst errors surrounding each insertion/deletion error.

Since the lower and upper SIR bounds for the DIDS channel with $L = 0, 1$ are

A.2 Symmetric Information Rate Lower and Upper Bounds of the DIDS Channel

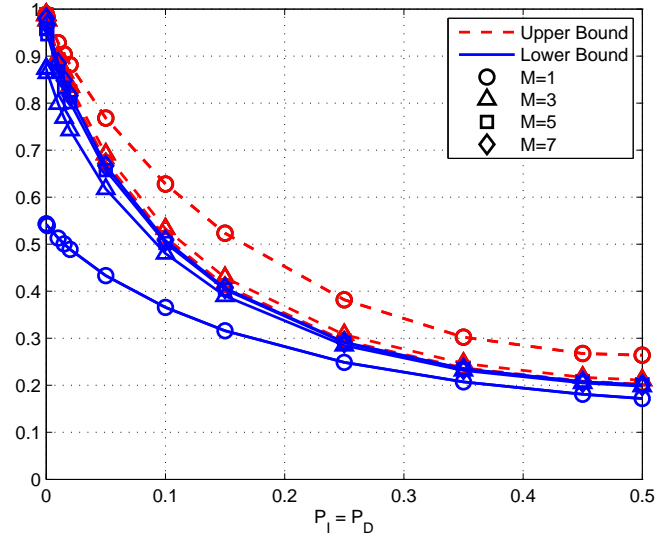


Figure A.2: Symmetric information rate lower and upper bounds for DIDS channel with $L = 1$.

almost identical when $M \geq 5$, we take the upper bounds with $M = 7$ to approximate the actual SIRs for the DIDS channel with $L = 0, 1$. To show the SIR loss due to the increase in L , we plot in Fig. 3.13 the SIRs for the DIDS channel with $L = 0, 1$ and the SIR lower and upper bounds with $M = 5$ for the DIDS channel with $L = 2$. The analysis and discussion concerning Fig. 3.13 can be found in Section. 3.4.2.

A.2 Symmetric Information Rate Lower and Upper Bounds of the DIDS Channel

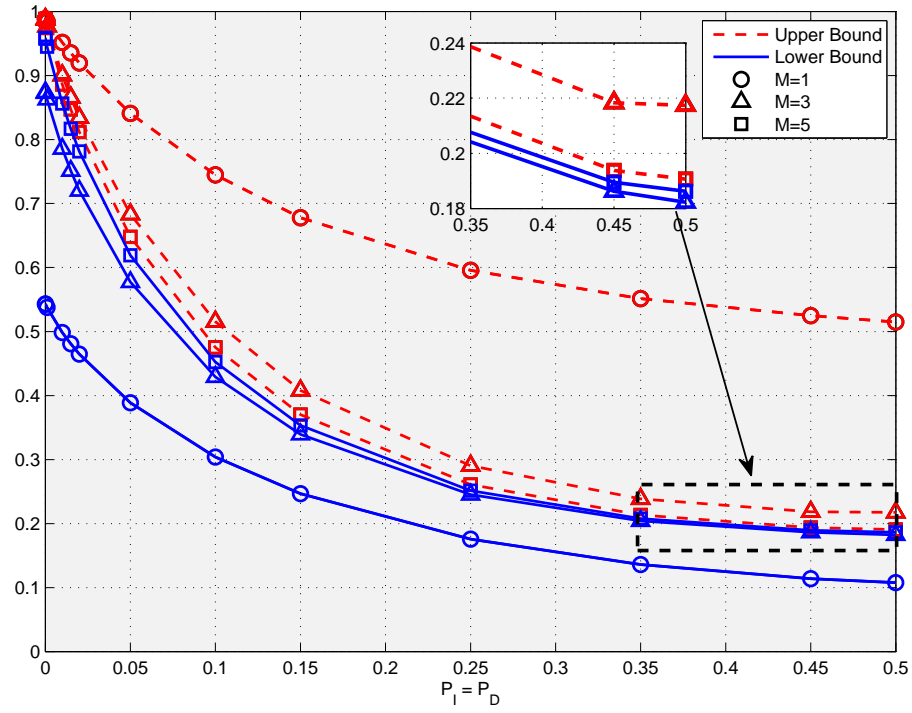


Figure A.3: Symmetric information rate lower and upper bounds for DIDS channel with $L = 2$.

Bibliography

- [1] R. E. Fontana, S. Hetzler, and G. Decad, “Technology roadmap comparisons for tape, hdd, and nand flash: Implications for data storage applications,” *IEEE Trans. Magn.*, vol. 48, no. 5, pp. 1692–1696, May 2012.
- [2] S. Wang and A. Taratorin, *Magnetic Information Storage Technology: A Volume in the Electromagnetism Series*, ser. Electromagnetism. Academic Press, 1999.
- [3] D. Weller and A. Moser, “Thermal effect limits in ultrahigh-density magnetic recording,” *IEEE Trans. Magn.*, vol. 35, no. 6, pp. 4423–4439, Nov. 1999.
- [4] B. Vasic and E. Kurtas, *Coding and Signal Processing for Magnetic Recording Systems*, ser. Computer Engineering Series. Taylor & Francis, 2004.
- [5] S. Iwasaki and K. Ouchi, “Co-cr recording films with perpendicular magnetic anisotropy,” *IEEE Trans. Magn.*, vol. 14, no. 5, pp. 849–851, Sep. 1978.
- [6] S. Iwasaki, “Perpendicular magnetic recording,” *IEEE Trans. Magn.*, vol. 16, no. 1, pp. 71–76, Jan. 1980.
- [7] R. Victora and M. Patwari, “Areal density limits for perpendicular magnetic recording,” *IEEE Trans. Magn.*, vol. 38, no. 5, pp. 1886–1891, Sep. 2002.
- [8] R. Wood, “The feasibility of magnetic recording at 1 Terabit per square inch,” *IEEE Trans. Magn.*, vol. 36, no. 1, pp. 36–42, Jan. 2000.

BIBLIOGRAPHY

- [9] S. Greaves, Y. Kanai, and H. Muraoka, "Shingled recording for 2 – 3 Tbit/in²," *IEEE Trans. Magn.*, vol. 45, no. 10, pp. 3823–3829, Oct. 2009.
- [10] K. Sann Chan, J. Miles, E. Hwang, B. Vijayakumar, J.-G. Zhu, W.-C. Lin, and R. Negi, "TDMR platform simulations and experiments," *IEEE Trans. Magn.*, vol. 45, no. 10, pp. 3837–3843, Oct. 2009.
- [11] R. Victora, S. Morgan, K. Momsen, E. Cho, and M. Erden, "Two-dimensional magnetic recording at 10 Tb/in²," *IEEE Trans. Magn.*, vol. 48, no. 5, pp. 1697–1703, May 2012.
- [12] H. Richter, A. Dobin, O. Heinonen, K. Gao, R. Veerdonk, R. Lynch, J. Xue, D. Weller, P. Asselin, M. Erden, and R. Brockie, "Recording on bit-patterned media at densities of 1 Tb/in² and beyond," *IEEE Trans. Magn.*, vol. 42, no. 10, pp. 2255–2260, Oct. 2006.
- [13] Y. Shiroishi, K. Fukuda, I. Tagawa, H. Iwasaki, S. Takenoiri, H. Tanaka, H. Mutoh, and N. Yoshikawa, "Future options for HDD storage," *IEEE Trans. Magn.*, vol. 45, no. 10, pp. 3816–3822, Oct. 2009.
- [14] Z. M. Yuan, B. Liu, T. J. Zhou, C. K. Goh, C. L. Ong, C. M. Cheong, and L. Wang, "Perspectives of magnetic recording system at 10 Tb/in²," *IEEE Trans. Magn.*, vol. 45, no. 11, pp. 5038–5043, Nov. 2009.
- [15] M. Kryder, E. Gage, T. McDaniel, W. Challener, R. Rottmayer, G. Ju, Y.-T. Hsia, and M. Erden, "Heat assisted magnetic recording," *Proceedings of the IEEE*, vol. 96, no. 11, pp. 1810–1835, Nov. 2008.
- [16] J.-G. Zhu, X. Zhu, and Y. Tang, "Microwave assisted magnetic recording," *IEEE Trans. Magn.*, vol. 44, no. 1, pp. 125–131, Jan. 2008.

BIBLIOGRAPHY

- [17] Y. Kamata, A. Kikitsu, N. Kihara, S. Morita, K. Kimura, and H. Izumi, “Fabrication of ridge-and-groove servo pattern consisting of self-assembled dots for 2.5 Tb/in² bit patterned media,” *IEEE Trans. Magn.*, vol. 47, no. 1, pp. 51–54, Jan. 2011.
- [18] A. Kikitsu, T. Maeda, H. Hieda, R. Yamamoto, N. Kihara, and Y. Kamata, “5 Tdots/in² bit patterned media fabricated by a directed self-assembly mask,” *IEEE Trans. Magn.*, vol. 49, no. 2, pp. 693–698, Feb. 2013.
- [19] M. Grobis, O. Hellwig, T. Hauet, E. Dobisz, and T. Albrecht, “High-density bit patterned media: Magnetic design and recording performance,” *IEEE Trans. Magn.*, vol. 47, no. 1, pp. 6–10, Jan. 2011.
- [20] J.-G. Zhu, X. Lin, L. Guan, and W. Messner, “Recording, noise, and servo characteristics of patterned thin film media,” *IEEE Trans. Magn.*, vol. 36, no. 1, pp. 23–29, Jan. 2000.
- [21] S. S. Malhotra, B. B. Lal, M. Alex, and M. A. Russak, “Effect of track edge erasure and on-track percolation on media noise at high recording density in longitudinal thin film media,” *IEEE Trans. Magn.*, vol. 33, no. 5, pp. 2992–2994, Sep. 1997.
- [22] R. L. White, R. Newt, and R. F. W. Pease, “Patterned media: a viable route to 50 Gbit/in² and up for magnetic recording?” *IEEE Trans. Magn.*, vol. 33, no. 1, pp. 990–995, Jan. 1997.
- [23] E. A. Dobisz, Z. Bandic, T.-W. Wu, and T. Albrecht, “Patterned media: Nanofabrication challenges of future disk drives,” *Proceedings of the IEEE*, vol. 96, no. 11, pp. 1836–1846, Nov. 2008.

BIBLIOGRAPHY

- [24] T. Thomson and B. D. Terris, “Patterned magnetic recording media: Progress and prospects,” *Developments in Data Storage: Materials Perspective*, pp. 256–276, 2012.
- [25] C. Ross, “Patterned magnetic recording media,” *Annual Review of Materials Research*, vol. 2, 2001. [Online]. Available: <http://www.annualreviews.org/doi/abs/10.1146/annurev.matsci.31.1.203>
- [26] A. N. Murthy, M. Duwensee, and F. E. Talke, “Numerical simulation of the head/disk interface for patterned media,” *Tribology Letters*, vol. 38, no. 1, pp. 47–55, Apr. 2010.
- [27] L. Li and D. B. Bogy, “Air bearing dynamic stability on bit patterned media disks,” *Microsystem Technologies*, vol. 19, no. 9-10, pp. 1401–1406, Jun. 2013.
- [28] M. Y. Lin, K. S. Chan, M. Chua, S. Zhang, C. Kui, and M. R. Elidrissi, “Modeling for write synchronization in bit patterned media recording,” *Journal of Applied Physics*, vol. 111, no. 7, p. 07B918, Mar. 2012.
- [29] S. Zhang, K. Cai, M. Lin-Yu, J. Zhang, Z. Qin, K. K. Teo, W. E. Wong, and E. T. Ong, “Timing and written-in errors characterization for bit patterned media,” *IEEE Trans. Magn.*, vol. 47, no. 10, pp. 2555–2558, Oct. 2011.
- [30] A. R. Iyengar, P. H. Siegel, and J. K. Wolf, “Write channel model for bit-patterned media recording,” *IEEE Trans. Magn.*, vol. 47, no. 1, pp. 35–45, Jan. 2011.
- [31] H. Muraoka and S. J. Greaves, “Statistical modeling of write error rates in bit patterned media for 10 Tb/in² recording,” *IEEE Trans. Magn.*, vol. 47, no. 1, pp. 26–34, Jan. 2011.

BIBLIOGRAPHY

- [32] J. Kalezhi, B. D. Belle, and J. J. Miles, “Dependence of write-window on write error rates in bit patterned media,” *IEEE Trans. Magn.*, vol. 46, no. 10, pp. 3752–3759, Oct. 2010.
- [33] J. Talbot, J. Kalezhi, C. Barton, G. Heldt, and J. Miles, “Write errors in bit patterned media: The importance of parameter distribution tails,” *IEEE Trans. Magn.*, 2014. [Online]. Available: <http://ieeexplore.ieee.org/>
- [34] S. H. Zhang, K. S. Chai, K. Cai, B. J. Chen, Z. L. Qin, S. M. Foo, Z. Songhua, C. Kao-Siang, C. Kui, C. Bingjin, Q. Zhiliang, and F. Siang-Meng, “Write failure analysis for bit-patterned-media recording and its impact on read channel modeling,” *IEEE Trans. Magn.*, vol. 46, no. 6, pp. 1363–1365, Jun. 2010.
- [35] J. Hu, T. M. Duman, M. F. Erden, and A. Kavcic, “Achievable information rates for channels with insertions, deletions, and intersymbol interference with i.i.d. inputs,” *IEEE Trans. Commun.*, vol. 58, no. 4, pp. 1102–1111, Apr. 2010.
- [36] D. Fertonani, T. Duman, and M. Erden, “Bounds on the capacity of channels with insertions, deletions and substitutions,” *IEEE Trans. Commun.*, vol. 59, no. 1, pp. 2–6, Jan. 2011.
- [37] Y. B. Ng, B. V. K. V. Kumar, K. Cai, S. Nabavi, and T. C. Chong, “Picket-shift codes for bit-patterned media recording with insertion/deletion errors,” *IEEE Trans. Magn.*, vol. 46, no. 6, pp. 2268–2271, Jun. 2010.
- [38] F. Wang, D. Fertonani, and T. Duman, “Symbol-level synchronization and LDPC code design for insertion/deletion channels,” *IEEE Trans. Commun.*, vol. 59, no. 5, pp. 1287–1297, May 2011.

BIBLIOGRAPHY

- [39] G. Han, Y. Guan, K. Cai, K. Chan, and L. Kong, “Embedded marker code for channels corrupted by insertions, deletions, and AWGN,” *IEEE Trans. Magn.*, vol. 49, no. 6, pp. 2535–2538, Jun. 2013.
- [40] S. Karakulak, P. Siegel, J. Wolf, and H. Bertram, “A new read channel model for patterned media storage,” *IEEE Trans. Magn.*, vol. 44, no. 1, pp. 193–197, Jan. 2008.
- [41] E. Kretzmer, “Generalization of a technique for binary data communication,” *IEEE Trans. Commun. Tech.*, vol. 14, no. 1, pp. 67–68, Feb. 1966.
- [42] J. Coker, R. Galbraith, G. Kerwin, J. Rae, and P. Ziporovich, “Implementation of PRML in a rigid disk drive,” *IEEE Trans. Magn.*, vol. 27, no. 6, pp. 4538–4543, Nov. 1991.
- [43] R. Cideciyan, F. Dolivo, R. Hermann, W. Hirt, and W. Schott, “A PRML system for digital magnetic recording,” *IEEE J. Selected Areas in Commun.*, vol. 10, no. 1, pp. 38–56, Jan. 1992.
- [44] K. Koo, S.-Y. Kim, J. J. Jeong, and S. W. Kim, “Two-dimensional partial response maximum likelihood at rear for bit-patterned media,” *IEEE Trans. Magn.*, vol. 49, no. 6, pp. 2744–2747, Jun. 2013.
- [45] M. Keskinöz, “Two-dimensional equalization/detection for patterned media storage,” *IEEE Trans. Magn.*, vol. 44, no. 4, pp. 533–539, Apr. 2008.
- [46] P. W. Nutter, I. T. Ntokas, and B. K. Middleton, “An investigation of the effects of media characteristics on read channel performance for patterned media storage,” *IEEE Trans. Magn.*, vol. 41, no. 11, pp. 4327–4334, Nov. 2005.
- [47] J. Moon and W. Zeng, “Equalization for maximum likelihood detectors,” *IEEE Trans. Magn.*, vol. 31, no. 2, pp. 1083–1088, Mar. 1995.

BIBLIOGRAPHY

- [48] S. Nabavi and B. V. K. V. Kumar, “Two-dimensional generalized partial response equalizer for bit-patterned media,” in *Proc. IEEE Int. Conf. Commun.*, Glasgow, Scotland, Jun. 2007, pp. 6249–6254.
- [49] W. Chang and J. R. Cruz, “Inter-track interference mitigation for bit-patterned magnetic recording,” *IEEE Trans. Magn.*, vol. 46, no. 11, pp. 3899–3908, Nov. 2010.
- [50] B. Livshitz, A. Inomata, H. Bertram, and V. Lomakin, “Semi-analytical approach for analysis of BER in conventional and staggered bit patterned media,” *IEEE Trans. Magn.*, vol. 45, no. 10, pp. 3519–3522, Oct. 2009.
- [51] W. Chang and J. R. Cruz, “Intertrack interference mitigation on staggered bit-patterned media,” *IEEE Trans. Magn.*, vol. 47, no. 10, pp. 2551–2554, Oct. 2011.
- [52] S. Nabavi, B. V. K. V. Kumar, and J. A. Bain, “Two-dimensional pulse response and media noise modeling for bit-patterned media,” *IEEE Trans. Magn.*, vol. 44, no. 11, pp. 3789–3792, Nov. 2008.
- [53] Y. Ng, K. Cai, B. Kumar, S. Zhang, and T. C. Chong, “Modeling and two-dimensional equalization for bit-patterned media channels with media noise,” *IEEE Trans. Magn.*, vol. 45, no. 10, pp. 3535–3538, Oct. 2009.
- [54] Y. Ng, K. Cai, B. V. K. V. Kumar, T. C. Chong, S. Zhang, and B. J. Chen, “Channel modeling and equalizer design for staggered islands bit-patterned media recording,” *IEEE Trans. Magn.*, vol. 48, no. 6, pp. 1976–1983, Jun. 2012.
- [55] J. Moon and J. Park, “Pattern-dependent noise prediction in signal-dependent noise,” *IEEE J. Selected Areas in Commun.*, vol. 19, no. 4, pp. 730–743, Apr. 2001.

BIBLIOGRAPHY

- [56] H. Mercier, V. K. Bhargava, and V. Tarokh, “A survey of error-correcting codes for channels with symbol synchronization errors,” *IEEE Commun. Surveys & Tutorials*, vol. 12, no. 1, pp. 87–96, Jan. 2010.
- [57] M. C. Davey and D. J. C. MacKay, “Reliable communication over channels with insertions, deletions, and substitutions,” *IEEE Trans. Inf. Theory*, vol. 47, no. 2, pp. 687–698, Feb. 2001.
- [58] J. Briffa and H. Schaathun, “Non-binary turbo codes and applications,” in *Proc. 5th IEEE International Symposium on Turbo Codes & Related Topics*, Sep. 2008, pp. 294–298.
- [59] H. Song and J. R. Cruz, “Reduced-complexity decoding of Q-ary LDPC codes for magnetic recording,” *IEEE Trans. Magn.*, vol. 39, no. 2, pp. 1081 – 1087, Mar. 2003.
- [60] J. Hu, T. Duman, E. Kurtas, and M. Erden, “Bit-patterned media with written-in errors: Modeling, detection, and theoretical limits,” *IEEE Trans. Magn.*, vol. 43, no. 8, pp. 3517–3524, Aug. 2007.
- [61] K. Cai, Z. Qin, S. Zhang, Y. Ng, K. Chai, and R. Radhakrishnan, “Modeling, detection, and LDPC codes for bit-patterned media recording,” in *IEEE GLOBE-COM Workshops*, Dec. 2010, pp. 1910 –1914.
- [62] R. Keele, “Advances in modeling and signal processing for bit-patterned magnetic recording channels with written-in errors,” Ph.D. dissertation, The University of Oklahoma, Norman, 2012.
- [63] S. Nabavi, “Signal processing for bit-patterned media channels with inter-track interference,” Ph.D. dissertation, Carnegie Mellon University, Pittsburgh, PA, 2008.

BIBLIOGRAPHY

- [64] C. He, D. Sridhara, A. Sridharan, and R. Venkataranmani, “Converting timing errors into symbol errors to handle write mis-synchronization in bit-patterned media recording systems,” U.S. Patent 2010/0 020 429A1, Jan., 2010.
- [65] R. Gallager, L. Laboratory, and M. I. O. T. L. L. LAB., *Sequential Decoding for Binary Channels with Noise and Synchronization Errors*, ser. Group report. Massachusetts Institute of Technology, Lincoln Laboratory, 1961.
- [66] E. Ratzner, “Marker codes for channels with insertions and deletions,” *Annales Des Tlcommunications*, vol. 60, no. 1-2, pp. 29–44, 2005.
- [67] L. Bahl and F. Jelinek, “Decoding for channels with insertions, deletions, and substitutions with applications to speech recognition,” *IEEE Trans. Inform. Theory*, vol. 21, no. 4, pp. 404–411, Apr. 1975.
- [68] Y. L. Guan, G. Han, L. Kong, K. S. Chan, K. Cai, and J. Zheng, “Coding and signal processing for ultra-high density magnetic recording channels,” in *2014 International Conference on Computing, Networking and Communications (ICNC)*, Feb. 2014, pp. 194–199.
- [69] E. A. Ratzner and D. J. MacKay, “Codes for channels with insertions, deletions and substitutions,” in *Proc. 2nd International Symposium on Turbo Codes and Applications*, 2000, pp. 149–156.
- [70] P.-M. Nguyen, M. A. Armand, and T. Wu, “On the watermark string in the Davey-MacKay construction,” *IEEE Commun. Letters*, vol. 17, no. 9, pp. 1830–1833, Sep. 2013.
- [71] J. Briffa, H. Schaathun, and S. Wesemeyer, “An improved decoding algorithm for the Davey-MacKay construction,” in *Proc. IEEE Intern. Conf. Commun.*, Cape Town, South Africa, May 2010, pp. 1 –5.

BIBLIOGRAPHY

- [72] X. Jiao and M. A. Armand, “Interleaved LDPC codes, reduced-complexity inner decoder and an iterative decoder for the Davey-MacKay construction,” in *Proc. IEEE Int. Symp. Inf. Theory*, St. Petersburg, Russia, Jul./Aug. 2011, pp. 742–746.
- [73] R. G. Gallager, *Low Density Parity Check Codes*. Cambridge, MA: MIT Press, 1963.
- [74] D. J. MacKay and R. M. Neal, “Near shannon limit performance of low density parity check codes,” *Electronics letters*, vol. 32, no. 18, pp. 1645–1646, 1996.
- [75] T. Richardson and R. Urbanke, “The capacity of low-density parity-check codes under message-passing decoding,” *IEEE Trans. Inform. Theory*, vol. 47, no. 2, pp. 599–618, Feb. 2001.
- [76] T. Richardson, M. Shokrollahi, and R. Urbanke, “Design of capacity-approaching irregular low-density parity-check codes,” *IEEE Trans. Inform. Theory*, vol. 47, no. 2, pp. 619–637, Feb. 2001.
- [77] S. Ten Brink, “Convergence behavior of iteratively decoded parallel concatenated codes,” *IEEE Trans. Commun.*, vol. 49, no. 10, pp. 1727–1737, Oct. 2001.
- [78] S. ten Brink, G. Kramer, and A. Ashikhmin, “Design of low-density parity-check codes for modulation and detection,” *IEEE Trans. Commun.*, vol. 52, no. 4, pp. 670–678, Apr. 2004.
- [79] R. M. Tanner, “A recursive approach to low complexity codes,” *IEEE Trans. Inform. Theory*, vol. 27, no. 5, pp. 533–547, Sep. 1981.
- [80] D. J. C. MacKay, “Good error-correcting codes based on very sparse matrices,” *IEEE Trans. Inform. Theory*, vol. 45, no. 2, pp. 399–431, Mar. 1999.

BIBLIOGRAPHY

- [81] M. Davey and D. MacKay, "Low-density parity check codes over $GF(q)$," *IEEE Commun. Lett.*, vol. 2, no. 6, pp. 165–167, Jun. 1998.
- [82] D. Declercq and M. Fossorier, "Decoding algorithms for nonbinary LDPC codes over $GF(q)$," *IEEE Trans. Commun.*, vol. 55, no. 4, pp. 633–643, Apr. 2007.
- [83] Y. Nakamura, Y. Bandai, Y. Okamoto, H. Osawa, H. Aoi, and H. Muraoka, "A study on nonbinary LDPC coding and iterative decoding system in BPM r/w channel," *IEEE Trans. Magn.*, vol. 47, no. 10, pp. 3566–3569, Oct. 2011.
- [84] I. S. Reed and G. Solomon, "Polynomial codes over certain finite fields," *Journal of the Society for Industrial & Applied Mathematics*, vol. 8, no. 2, pp. 300–304, Jun. 1960.
- [85] S. Lin and D. J. Costello, *Error Control Coding, Second Edition*. Upper Saddle River, NJ, USA: Prentice-Hall, Inc., 2004.
- [86] J. Jiang and K. R. Narayanan, "Iterative soft decoding of Reed-Solomon codes," *IEEE Commun. Letters*, vol. 8, no. 4, pp. 244–246, Apr. 2004.
- [87] W. Peterson, "Encoding and error-correction procedures for the bose-chaudhuri codes," *IRE Trans. on Inform. Theory*, vol. 6, no. 4, pp. 459–470, September 1960.
- [88] M. El-Khamy and R. J. McEliece, "Iterative algebraic soft-decision list decoding of Reed-Solomon codes," *IEEE J. Selected Areas in Commun.*, vol. 24, no. 3, pp. 481–490, Mar. 2006.
- [89] R. Koetter and A. Vardy, "Algebraic soft-decision decoding of Reed-Solomon codes," *IEEE Trans. Inform. Theory*, vol. 49, no. 11, pp. 2809–2825, Nov. 2003.

BIBLIOGRAPHY

- [90] J. Jiang and K. R. Narayanan, "Iterative soft-input soft-output decoding of Reed-Solomon codes by adapting the parity-check matrix," *IEEE Trans. Inform. Theory*, vol. 52, no. 8, pp. 3746–3756, Aug. 2006.
- [91] V. Guruswami and M. Sudan, "Improved decoding of Reed-Solomon and algebraic-geometry codes," *IEEE Trans. Inform. Theory*, vol. 45, no. 6, pp. 1757–1767, Sep. 1999.
- [92] R. McEliece, "On the average list size for the Guruswami-Sudan decoder," in *Proc. 7th Int. Symp. on Comm. Theory Applications*, 2003.
- [93] S. Wicker, *Error control systems for digital communication and storage*. Prentice Hall, 1995.
- [94] X. Y. Hu, E. Eleftheriou, and D. M. Arnold, "Regular and irregular progressive edge-growth Tanner graphs," *IEEE Trans. Inf. Theory*, vol. 51, no. 1, pp. 386–398, Jan. 2005.
- [95] G. Han, Y. Guan, K. Cai, K. Chan, and L. Kong, "Coding and detection for channels with written-in errors and inter-symbol interference," *IEEE Trans. Magn.*, pp. 1–6, 2014. [Online]. Available: <http://ieeexplore.ieee.org>
- [96] E. Gilbert, "Capacity of a burst-noise channel," *Bell System Technical Journal*, vol. 39, no. 5, pp. 1253–1265, Sept 1960.
- [97] W. Chang, "Advanced signal processing for magnetic recording on perpendicularly magnetized media," Ph.D. dissertation, The University of Oklahoma, Norman, 2010.
- [98] S. Yuan and H. Bertram, "Correction to "off-track spacing loss of shielded mr heads"," *IEEE Trans. Magn.*, vol. 32, no. 4, pp. 3334–, July 1996.

BIBLIOGRAPHY

- [99] A. Iyengar, P. Siegel, and J. Wolf, “LDPC codes for the cascaded BSC-BAWGN channel,” in *Proc. 47th Annu. Allerton Conf. Communication, Control and Computing*, Sep./Oct. 2009, pp. 620–627.
- [100] P.-M. Nguyen, M. A. Armand, and T. Wu, “Improved codes for synchronization error correction on the BPMR channel,” in *Digest of Technical Papers of TMRC2014*, Berkeley, California, US, Aug. 2014.
- [101] J. Sellers, F., “Bit loss and gain correction code,” *Information Theory, IRE Transactions on*, vol. 8, no. 1, pp. 35–38, Jan. 1962.
- [102] Y. Ng, “Signal processing for bit-patterned media recording and heat-assisted magnetic recording with media noise,” Ph.D. dissertation, Carnegie Mellon University, 2012.
- [103] J. Moon and J. Park, “Pattern-dependent noise prediction in signal-dependent noise,” *IEEE J. Selected Areas in Commun.*, vol. 19, no. 4, pp. 730–743, Apr. 2001.
- [104] T. Richardson and R. Urbanke, *Modern coding theory*. Cambridge University Press, 2008.
- [105] S. Verdú and T. Han, “A general formula for channel capacity,” *IEEE Trans. Inform. Theory*, vol. 40, no. 4, pp. 1147–1157, Jul 1994.
- [106] P.-M. Nguyen and M. A. Armand, “Capacity of a class of channels with dependent insertions and deletions,” *Submitted to Trans. Inform. Theory*.

List of Publications

Journal Papers

1. **T. Wu** and M. A. Armand, “The Davey-MacKay coding scheme for channels with dependent insertion, deletion and substitution errors,” *IEEE Transactions on Magnetics*, vol. 49, no. 1, pp. 489-495, Jan. 2013.
2. **T. Wu** and M. A. Armand, “Joint and separate detection-decoding on BPMR channels,” *IEEE Transactions on Magnetics*, vol. 49, no. 7, pp. 3779–3782, Jul. 2013.
3. P. Nguyen, M. A. Armand, and **T. Wu**, “On the watermark string in the Davey-MacKay construction,” *IEEE Communications Letters*, vol. 17, no. 9, pp. 1830–1833, Sept. 2013.
4. **T. Wu**, M. A. Armand, J. R. Cruz, ”Detection-decoding on BPMR channels with written-in error correction and ITI mitigation,” *IEEE Transactions on Magnetics*, vol. 50, no. 1, Jan. 2014.

Conference Papers

1. **T. Wu**, M. A. Armand and X. Jiao, “On Reed-Solomon codes as outer codes in the Davey-MacKay construction for channels with insertions and deletions,”

in *Proceedings of 8th International Conference on Communications and Signal Processing*, Singapore, Dec. 13-16, 2011.

2. **T. Wu**, M. A. Armand, “Iterative bidirectional detection for BPMR channels,” in *Digest of Technical Papers of Intermag Conf.*, Dresden, Germany, May 4-8, 2014, pp. 3462–3463
3. **T. Wu**, M. A. Armand and J. R. Cruz, “Detection-decoding on staggered BPMR channels with written-in errors and inter-track interference,” in *Digest of Technical Papers of Intermag Conf.*, Dresden, Germany, May 4-8, 2014, pp. 1068–1069
4. P. Nguyen, M. A. Armand, and **T. Wu**, “Improved codes for synchronization error correction on the BPMR channel,” in *Digest of Technical Papers of TMRC2014*, Berkeley, California, US, Aug. 11-13, 2014